# Identification of Chromatin Modifiers Regulating Vincristine Resistance in Medulloblastoma

by

**Göktuğ Karabıyık**

A Dissertation Submitted to the
Graduate School of Health Sciences
in Partial Fulfillment of the Requirements for
the Degree of

Doctor of Philosophy

In

Cellular and Molecular Medicine


August 10, 2023

**Identification of Chromatin Modifiers Regulating Vincristine Resistance in Medulloblastoma**

Koç University

Graduate School of Health Sciences

This is to certify that I have examined this copy of a doctoral dissertation by

**Göktuğ KARABIYIK**

and have found that it is complete and satisfactory in all respects,

and that any and all revisions required by the final

examining committee has been made.

Committee Members:

_____

Prof. Tuğba Bağcı Önder (Advisor)

_____

Prof. Tamer Önder

_____

Assoc. Prof. Umut Şahin

_____

Assoc. Prof. Adam P. Cribbs

_____

Assist. Prof. Ece Öztürk

Date: 10.08.2023

*I dedicate my thesis*

*To J.R.R. Tolkien;*

*“There is some good in this world,*
*and it's worth fighting for.”*

## ABSTRACT

### Identification of Chromatin Modifiers Regulating Vincristine Resistance in Medulloblastoma

Göktuğ Karabıyık

Doctor of Philosophy in Cellular and Molecular Medicine

August 10, 2023

Medulloblastoma (MB) is the most prevalent brain cancer in children, typically occurring between the ages of six and eight. While primary MB treatments have a success rate of over 50%, relapse affects more than 30% of the patients, resulting in a poor prognosis with survival rates dropping below 25%. Furthermore, acquired-drug resistance is widely observed in patients with relapse, posing a significant challenge for the treatment of MB. Recent cohorts revealed mutations and differential regulation of chromatin modifiers in distinct subgroups of MB, emphasizing the importance of epigenetic regulations in MB tumorigenesis.

In this study, we aimed to identify the epigenetic vulnerabilities of MB by employing loss-of-function screening approaches. Using paired parental and vincristine-resistant MB cells previously generated in our lab, we first conducted a chemical screen with an epigenetic probe library. Second, we performed genetic perturbation screens using our CRISPR/Cas9-based epigenome-wide knockout library (EPIKOL). The ultimate goal was to discover new epigenetic mechanisms of drug response in MB.

The established vincristine-resistant MB cells showed up to 100-fold resistance to vincristine, displaying Multi-Drug Resistance (MDR) characteristics primarily attributed to a significant upregulation of *ABCB1*. With chemical screens, we demonstrated that inhibition of the bromodomain of CBP/p300 histone acetyltransferases leads to sensitization of vincristine-resistant MB by regulating the expression of ABC and SLC transporters. With genetic screens using EPIKOL, we further validated the sensitizing effect of CBP inhibition on drug resistance. Additionally, we identified KEAP1, the regulator of NRF2, as a novel target. Accordingly, KEAP1 was identified from 3 different screens on vincristine-resistant MB, where the negative selection was applied with increasing doses of vincristine, but not on parental MB cells. KEAP1 loss by CRISPR/Cas9 using multiple sgRNAs also confirmed the sensitizing effect through viability assays. Moreover, upon exposure to vincristine, a significant increase in apoptosis was also observed in KEAP1-KO vincristine-resistant cells. Additionally, the transcriptomic analysis revealed the downregulation of *ABCB1*, the main efflux pump of vincristine, on KEAP1-KO vincristine-resistant cells, further supporting the sensitizing effect of KEAP1 loss.

This thesis identified two major regulators of acquired vincristine resistance in MB, which have the potential to serve as therapeutic intervention points in the future.

# ÖZETÇE


**Medulloblastomada Vinkristin Direncini Regüle eden Kromatin Regülatörlerlerinin Araştırılması**

Göktuğ Karabıyık

Hücresel ve Moleküler Tıp, Doktora

10 Ağustos 2023

Medulloblastoma (MB), genellikle 6-8 yaş arasında teşhis edilen, çocukluk çağının en yaygın beyin kanseri tipidir. Primer MB tedavilerinde başarı oranı %50'nin üzerindeyken, hastaların %30'unun üzerinde bir bölümünde nüks görüldüğü ve sağ kalım oranının %25'in altına düştüğü belirtilmiştir. Buna ek olarak, nüks görülen hastalarda, edinilmiş ilaç direnci yaygın olarak gözlenmekte, ve bu durum, tedavide önemli zorluklara yol açmaktadır. Son çalışmalar, MB'nin farklı alt gruplarına özel olarak, kromatin düzenleyicilerinde mutasyonlar gözlemlendiğini ve gen anlatımında anlamlı farklılıklar olduğunu açığa çıkartmıştır, bu da MB tümörü oluşumunda ve gelişiminde epigenetik faktörlerin önemini göstermektedir.

Bu çalışmada, hem ana MB hücrelerinde, hem de ilaç direnci geliştirilmiş MB hücrelerinde epigenetik prob kütüphanesi ve CRISPR/Cas9 tabanlı genetik ablasyon kütüphanesi (EPIKOL) kullanılarak MB'nin epigenetik zayıflıklarının belirlenmesi ve MB tümörü oluşumundaki ve ilaç direncinin gelişimindeki etkisinin gösterilmesi amaçlanmıştır.

Oluşturulan ilaç dirençli MB hatlarında, vinkristine karşı 100 kata varan çoklu ilaç direnci gözlemlenmiş ve önemli bir ilaç pompası olan *ABCB1* gen anlatımı seviyesinde anlamlı fark gösterilmiştir. Kimyasal prob kütüphanesinin kullanımı ile CBP/p300 bromodomain'lerinin inhibisyonunun ilaç dirençli MB hücrelerinin vinkristine olan duyarlılığını arttırdığı ve bunun ABC ve SLC pompalarını gen anlatımının düzenlenmesiyle oluştuğu gösterilmiştir. EPIKOL taraması ile de, CBP inhibisyonunun ilaç dirençli MB üzerindeki duyarlılığı arttırıcı etkisi yeniden doğrulanmıştır. Buna ek olarak, NRF2'nin negatif düzenleyicisi KEAP1 geninin inhibisyonunun da *ABCB1* gen anlatımını dolaylı olarak düzenleyerek, vinkristin dirençli hücrelere spesifik olarak duyarlılığı arttırdığı gözlemlenmiştir. Ana MB hücre hattında ise aynı etki gözlemlenmemiştir. Birden fazla sgRNA kullanılarak yapılan doğrulama deneylerinde vinkristin dirençli MB hücrelerinde KEAP1 geni ablasyonu üzerine vinkristine maruz bırakıldıklarında apoptoz seviyelerinde artış gösterilmiştir. Bunlara ek olarak KEAP1-KO vinkristin dirençli hücrelerde yapılan transkriptom analizinde, vinkristinin ana pompası olan ABCB1 sevisinde düşüş gözlemlenmiştir.

Bu tez, MB'de edinilmiş vincristin direnincinin iki önemli düzenleyicisini tanımlamış olup, bu düzenleyicilerin, gelecekteki çalışmalarla beraber olası terapötik etki potansiyaline sahip olduğu ortaya koymuştur.

## ACKNOWLEDGEMENT

"It's a dangerous business, going out your door. You step onto the road, and if you don't keep your feet, there's no knowing where you might be swept off to." Ph.D. was a great adventure for me, and I was lucky to share this journey with many loved and respected ones. When I got lost, they helped me to find the way. There were the ones I met every day, and there were the ones, I have not had a chance to meet throughout this journey, but I would like to thank each and every one of them who shared even a brief moment of joy, sincere laughter, and wisdom.

I would like to express my sincere gratitude and thank my supervisor first. This journey started with Dr. Tuğba Bağcı-Önder. She was the only person I chose at the beginning of the journey, and the rest were either the ones she chose to create my TBO lab family or the ones I met, thanks to her letting me join TBO lab. We shared many memories, and I will remember all with a smile on my face. Both scientifically and personally, I learned a lot from her. I am grateful for her guiding light, encouraging us to become the best of what we can be.

I am sincerely grateful to my thesis committee members, Dr. Tamer Önder and Dr. Umut Şahin, for their guidance throughout this journey. Even though I stumbled occasionally, their critical thinking helped me stand up and continue walking to this moment. I am also immensely grateful to my thesis defense committee members, Dr. Adam P. Cribbs and Dr. Ece Öztürk, for their genuine interest in my research. Their participation in my jury has been precious.

I would like to thank Koç University Research Center for Translational Medicine (KUTTAM) and the Newton Royal Fellowship for their financial support.

The greatest chapters of this journey were among my TBO Lab family. I learned a lot from every individual, and I can only hope that I played a role for them to discover a new perspective or help them find the knowledge they pursued. While many members of the family I met on the first days of my journey already carried on with their academic career, TBO Lab is a whole, and I would like to thank every one of them: Dr. Ahmet Cingöz, Dr. İlknur Sur-Erdem, Dr. Alişan Kayabölen, Dr. Filiz Şenbabaoğlu-Aksu, Dr. Fidan Şeker-Polat, Dr. Ezgi Özyerli, Dr. Ayşe Derya Cavga, Dr. Ali Cenk Aksu, Dr. Tolga Lokumcu, Dr. Özlem Yedier-Bayram, Ezgi Yağmur Kala, Nareg Değirmenci, Canan Bayraktar, Vuslat Akçay, Beril Esin, Ebru Yılmaz, Mina Küçüktaş, Aksel Çelikkol, Beyza Köseoğlu, Gizem Doğan-Yılmaz, İpek Kök, and Sedef Saraç. And I would like to thank my interns, Can Dedeköy and Mehmet Eren Kule, for their enthusiasm about the project, help, support, and patience.

Koç University has been more than just an educational institution; it has been my home for one-third of my life, shaping a significant part of my academic journey. I forged many friendships that I will carry with me for a lifetime. These connections continue to walk with me in my journey ahead. I am profoundly thankful unwavering support of my companions from my undergraduate days - Yunus Can Erol, Dr. Büşra İzgi, Dr. Eray Enüstün, Ilgın Kotan, and Dr. Betül Ersoy. Alongside Yunus Can Erol and Vuslat Akçay, we shared a common fascination with gazing up at the night sky, and I extend my heartfelt gratitude to them for being by my side through those adventures.

Within the open and collaborative atmosphere of KUTTAM, I had the privilege of getting to know exceptional individuals Dr. Doğancan Özturan, Dr. Uğur Akcan, Dr. Deniz Ata, Dr. Özen Leylek and Dr. Ceren Şeref. Their friendship and distinctive qualities have been an invaluable source of support and inspiration, enriching my academic career and my personal growth in countless ways. Throughout my academic journey, one individual, Batuhan Mert Kalkan, has been a constant companion. His friendship, accompanied by his unconventional thinking, has added an indispensable dimension to this path of learning and discovery.

Dr. Filiz Şenbabaoğlu-Aksu was an exceptional mentor, guiding me academically and personally, and fostering a fresh perspective in me. Together with Dr. Özlem Yedier-Bayram and Ezgi Yağmur Kala, comprising the EPIKOL team, we surmounted various challenges, stepping into each other's shoes and nurturing a profound spirit of collaboration and friendship. Sharing a house with Dr. Alişan Kayabölen was a delight as it led to countless sleepless nights filled with enriching discussions about the universe and everything in it. Dr. Fidan Şeker-Polat set an inspiring example of determination and courage, qualities I wholeheartedly admire. Dr. Ahmet Cingöz, akin to an older brother, shared two profound passions with me - our love for Istanbul and photography. Nareg Değirmenci, a cherished friend, possessed an extraordinary gift for being there when you needed her, adding a layer of her preciousness to every moment. Dr. Ali Cenk Aksu's unwavering support and consistent presence, even when I was unaware of my need for it, left an indelible mark of gratitude. May the stars shine upon his face. Canan Bayraktar was a friend I thought I had even before I met her. She not only proved to be a thoughtful gift but also a source of invaluable lessons along the way. Arda Odabaş akin to the younger brother I have never had served as a reminder what academia meant to me when I began this journey. Completing my thesis demanded far more moral support than I initially anticipated. I feel fortunate to have had the support of two young scientists who have accompanied me on this final part of the journey. I want to thank Mina Küçüktaş, my bench mate, for consistently reminding me of the importance of determination bolstered by unwavering hope. I also extend my gratitude to Beril Esin for her enormous support, her keen ear for me at all times, and for entrusting me with the role of the 'first officer' when it came to the data.

I extend my gratitude to the countless bright smiles I met on this journey. They became a light in dark places when all other lights go out. Lastly, I pay a tribute to the individual who imparted those illuminating words on me, John Ronald Reuel Tolkien. From the moment he told me the tale of the Moon and the Sun, he became the guiding star on my path despite our never having met. As we commemorate the passing of fifty years since he embarked on his own journey, his enchanting words remain eternally etched in memory.

Finally, I would like to express my deepest gratitude to two of the strongest women I have ever known, my family: my sister İpek Öykü and my mother, Sevgi Yallagöz. Their support has been the cornerstone of my journey, providing me with the essential strength and encouragement needed to persevere.

## TABLE OF CONTENTS

# LIST OF TABLES

# LIST OF FIGURES

# ABBREVIATIONS

| | |
|---|---|
| ABC | ATB Binding Cassette |
| ARE | Antioxidant-Response-Element |
| BET | Bromodomain and extra-terminal domain |
| BPTF | Bromodomain PHD Finger Transcription Factor |
| BRD | Bromodomain |
| BTB | a broad complex, tram track, bric-a-brac |
| bZip | basic leucine zipper |
| C-MB | Classic Medulloblastoma |
| Cas9 | CRISPR associated nuclease 9 |
| CBP | CREB binding protein |
| cDNA | complementary DNA |
| CDP | Cumulative Distribution Plot |
| c-PARP | Cleaved PARP |
| CRISPR | Clustered Regularly Interspaced Short Palindromic Repeats |
| CT | Computed Tomography |
| CTG | Cell Titer Glo |
| CTR | C-Terminal Region |
| CUL3 | Cullin 3 |
| DEGs | Differentially Expressed Genes |
| DepMap | Cancer Dependency Map |
| DGR | Double Glycine Repeat |
| DMEM | Dulbecco's Modified Eagle Medium |
| DN-MB | Desmoplastic/nodular Medulloblastoma |
| DNMT | DNA methyl transferase |
| EPIKOL | Epigenetic Knockout Library |
| EZH2 | Enhancer of zeste homolog 2 |
| FBS | Fetal Bovine Serum |
| FDR | False Discovery Rate |
| gDNA | Genomic DNA |
| GFP | Green Fluorescent Protein |
| GSEA | Gene Set Enrichment Analysis |
| HAT | Histone Acetyl Transferase |

| | |
|---|---|
| HDAC | Histone Deacetylase |
| HDR | Homology Directed Repair |
| hGFP | eGFP vector with hygromycin selection |
| HMT | Histone methyltransferase |
| HDM | Histone Demethylase |
| IC50 | Inhibitory Concentration 50 |
| IVR | Intervening Region |
| JAK2 | Janus Kinase 2 |
| KEAP1 | Kelch-like ECH-associated protein 1 |
| KIR | KEAP1-interacting region |
| LC3 | Microtubule-associated protein 1A/1B-light chain 3 |
| LCA-MB | Large cell/anaplastic Medulloblastoma |
| LFC | $Log_2$ Fold Change |
| MB | Medulloblastoma |
| MBEN | Medulloblastoma with extensive nodularity |
| MDR | Multidrug resistance |
| MOI | Multiplicity of Infection |
| MRI | Magnetic Resonance Imaging |
| NEH | Nrf2-ECH Homology |
| NES | Normalized Enrichment Score |
| NHEJ | Nonhomologous end joining |
| NRF2 | Nuclear factor erythroid 2-related factor 2 |
| NT | Non-targeting |
| OE | Overexpression |
| P300 | E1A Binding Protein P300 |
| PCA | Principal Component Analysis |
| PCR | Polymerase chain reaction |
| PD | Population Doubling |
| Pen/Strep | Penicillin/Streptomycin |
| P-gp | P-glycoprotein |
| PT | Post Transduction |
| RPM | Read per million |
| rpm | revolutions per minute |

| | |
|---|---|
| ROS | Reactive Oxygen Species |
| qRT-PCR | Quantitative Real-Time PCR |
| SAM | S-adenosyl-L-methionine |
| SHH | Sonic Hedgehog |
| sgRNA | small guide RNA |
| sMaf | small musculoaponeurotic fibrosarcoma |
| TET | Ten-eleven translocation |
| TPM | Transcript per million |
| WHO | World Health Organization |
| WNT | Wingless |
| WT | Wildtype |

# 1 INTRODUCTION

## 1.1 Medulloblastoma

Medulloblastoma (MB) is a malignant embryonal tumor formed in the cerebellum or around the posterior fossa. MB is classified as grade IV according to the World Health Organization (WHO) classification, indicating rapid cell division, extensive spreading, and lack of resemblance to the original tissue (Quinlan & Rizzolo, 2017). MB is most commonly diagnosed in children under nine, with the peak incidence between six and eight years old (Northcott et al., 2019). MB is the most prevalent childhood brain tumor, accounting for approximately 20% of all cases (Juraschka & Taylor, 2019; Ostrom et al., 2018).

While the 5-year survival rate for MB is greater than 50% on primary MB, approximately 30% of patients experience tumor recurrence, leading to a significant drop in the survival rate to 25%. Management of relapsed tumors poses significant clinical difficulties and requires a more aggressive treatment strategy (Johnston et al., 2018; Juraschka & Taylor, 2019; Sabel et al., 2016). Additionally, even with successful treatment, young patients experience long-term complications due to the adverse effects of chemotherapy and radiotherapy, dramatically affecting their quality of life (Chevignard et al., 2017; Fric et al., 2020).

The 2016 WHO Classification of Central Nervous System Tumors recognizes both histological and molecular subtypes of Medulloblastoma for the diagnosis. Histological classification has been proven to be a valuable tool for the diagnosis of subtypes and prognostic stratification (Eberhart et al., 2002; Triscott et al., 2021). The 2016 WHO classification includes four distinct histological subtypes, namely, Classic MB (C-MB), Desmoplastic/nodular MB (DN-MB), MB with extensive modularity (MBEN), and large cell/anaplastic MB (LCA-MB). 2021 WHO Classification also confirms established clinical associations of histological subtypes of MB (Louis et al., 2021). Recent cohort studies conducted over the past few decades have led to the identification of four distinct molecular subtypes of MB based on their specific genetic, pathophysiologic, and gene expression profiles. These subtypes include Wingless (WNT)-activated, Sonic Hedgehog

(SHH)-activated, Group 3, and Group 4 (Louis et al., 2016; Taylor et al., 2012). The driving mutations observed in these MB subgroups are primarily associated with developmental pathways for respective subtypes. Several mutations on chromatin-modifying genes have also been observed in large cohorts. However, each subgroup displays distinct mutation signatures (Cavalli et al., 2017; Northcott et al., 2017; Pugh et al., 2012; Robinson et al., 2012).

## 1.2 Histological Classification of Medulloblastoma

### *1.2.1 Classic Variant (C-MB)*

Classical Variant is the most commonly prevalent histological subtype of MB, accounting for more than 70% of all cases (Orr, 2020). Most WNT-activated MB tumors are highly associated with this histological subtype (Ellison et al., 2011). MB cases in this variant are characterized by densely packed cells with relatively round nuclei, a lack of increased cell size, and frequent mitotic activity. Homer Wright rosettes are commonly seen in this variant (Millard & De Braganca, 2016). The presence of those rosettes is thought to relate to the presence of neural differentiation (Wippold & Perry, 2006).

### *1.2.2 Desmoplastic/nodular Variant (DN-MB)*

The desmoplastic/nodular variant is characterized by the presence of “desmoplastic” areas within the tumor, indicating excessive growth of fibrous or connective tissue surrounding the tumor cells. This histological subtype of MB is predominantly seen in children younger than the age of two (Siegfried et al., 2016). Almost all DN-MB tumors are associated with the SHH-activated subtype of MB and are generally associated with an intermediate clinical risk (AbdelBaki et al., 2018; Orr, 2020)

### *1.2.3 MB with extensive nodularity (MBEN)*

MBEN is a special variant of DN-MB, where tumor cells are densely packed as nodules rather than primitive elements seen in DN-MB. While this histological subtype is the rarest subtype, it is associated with good to excellent prognosis. Nearly all MBEN tumors are located in p53 mutant SHH-activated MB (Korshunov et al., 2018; Siegfried et al., 2016)

### *1.2.4 Large cell/anaplastic Variant (LCA-MB)*

Large cell/anaplastic variant encompasses two distinct histological subtypes; however, they are combined in the 2016 histological classification due to the presence of anaplastic features in most large cell tumors (Brown et al., 2000). Generally, this subtype exhibits increased cell size, a large nuclear-to-cytoplasmic ratio, frequent mitosis, and increased apoptotic bodies (Eberhart et al., 2002).

## 1.3 Molecular Classification of Medulloblastoma

### *1.3.1 WNT-activated MB*

The Wingless (WNT) subgroup of MB is characterized by activating mutations on the *CTNNB1* gene, which encodes the β-Catenin protein (Kool et al., 2012). These mutations result in constitutive expression and stabilization of β-catenin, leading to activation of the WNT pathway and promoting tumor growth and tumorigenesis (Northcott et al., 2019). While WNT-activated MB accounts for approximately 10% of all medulloblastoma cases, it is most observed in older children. This subtype is associated with the best prognosis among all MB subtypes, and patients within this subtype have a higher rate of event-free survival even with the standard therapy (Taylor et al., 2012).

### *1.3.2 SHH-activated MB*

The Sonic Hedgehog (SHH) subgroup of MB is characterized by mutations in the integral components of the SHH pathway, such as tumor suppressor *PTCH1*, *SUFU* genes, or activating mutations on proto-oncogenes like *SMO*. These mutations result in dysregulation of the SHH signaling pathway, leading to uncontrolled cell proliferation (Millard & De Braganca, 2016). SHH-activated MB accounts for approximately 25% of all MB cases and is more commonly seen in children (Northcott et al., 2012). Also, the SHH subgroup of MB is further divided into two groups based on p53 mutation status. SHH/p53 mutant patients have poorer outcomes than the SHH/p53 wild-type group (Northcott et al., 2019).

### *1.3.3 Group 3 MB*

*MYC* amplification is a particular factor and one of the characterizing properties of Group 3 MB. Amplification of MYC signaling plays an important role in cell growth and proliferation (Northcott et al., 2019). Unlike other subgroups, patients of Group 3 show patient-specific mutation signatures with driver mutations accumulated around one common molecular pathway (Northcott et al., 2019). Approximately a quarter of all MB patients are classified under Group 3, and this subtype is more frequently seen in infants and children with peak diagnosis age between 3 and 5 years, while it is almost never seen in adults (Menyhart et al., 2019; Millard & De Braganca, 2016; Taylor et al., 2012). Compared to other MB subgroups, a worse prognosis is expected for Group 3 patients with a 5-year survival rate of less than 50% (Kool et al., 2012; Schroeder & Gururangan, 2014).

### *1.3.4 Group 4 MB*

Group 4 is the most prevalent subtype of MB, accounting for approximately 40% of all patients, and predominantly seen in patients between 3 and 16 years old. Group 4 MB patients may exhibit *MYCN,* and *CDK6* amplifications are observed in patients. However, in large cohorts, no specific commonly mutated gene has been detected in patients (>10% of all patients), hindering the understanding of the disease's pathogenesis (Northcott et al., 2017; Northcott et al., 2019). Even though patients in Group 4 generally have better prognoses in comparison to Group 3 patients, approximately 30% of the patients present metastasis at diagnosis and are included in the high-risk group (Millard & De Braganca, 2016).

Recent advancements in informatics technology and single-cell transcriptomics have shed light on the clinical and biological relevance of Group 3 and Group 4 MB tumors. According to a recent study, these tumors are thought to represent a continuum reflecting human cerebellar development. Study showed that identified tumors in group 3 and group 4 MB are intermediates of this bipolar continuum. While group 4 tumors represent late-stage differentiated cerebellar nuclei/ unipolar brush cells in cerebellum development, group 3 tumors represent poorly differentiated rhombic lip precursor cells, leading to poorer survival characteristics (Williamson et al., 2022).

**Table 1.1: Molecular and Histological Subtypes of Medulloblastoma.** Table adapted from (Louis et al., 2016)

| Molecular Subtype | Histological Subtype | Prognosis |
|---|---|---|
| WNT-Activated MB | Classic | Low risk- Classic morphology |
| | Large cell/Anaplastic | Uncertain clinicopathological significance |
| SHH-Activated MB TP53-mutant | Classic | Uncommon high-risk tumor |
| | Large cell/Anaplastic | High-risk tumor |
| | Desmoplastic/Nodular | Uncertain clinicopathological significance |
| SHH-Activated MB TP53-wildtype | Classic | Standard risk tumor |
| | Large cell/Anaplastic | Uncertain clinicopathological significance |
| | Desmoplastic/Nodular | Low-risk tumors in infants |
| | Extensive nodularity | Low-risk tumors in infants |
| Group 3 MB | Classic | Standard risk tumor |
| | Large cell/Anaplastic | High-risk tumor |
| Group 4 MB | Classic | Standard risk tumor |
| | Large cell/Anaplastic | Uncertain clinicopathological significance |

## 1.4 Diagnosis and Treatment of Medulloblastoma

MB diagnosis in clinics involves multiple approaches, including cerebrospinal fluid cytology, imaging through head computed tomography (CT) or brain Magnetic Resonance Imaging (MRI), and molecular analysis on symptomatic patients. The onset of symptoms can vary, ranging from a few days to years after the pathogenesis of MB (Martirosian. & Neman., 2018). Common symptoms are often nonspecific and related to increased intracranial pressure, such as nausea, headaches, vomiting, and behavioral changes in children (Millard & De Braganca, 2016; Northcott et al., 2019).

Based on the clinical findings, patients diagnosed with MB are typically classified into two main prognostic groups. The high-risk group includes patients with incomplete

tumor removal (postsurgical residual disease greater than 1.5 $cm^2$) due to safety reasons, young age, and the presence of metastatic tumors. Conversely, the low-risk group consists of patients who undergo close to complete removal of tumor removal, exhibit non-metastatic behavior, and increased age are the factors decreasing the risk, thus forming the low-risk group and older in age. Standard treatment approaches for MB usually involve maximal safe surgery followed by chemotherapy and radiotherapy (Millard & De Braganca, 2016).

However, radiotherapy is not preferred for patients younger than three years old due to outcomes of previous studies indicating significant decreases in IQ score and impaired cognitive and motor functions in patients who received radiotherapy before the age of three (Ottensmeier et al., 2020; Thomas & Noel, 2019). More recently, to decrease the toxic effect of radiation on both standard and high-risk patients, the autologous stem-cell rescue has been shown to increase the survival of patients and decrease the toxic, effect improving the success rate, especially for patients in high-risk risk group compared to published trials (Gajjar et al., 2006; Grill et al., 2006)

**Table 1.2: Medulloblastoma Risk Stratification.** Table adapted from (Ramaswamy, Remke, Adamski, et al., 2016; Ramaswamy, Remke, Bouffet, et al., 2016)

| Risk Group | The 5-year overall survival rate | Molecular Subtype |
|---|---|---|
| Very High | <50% | Metastatic Group 3 MB |
| | | SHH-activated MB TP53-mutant |
| High | 50-70% | Metastatic or MYCN amplified SHH group |
| | | Metastatic Group 4 MB |
| Standard | 75-90% | Localized SHH-activated MB TP53-wildtype |
| | | Group 3 MB without MYC amplification |
| | | Group 4 MB without loss of chromosome 11 |
| Low | >90% | Localized WNT-activated MB |
| | | Localized Group 4 MB with loss of chromosome 11 |

### *1.4.1 Chemotherapy*

Medulloblastoma treatment consisted of only surgery in the 1960s, followed by radiotherapy for most cases (Brown et al., 1977). The addition of multidrug chemotherapeutic application to MB treatment in the 1980s significantly increased the survival rate even with the reduced radiotherapy doses in standard-risk MB. The reduction of radiotherapy in the treatment of MB was aimed to decrease the side effects of radiotherapy, especially in young individuals. However, even in standard risk of MB, the exclusion of radiotherapy led to decreased survival (Packer et al., 1999; Varan, 2011).

Current chemotherapy regimens applied for MB patients mainly depend on the risk group, molecular subgroups, age, metastatic disease, and prognosis of the MB patients (Robinson et al., 2018). For standard-risk and low-risk MB patients, chemotherapy regimens mainly include a combination of cisplatin, cyclophosphamide, lomustine, and vincristine in addition to radiotherapy (Martin et al., 2014; Parkes et al., 2015). Since the introduction of chemotherapeutic regimens in MB treatment, new approaches have been utilized to optimize the dosage of drugs and radiation, and increased survival rates were observed with new clinical trials (Choi, 2023).

Several approaches have been utilized to improve the survival rate of high-risk MB. Patients with metastasis and relapse were included in this group. Clinical trials were mostly focused on the presentation of high doses of multiple drugs in multiple cycles supported by radiation therapy. However, no consensus has been reached for high-risk MB treatment strategies (Lafay-Cousin & Dufour, 2022). Furthermore, patients younger than three years of age are usually accepted as high-risk. Since the maturation of the central nervous system is approximately completed around three years of age, radiotherapy is not administered or delayed for those patients to prevent sequels, including mental motor retardation and severe cognitive problems, increasing the importance of chemotherapy (Kalifa & Grill, 2005).

*Vincristine*

The usage of a diverse array of drugs targeting essential mechanisms in rapidly dividing cancer cells has been crucial for MB treatment. However, standing out as a widely employed drug in all regimens, vincristine has been an important part of the

backbone of the standard treatment of MB.

Vincristine belongs to the vinca alkaloid group, identified in *Catharanthus roseus.* It exerts its mechanism of action by binding to the plus (+) end of microtubules, thereby impeding GTP absorption and preventing microtubule polymerization. Subsequently, inhibition of microtubule polymerization disrupts important cellular functions for dividing cells, such as mitotic spindle formation, leading to impaired cell division. While a low concentration of Vincristine prevents the polymerization of microtubules, a high concentration leads to the depolymerization of formed microtubules (Martino et al., 2018) **(Figure 1.1)**. Like most chemotherapeutic agents, vincristine affects rapidly dividing cells all over the body. Even though it has been successfully used for various cancer types for decades, several dose-limiting side effects were reported, including weight loss, nausea, vomiting, and, most importantly, peripheral neuropathy. Those side effects, especially neuropathy, are major drawbacks of vincristine treatment and might dramatically affect a patient's life in the long term, even after successful treatment. Because of this reason, vincristine is usually used in low concentration, and in most regimens, vincristine is prescribed in a cocktail with cyclophosphamide and doxorubicin (Skubnik et al., 2021). In a case study where a desmoplastic nodular MB patient had inherited neuropathy, the patient was treated with a regimen without vincristine, and according to this study, it was the first case where a successful MB treatment without vincristine was achieved (Bernstock et al., 2019).

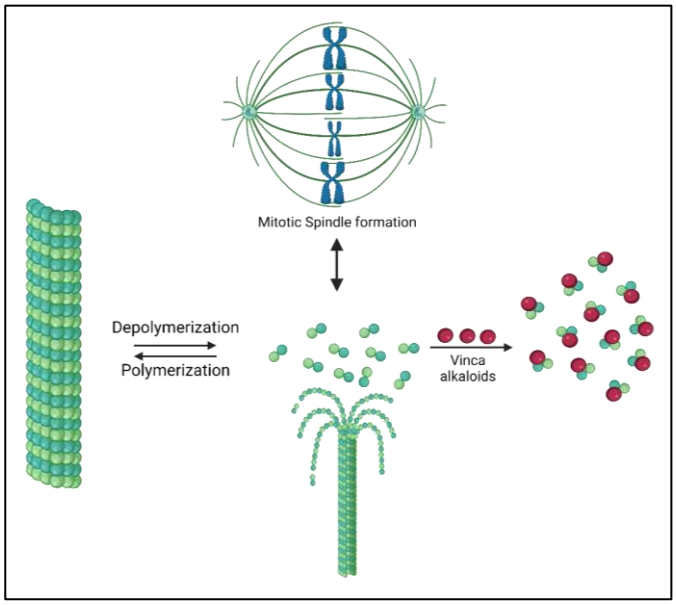


**Figure 1.1: Mechanism of Action of Vincristine.** Figure created in biorender.com

## 1.5 Multi-Drug Resistance in Medulloblastoma

Especially in high-risk MB patients, drug resistance poses a significant and unmet challenge for the treatment of MB. Despite newer approaches and several clinical trials that improved the treatment of MB over the years, the emergence of drug resistance limits the effectiveness of chemotherapeutic agents used in MB treatment. One known mechanism that leads to acquired drug resistance involves upregulation or gain-of-function mutation in drug transporters (Taylor et al., 2023).

### *1.5.1 ABC transporters*

There are dozens of drug transporter coding genes in the human genome; each has its specific affinity against several drugs. The ATP-binding Cassette (ABC) family is one of the most prominent families, consisting of 48 transporters. They transport their substrate outside with the hydrolyzation of ATP molecules (Wilkens, 2015) (**Figure 1.2**). Drug resistance related to upregulation or gain-of-function mutations in members of the ABC family has been reported in various cancer types (El-Awady et al., 2016). *ABCB1* (P-glycoprotein (Pgp)) is especially important for MB therapeutics since it transports several chemotherapeutic agents used for MB treatment, including vincristine, etoposide, and carboplatin. Because of that reason, resistance against one compound may cause multidrug resistance (MDR), which is much harder to treat with conventional chemotherapy/ radiotherapy approaches. Studies on microarrays suggest that *ABCB1* upregulation is also high-risk for MB patients, given that ABCB1 positive samples were significantly within the high-risk group (Othman et al., 2014; Wijaya et al., 2017). Especially for Group 3 and Group 4, amplification of *MYC* and *MYCN* has been associated with higher *ABCB1* expression due to the proposed regulatory action of those genes over *ABCB1*. Interestingly, on radiation-resistant MB cells, the upregulation of genes within the ABC family has also been observed (Ingram et al., 2013). Inhibition of drug transporters in this family by verapamil led to the sensitization of drug-resistant MB cells (Othman et al., 2014).

Another problem encountered by MB patients is tumor relapse following treatment. While the 5-year survival rate is greater than 50% on MB subgroups in general, on relapsed tumors, it drops down below 25%. The recurrence rate ranges between 20-40%, mainly depending on the subgroup. Acquired drug resistance is also a critical factor

contributing to the poorer prognosis observed in patients with relapsed or metastatic tumors compared to those with primary tumors (Bowers et al., 2007; Millard & De Braganca, 2016; Schroeder & Gururangan, 2014).

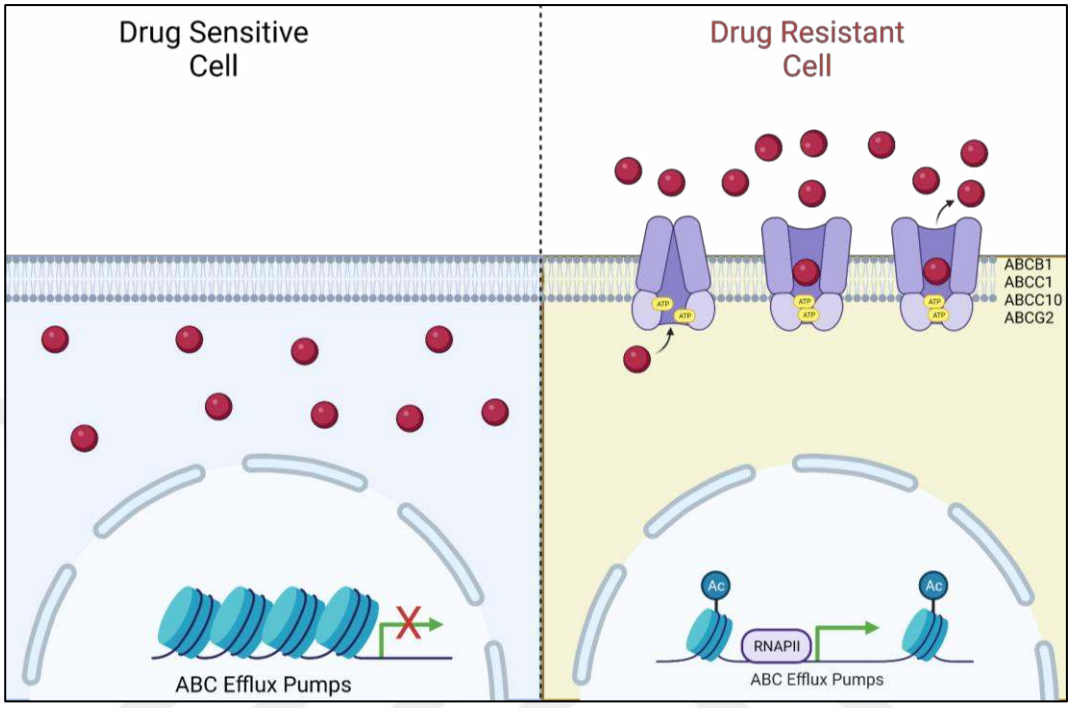


**Figure 1.2: ABC transporter's mechanism of action.** Figure created in biorender.com

## 1.6 Epigenetics

Over the years, identifications of mutations in DNA sequence have significantly contributed to understanding of various human diseases, including cancer. However, it is noteworthy that, particularly in embryonal tumors like medulloblastoma and AT/RT, the mutation burden is much lower than in tumors associated with advanced age, such as melanoma and lung cancer. In diseases with a limited number of mutations, dysregulation of gene expression associated with the development and cellular differentiation processes are observed. Throughout the differentiation from stem cells to fully developed, differentiated cells, gene expression is tightly controlled through epigenetic mechanisms (Jackson et al., 2018).

Epigenetics studies the heritable changes in gene expression without alterations in DNA sequence. Epigenetic regulators, including writers, erasers, and readers, control gene expression through DNA methylation and histone acetylation modifications (Sharma et al., 2010) **(Figure 1.3)**.

### *1.6.1 DNA Methylation*

DNA methylation is a common epigenetic regulation occurring on cytosine residues of gene regulatory regions called CpG islands. While methylation of these regions is highly associated with repressed gene signatures, especially in cancer cells, de novo methylation of DNA might be utilized to prevent the reactivation of repressed genes. Similarly, methylation of tumor suppressor promoters and genes that regulate differentiation is widely seen in cancer patients (Baylin & Jones, 2011; Cheng et al., 2019; Jackson et al., 2018).

Methylation has been used as an important biomarker for various cancer types. While studies showed that methylation is correlated with increasing tumor size and stage of breast cancer (Christensen et al., 2010), methylation signature has been utilized to identify subgroups of MB (Northcott et al., 2015).

DNA methylation is catalyzed by enzymes called DNA methyltransferases (DNMT) via transferring methyl group of S-adenosyl-L-methionine (SAM) to cytosine nucleotide as writers for this epigenetic modification (Schubeler, 2015). Overexpression of DNMTs is commonly observed in various cancer types, including CML, breast, pancreatic, and lung cancers, where the increasing level of DNMT expression has been linked to a worse prognosis (Cheng et al., 2019). In contrast, erasers of methylation are Ten-eleven translocation enzymes (TET). TET genes were found frequently mutated in various cancer types (Rasmussen & Helin, 2016). Finally, several proteins have reader domains for DNA methylation, such as methyl-CpG binding domain (MBD), zinc-finger and BTB domain, PHD, and RING finger domains. While specific functions of those domains in various diseases remain to be elucidated, mutations in several DNA methylation readers have been identified (Riccio et al., 1999)

### *1.6.2 Histone Acetylation*

Chromatin consists of nucleosomes where DNA is packaged with octamers of core histone proteins (H2A, H2B, H3, and H4) surrounding ~147-base-pair of DNA. While “closed” chromatin is associated with repressed genes, “open” chromatin is associated with actively transcribed genes. Regulation of gene expression at the histone level is determined by histone code, where histone tails are covalently modified by

epigenetic regulators (Cheng et al., 2019). Histone acetylation is an important epigenetic regulation where specific lysine (K) residues on histone tails are covalently linked with acetyl groups from acetyl-CoA cofactors by Histone acetyltransferases (HATs) and histone deacetylases (HDACs) remove acetyl residues. Histone modifications are important for development and differentiation. Due to decreased positive charge on core histone after acetylation, histone acetylation is mostly an activating marker, however, depending on the histone code, it might have different functions. Differentially expressed HATs are associated with tumorigenesis (Seligson et al., 2009). Similar to DNA methylation, reader domains for histone acetylation are essential. Bromodomain (BRD) are important motifs for the recognition of acetylated lysine residues on specific histone tails, and BRD-containing proteins have been extensively studied in the field of cancer. Moreover, some HATs also have bromodomains such as CBP, PCAF, and GCN5 (Dhalluin et al., 1999)

### *1.6.3 Histone Methylation*

Lysine and Arginine residues on histone tails can be methylated by histone methyltransferases (HMTs) as writers for histone methylation and demethylated by histone demethylases (HDMs). While arginine can be monomethylated or demethylated, lysine residues can also be trimethylated. Unlike histone acetylation, the effect of histone methylation depends on the methylated residue and the histone code. In general, H3K27 and H3K9 methylations are associated with repressed gene expression, and H3K4 and H3K36 methylations are associated with gene activation (Volkel & Angrand, 2007). Histone methylation is associated with transcriptional regulation by influencing chromatin structure and recruitment of key transcriptional factors (Zhao & Shilatifard, 2019)

Aberrant histone methylation has been linked to cancer, especially extensive loss or gain of H2K27me3 or H4K20, and has been linked with deregulated gene expression. Similarly, mutations on histone residues that can be methylated, such as H2K27M, H3K27I, and H3G34R, have been shown to be oncogenic. Several reader motifs for histone methylation have been identified to date, such as chromodomains, Tudor domain, and PHD motif. In general, they play an essential role in interpreting the information through histone methylation. Dysregulation of histone methylation readers has been

linked with aberrant methylation and linked with cancer (Mohammad & Helin, 2017; Park et al., 2022).

### *1.6.4 Histone Phosphorylation*

Similar to acetylation and methylation, histone phosphorylation is a post-translational modification on the tails of core histone protein and has several functions for cellular processes, including chromatin remodeling during cell division and apoptosis and gene expression regulation during DNA damage. The phosphorylation of histones is regulated by kinases and phosphatases. Serine, threonine, and tyrosine residues on the tails of all core histone proteins can be phosphorylated (Shanmugam et al., 2018). Phosphorylation of H2AX is an important event for DNA damage response. It serves as a marker for the recruitment of DNA repair machinery (Rossetto et al., 2012)

Histone phosphorylation has been linked to cancer in specific regulation of gene expression. Extensive phosphorylation of H2BS32p by RSK2 kinase has been seen in skin cancer cells (Lau et al., 2011). H3Y41 phosphorylation by Janus Kinase 2 (JAK2) has been shown to disrupt heterochromatin protein 1α, thus leading to constitutive activation of JAK2 signaling and oncogenesis (Dawson et al., 2009). Aurora kinase B overexpression, which takes part in chromosome segregation by H3 phosphorylation, has been shown in colorectal and breast cancer and associated with poor prognosis and drug resistance, suggesting histone phosphorylation as an important post-translational modification on histones (Zhang et al., 2015).

### *1.6.5 Histone Ubiquitination*

Ubiquitination is a significant post-translational modification that regulates several essential cellular functions. Ubiquitin is a polypeptide that consists of 76 amino acids containing seven lysine residues (K6, K11, K27, K29, K33, K48, and K63). Ubiquitination is initiated by E1 ubiquitin-activating enzymes in an ATP-dependent manner, followed by E2 ubiquitin-conjugating enzymes, followed by E3 ubiquitin ligases (Cockram et al., 2021).

Depending on the linkage of poly-ubiquitin chains, ubiquitination can lead to proteasomal degradation, cell cycle progression regulation, and lysosomal degradation. However, the ubiquitination of histones has distinct functions, which regulate DNA

repair, transcriptional regulation, and genome stability. While H2A ubiquitination has been associated with transcriptional silencing and genome maintenance, H2B monoubiquitination has been associated with transcriptional activation and tumor suppression (Zhu et al., 2007). H2B monoubiquitination maintenance depends on one tumor suppressor cell division cycle 73 (CDC73). Mutations in this protein leads to the failure of ubiquitination of H2B, which has been reported in various cancer types (Hahn et al., 2012).

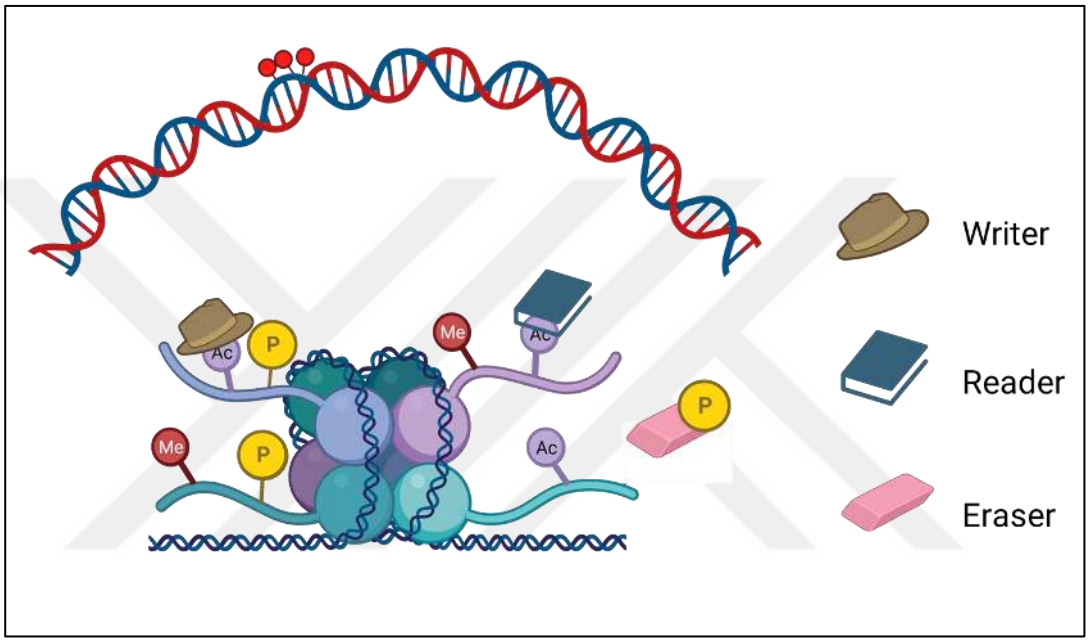


**Figure 1.3: Summary of Epigenetic Regulations.** Epigenetic modifications can influence gene expression in several different ways and contribute to diverse biological processes. The figure illustrates DNA methylation, shown on top, and histone modifications, including methylation, acetylation, and phosphorylation. Epigenetic regulations are carried out by complexes consisting of several proteins, mainly categorized as writers, readers, and erasers. Figure created in biorender.com.

## 1.7 Medulloblastoma and Epigenetics

Advancements in functional genomics have allowed extensive cohort studies to identify several candidate driver genes for specific subgroups of MB. Especially for WNT and SHH subgroups, several driver mutations within respective pathways (SHH, WNT) were identified. However, recent cohort studies for MB indicated the absence of commonly mutated genes in Group 3 and Group 4 MB. This situation may be attributed to the dysregulation of chromatin-modifying genes that disrupt normal differentiation and promote tumorigenesis. Cohort studies estimate that approximately 50% of all MB cases exhibit at least one somatic mutation in chromatin modifiers,

including demethylases, acetyltransferases, and nucleosome remodelers (Batora et al., 2014; Northcott et al., 2017; Robinson et al., 2012; Roussel & Stripay, 2018). The specific roles of several observed mutations in MB are still poorly understood, highlighting the importance of unraveling the mechanisms by which these modifiers operate to provide new therapeutic approaches.

Mutations in the chromatin modifiers can either regulate the main driver genes of a particular MB subgroup or interfere with differentiation pathways, leading to either blockage of normal differentiation or induction of undifferentiated state (Roussel & Stripay, 2018) **(Table 1.3**). Observed mutations from patient data show that most genes are subtype-specific; and also, the majority of identified mutations result in loss of function in tumor suppressor genes. For example, Lysine Methyltransferase 2D, *KMT2D* (*MLL2*) emerges to be the only commonly mutated chromatin modifier among all MB subgroups (Northcott et al., 2017; Robinson et al., 2012; Roussel & Stripay, 2018). *KMT2D'*s methylation activity on H3K4 is crucial for normal brain development and differentiation **(Figure 1.4)**. In most cases, truncated mutations, leading to loss of function, were observed, resulting in truncated proteins, lacking methylation activity (Parsons et al., 2011). Lysine Demethylase 6A, *KDM6A* (*UTX*), also involved in neural differentiation, exhibits loss of function mutations, particularly in Group 3 and Group 4. However, mutations on *KMT2D* and *KDM6A* were mutually exclusive (Batora et al., 2015; Roussel & Stripay, 2018). Loss of function mutations in subunits of the SWI/SNF nucleosome remodeling complex is common in 20% of all cancer types also detected in multiple MB subgroups, including *SMARCA4, ARID1A, ARID2* (Batora et al., 2014; Helming et al., 2014). Additionally, several subgroup-specific somatic mutations have been identified in the aforementioned studies. From those, the loss of function mutations in the SHH subgroup fails to repress GLI proteins, promoting growth in this subtype (Tiberi et al., 2014). In cases where *PTCH1* mutation is present (Gorlin syndrome), loss of function mutation on *GSE1* (Genetic Suppressor element 1), an interacting partner of HDAC2, promotes tumorigenesis while the presenting a WT copy of *GSE1 in vivo* suppresses tumor growth (M. Huang et al., 2019). As previously mentioned, most mutations are patient-specific for Group 3 and Group 4. Loss of function mutation on *KDM6A* is present in both Group 3 and Group 4 subgroups, preventing KDM6A from promoting lineage-specific differentiation

promoting tumorigenesis. Furthermore, *EZH2*, histone-lysine N-methyltransferase, that methylates H3K27 to repress differentiation, has been significantly upregulated in Group 4 patients. Inhibitors for EZH2 are on clinical trials (Robinson et al., 2012; H. Zhang et al., 2020)

**Table 1.3:Mutations and alterations in Epigenetic Regulators in Medulloblastoma**. Differential regulation or mutations on chromatin modifiers have been observed for different subtypes of MB in cohort studies. (1: (Pugh et al., 2012); 2: (Northcott et al., 2017); 3: (Robinson et al., 2012); 4: (Jones et al., 2012); 5: (Yi & Wu, 2018). Table adapted from (Roussel & Stripay, 2018))

| **Gene** | **WNT** | **SHH** | **Group 3** | **Group 4** | Reference |
|---|---|---|---|---|---|
| ARID1A | X | X | X | | 2 |
| ARID2 | X | X | | | 2 |
| BCOR | | X | | X | 2,1 |
| BMI1 | X | X | X | X | 5 |
| CDH1 | X | | | | 3 |
| CHD7 | | | X | X | 2, 3 |
| CBP | X | X | X | | 1 |
| EZH2 | | | X | X | 5 |
| GPS3 | | | X | X | 2 |
| GSE1 | | X | X | | 3 |
| KDM1A | | | | X | 3 |
| KDM3A | | | X | | 3 |
| KDM5A | | | X | X | 3 |
| KDM5B | | | X | | 3 |
| KDM6A | | | X | X | 1, 2, 3,4 |
| KDM7A | | | X | | 3 |
| KMT2C | | X | X | X | 1, 2 |
| KMT2D | X | X | X | X | 1, 2, 3, 4 |
| LDB1 | | X | | | 1 |
| NCOR2 | | X | | | 1 |
| PRDM6 | | | | X | 2 |
| SMARCA4 | X | X | X | X | 1, 2, 3, 4 |
| ZMYM3 | | | | X | 2, 3 |

In addition to mutations in chromatin modifiers, alterations in gene expression might also affect the growth and progression of the disease. A large cohort study reported that DNA methylation patterns of MB patients are similar within subgroups, which can aid in further classification of the cases and in predicting the prognosis of the disease. However, no specific therapeutic approach was proposed (Schwalbe et al., 2017).

HDAC inhibitors have been used for a variety of cancer types. Even though there is no approved drug for MB in this category, it has been shown that, especially in the SHH subgroup of MB, HDAC inhibitors can block GLI activity and inhibit the growth of cancer cells. Also, those inhibitors can target MYC-amplified MB specifically and downregulate *MYC* expression. In this way, growth and proliferation can be inhibited in those cells (Canettieri et al., 2010; Ecker et al., 2015).

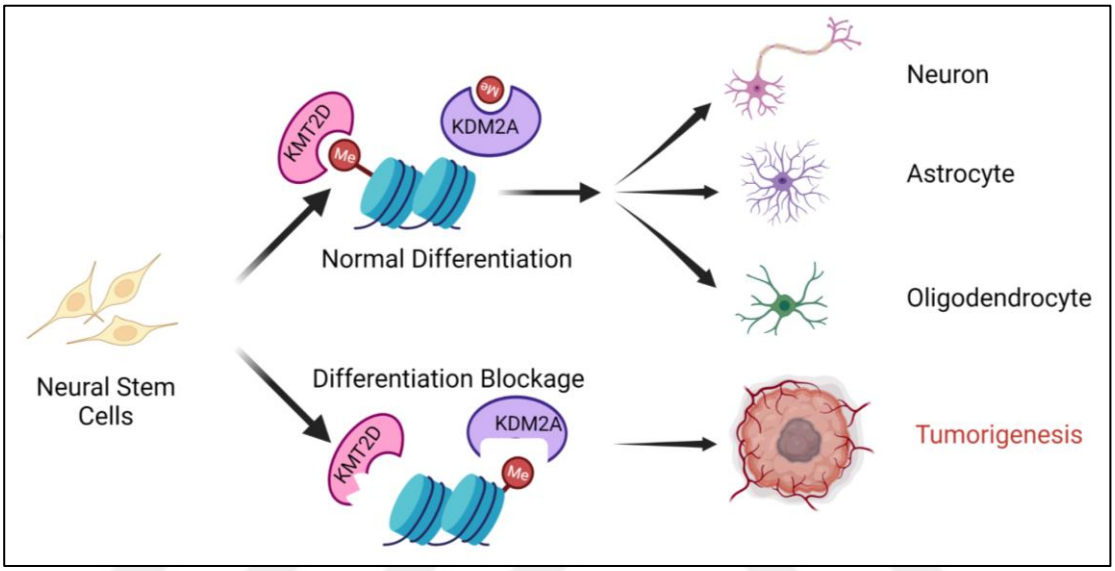


**Figure 1.4: Effect of Epigenetic Regulators on Neural Development.** Epigenetic regulators are crucial in the normal development of Neural Stem Cells into specialized cells such as neurons, astrocytes, and oligodendrocytes. Mutations or abnormalities in the expression in these epigenetic regulators might disrupt the differentiation process, leading to blockage and potentially triggering tumorigenesis. Figure created in biorender.com.

Finally, Bromodomain inhibitors are effective against the SHH subgroup and Group 3 for similar reasons (Zwergel et al., 2018). Bromodomains are present in a wide range of chromatin modifiers and recognize acetyl-lysine and acetylated chromatin, which are presented on active genes, and active enhancers are also marked by those modifications. Bromodomain inhibitors are shown to reduce the expression of *GLI* genes in the SHH subgroup (Tang et al., 2014). They also downregulated *MYC* expression in Group 3 MB (Henssen et al., 2013); animal experiments have further validated their efficacy in MB (Bandopadhayay et al., 2014; Long et al., 2014).

## 1.8 CRISPR/Cas9 and Negative Selection Screens

Several gene editing technologies have been used since the early gene targeting

efforts, with the Clustered Regularly Interspaced Short Palindromic Repeats/ CRISPR associated nuclease 9 (CRISPR/Cas9) system emerging as one of the most successful approach due to its high efficiency, speed, and cost-effectiveness. Originally identified as a bacterial adaptive immune system that stores the genetic material of invading organisms in its own CRISPR motif, when reencountered, the invader triggers the transcribed crRNA (short CRISPR RNA) to recognize the foreign genetic material. The Cas9 nuclease then introduces a double-strand cleavage (Doudna & Charpentier, 2014).

This adaptive immune system has been adapted to function in mammalian cells for gene editing purposes. In this system, a specific locus in the mammalian genome can be targeted by introducing a small guide RNA (sgRNA) along with Cas9 endonuclease. Once the sgRNA recognizes the target locus, Cas9 introduces a double-strand break, prompting the cell to initiate repair mechanisms. Homology Directed Repair (HDR) might be utilized if a template DNA with high homology is available. In the absence of a template, a non-homologous end joining (NHEJ) repair mechanism can be utilized to ligate free ends of the DNA break. Since NHEJ works in an error-prone manner, during repair, it might introduce insertions or deletions (Doudna & Charpentier, 2014; Sharma & Petsalaki, 2018). Over time, several tools have been developed utilizing the CRISPR/Cas9 system for diverse purposes, such as correcting mutations, modulating gene expression levels, RNA targeting, and imaging specific genomic loci (Pickar-Oliver & Gersbach, 2019).

In addition to those applications, CRISPR/Cas9 system has also been employed for genome-wide screens. Various approaches have been developed leveraging the viability of the cells treated with gRNA pools as a factor for positive or negative selection screens. While positive selection screens select for the resistance to induced conditions, negative selection (Dropout) screens are used to identify the essentiality of genes targeted by the depleted sgRNAs (J. Huang et al., 2019; Wei et al., 2019).

In this study, a negative selection screen on MB cells with the CRISPR/Cas9 library was used to identify essential chromatin modifiers for MB and chromatin modifiers that take part in drug resistance. The CRISPR/Cas9 library, Epigenetic Knock-Out Library (EPIKOL), has been generated by the combined effort of research

groups in our institute (O. Yedier-Bayram et al., 2022).

## 1.9 Epigenetic Knock-Out Library (EPIKOL)

EPIKOL is a CRISPR/Cas9-based epigenetic-focused sgRNA pool library consisting of a total of 7870 sgRNAs, targeting 719 chromatin modifier genes (Histone readers, writers, erasers, histone chaperones, and chromatin remodelers **(Figure 1.5)**, 25 context-specific genes, including ABC transporters, nuclear receptors and cancer-related genes regulating apoptosis and metastasis, and 35 general essential genes, and 80 non-targeting sgRNAs. Ten sgRNA per gene was included in the library from previous genome-wide KO libraries.

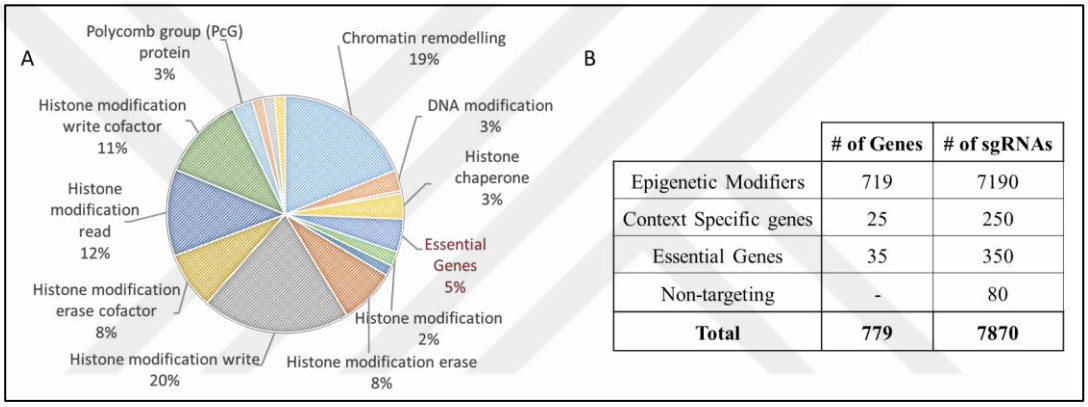


| | # of Genes | # of sgRNAs |
|---|---|---|
| Epigenetic Modifiers | 719 | 7190 |
| Context Specific genes | 25 | 250 |
| Essential Genes | 35 | 350 |
| Non-targeting | - | 80 |
| **Total** | **779** | **7870** |

**Figure 1.5: Composition of EPIKOL.** A. Pie chart of epigenetic modifiers included in EPIKOL. B. Distribution of Gene sets and sgRNAs in EPIKOL.

The main principle of the EPIKOL library is that cells of interest, which express Cas9, will be transduced with pLentiGuide_EPIKOL. With low MOI, each cell is expected to receive at most one infectious particle-carrying vector for one sgRNA. Cells that require the gene product of the sgRNAs target will die, and relevant sgRNAs will be depleted in the population, while sgRNAs that target genes that do not take part in essential pathways for that cell line will remain in the population. At the end of the screen, DNA sequences that code for the sgRNAs will be amplified by Nested-PCR and sequenced to determine depleted sgRNAs by comparing the population at the end of the antibiotic selection to the population at the end screen. It is expected to observe depleted general essential genes while non-targeting sgRNAs should remain similar in both conditions.

## 1.10 CREB binding Protein (CBP) / E1A Binding Protein P300 (p300)

CBP and p300, also known as KAT3A and KAT3B, are histone acetyltransferases that play crucial roles as ubiquitously expressed transcriptional coactivators. While CBP and p300 are highly homologous, with 63 % homology sharing HAT and bromodomains, and many common roles in several cellular mechanisms, including DNA damage response, growth and embryonic development and differentiation, non-overlapping, distinct roles have also been shown (Iyer et al., 2004).

The primary functions of CBP/p300 encompass bridging between gene-specific transcription factors with basal transcription factors, acting as scaffolds due to their large size around the transcriptionally active foci and histone acetylation activity through their HAT domain (Chan & La Thangue, 2001; Vo & Goodman, 2001). While the HAT activity of CBP/p300 has been extensively studied, the roles of the bromodomain are less known. However, bromodomain-acetyl-lysine interaction has been shown to significantly affect HAT function (Hassan et al., 2002). With the utilization of inhibitors such as SGC-CBP30 and I-CBP112, targeting bromodomains of CBP/p300, the importance of bromodomain on CBP/p300 function has been shown, including its interaction with p53 on activation of CDKN1A (Mujtaba et al., 2004). CBP/p300 was also identified as driver mutations in some medulloblastoma subtypes, while overexpression of CBP/p300 has also been reported in various cancer types, including prostate cancer and melanoma (Chen et al., 2022; Merk et al., 2018).

Similarly, the effect of other bromodomains and bromodomain and extra-terminal domain (BET) inhibitors such as BET151 and JQ1 targeting BRD4 were studied in medulloblastoma, especially on SHH and Group 3 MB and shown to prevent interaction of BRD4 with the driver genes of the specific subtypes of MB, inhibiting growth and tumorigenesis (Tang et al., 2014)

## 1.11 Kelch-like ECH-associated protein 1 (KEAP1)

Nuclear factor erythroid 2-related factor 2 (NRF2) serves as the master regulator of antioxidant response in cooperation with small musculoaponeurotic fibrosarcoma (sMaf) proteins through heterodimerization, operating as a transcription factor (Katsuoka et al., 2005; Moi et al., 1994). Since its discovery in 1994, researchers have identified over 250

genes that contain an enhancer sequence named Antioxidant-Response-Element (ARE) within their promoter regulatory regions that are regulated by NRF2. NRF2 targets include members of several different gene families, including antioxidant enzymes (e.g., superoxide dismutase 1 (*SOD1*), catalase (*CAT*), cytochrome P450 (CYPs) genes), phase II detoxification enzymes (e.g., glutathione S-transferases), drug transporters (NQO1, *ABCB6*, *ABCC1*, *ABBC3*), iron homeostasis genes (ferritin), anti-inflammatory genes. Collectively, those play essential roles in the regulation of stress response, particularly under conditions involving electrophiles and reactive oxygen species (ROS) (Cuadrado et al., 2019; Hayes & Dinkova-Kostova, 2014; He, Antonucci, et al., 2020; Wu et al., 2012).

Five years after the discovery of *NRF2*, studies examining differential NRF2 activity identified Kelch-like ECH-associated protein 1 (KEAP1) as the negative regulator of NRF2 (Itoh et al., 1999). Another five years after its discovery, KEAP1's function as a substrate adaptor protein of Cullin 3 (CUL3) dependent E3 ubiquitin ligase complex facilitating 26 S proteasomal degradation of NRF2 via ubiquitination was identified (Cullinan et al., 2004; Wakabayashi et al., 2003; Zhang et al., 2004).

Under physiological conditions, KEAP1 binds to NRF2 and promotes its degradation through ubiquitination, ensuring low concentration and short half-life of NRF2 in the cytoplasm (Kobayashi et al., 2004). However, during stress conditions, such as exposure to ROS or electrophiles, specific cysteine residues on KEAP1 (C151, C226, C273, and C278) undergo oxidation and disrupt KEAP1's function as the adaptor protein. Consequently, NRF2 translocates into the nucleus and initiates an antioxidant response by promoting transcriptional activation of target genes (He, Ru, et al., 2020; Horie et al., 2021) (**Figure 1.6).**

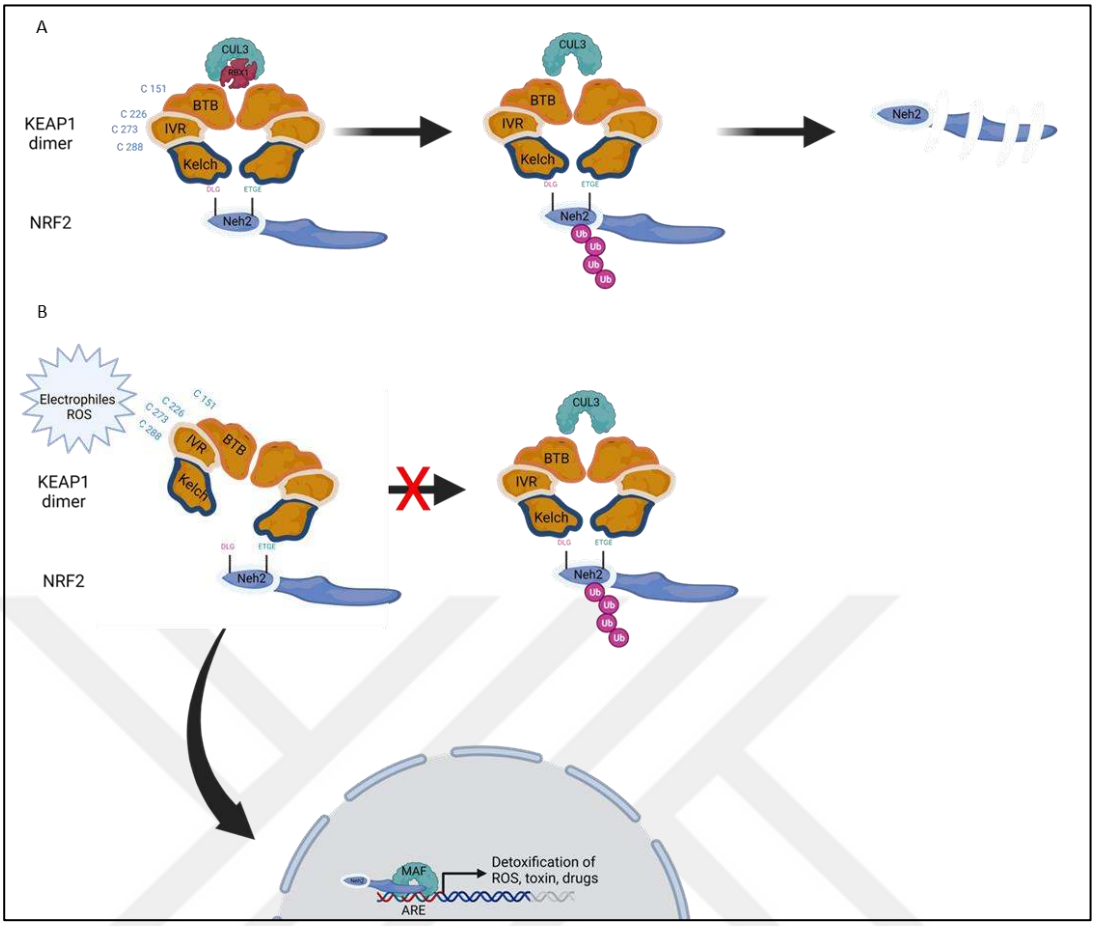


**Figure 1.6: KEAP1 Mechanism of Action.** A. KEAP1 is an adapter protein facilitating correct localization of its target NRF2 for ubiquitination and proteasomal degradation. B. In the presence of electrophiles or ROS, oxidization of cysteine sensors on KEAP1 leads to a conformational change, and NRF2 is translocated into the nucleus, activating downstream targets. Figure created in biorender.com modified from Horie et al, 2021.

The KEAP1 protein comprises three distinct functional domains: The broad complex, tramtrack, bric-a-brac (BTB) domain is located in the N-terminus of the protein and mediates both homodimerization of KEAP1 and its interaction with E3 Ubiquitin ligase CUL3 (Cleasby et al., 2014). On the other hand, the Kelch domain, formed by six repeats, is located in the C-terminus. This domain contains two distinct regions: double glycine repeat (DGR) and C-terminal region (CTR). These regions form the core β-propeller structure, which interacts with the Nrf2-ECH Homology (Neh) 2 domain of NRF2 (Li et al., 2004; Ogura et al., 2010). The intervening region (IVR) domain is in the middle of the BTB and Kelch domains. It surrounds the core β-propeller structure, further contributing to KEAP1-CUL3 interaction, particularly through the proximal 3-box region. Cysteine residues that sense oxidizing conditions are also located in the BTB and IVR domains (He, Ru, et al., 2020) (**Figure 1.7**).

The NRF2 protein has seven conserved Neh domains, each serving distinct functions. Neh1 domain contains a basic leucine zipper (bZip) motif, takes part in DNA binding and heterodimerization with sMaf proteins, and plays an essential role in downstream activation. The Neh2 domain of NRF2 possesses two essential binding motifs for KEAP1, namely DLG, and ETGE, and seven lysine residues, which are the targets of ubiquitination (Tonelli et al., 2018). While the KEAP1 homodimer shows low affinity towards the DLG motif, it binds to the ETGE motif with high affinity (Cuadrado et al., 2019; Horie et al., 2021; Tong et al., 2006). Interestingly, disruption of DLG motif – Kelch domain interaction prevents degradation of NRF2 even when the ETGE motif still remains bound to the Kelch domain, which suggests that weak binding of DLG motif might be susceptible to perturbations caused by conformational change resulting from oxidation of Cysteine residues (Yamamoto et al., 2008).

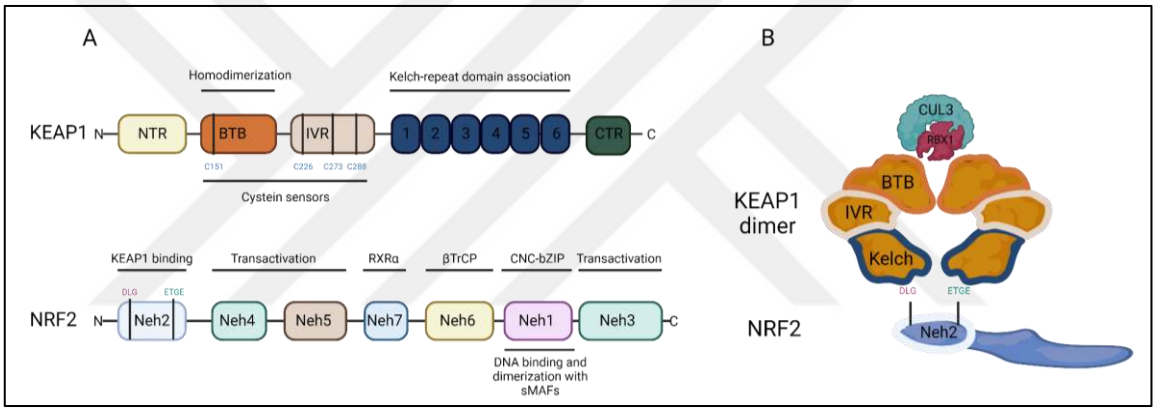


**Figure 1.7: Structure and Domains of KEAP1 and NRF2.** A. KEAP1 consists of BTB, IVR, and Kelch-repeat domains, NRF2 has several Neh domains with distinct functionality, where ETGE and DLG motifs of NRF2 interacts with Kelch-repeat domains of the KEAP1 dimer. B. Interaction of NRF2 with KEAP1-CUL3-RBX1 E3 ligase protein complex. Figure created in biorender.com.

## 1.12 Validated Substrates of KEAP1

KEAP1 has been identified as the negative regulator of NRF2 function under physiological conditions. KEAP1's Kelch domain interacts with ETGE and DLG motifs of NRF2's Neh2 domain, promoting proteasomal degradation of NRF2 via ubiquitination, as described above. However, recent studies showed that NRF2 is not the sole target of KEAP1. Several noncanonical substrates of KEAP1 that possess ETGE (-like) or DLG (-like) motifs were shown (Y. Zhang et al., 2020). While the precise function of these newly identified KEAP1 substrates in the KEAP1-NRF2 axis is still being investigated, proteins such as p62 (SQSTM1) and Nestin (NES) were found to bind to

KEAP1 along with NRF2 competitively. Interestingly, both SQSTM1 and NES are NRF2 downstream targets. Their interaction with KEAP1 stabilizes NRF2 and facilitates its translocation to the nucleus, activating a positive feedback loop (Wang et al., 2019) (**Figure 1.8**).

| Substrate | Biological Process | KEAP1 binding motif | Affinity |
|---|---|---|---|
| AMER1 | Wnt signaling | ETGE | - |
| DPP3 | Proteolysis | ETGE | $K_d$ = 661 ± 87 nM |
| NES | Neural development | ESGE | - |
| FAM129B | Wnt signaling | ETGE | - |
| iASPP | Apoptosis | QDDLT | - |
| IKBKB | IKK/NF-κB signaling | ETGE | - |
| MCM3 | DNA replication inhibitor | ETGE | - |
| NFE2L1 | Cell Redox homeostasis | QDIDLG | - |
| | | ETGE | - |
| NFE2L2 | Cell Redox homeostasis | QDIDLG | $K_a$ =1-2 x $10^6$ $M^{-1}$ |
| | | ETGE | $K_a$ =1-2 x $10^8$ $M^{-1}$ |
| PALB2 | Homologous Recombination Repair | ETGE | - |
| PGAM5 | Mitophagy, Necroptosis | ESGE | - |
| SQSTM1 | Autophagy | STGE | p62 $K_a$ = 3-5 x $10^7$ $M^{-1}$ |
| | | | p-P62 $K_a$ = 8.5 x $10^6$ $M^{-1}$ |
| PTMA | Histone exchange, apoptosis | ENGE | $K_a$ = 0.38 x $10^6$ $M^{-1}$ |

**Figure 1.8: Validated Substrates of KEAP1. Substrates interacting with KEAP1 with DLG-like motif and ETGE-like motif.**

### *1.12.1 p62/SQSTM1*

p62/SQSTM1 is a stress-inducible multifunctional protein that takes part in various cellular processes, including selective autophagy, a process by which selected cargoes, such as protein aggregates or damaged proteins in this case, is recognized by p62 and delivered to proteasomal degradation machinery. Similar to other autophagy receptor proteins, p62 has ubiquitin-binding-domain (UBD) and Microtubule-associated protein 1A/1B-light chain 3 (LC3) interacting region (LIR) (Katsuragi et al., 2016). L3 is an important protein for the formation of autophagosomes and the transportation of damaged protein cargo via the microtubule network. p62 interacts with KEAP1 on ETGE(-like) motif, KEAP1-interacting region (KIR). Especially under stress conditions, Serine 349 residue of p62 on KIR increases its affinity to KEAP1 and facilitates NRF2 stabilization and activation of NRF2-dependent antioxidant response mechanism in a noncanonical way. A splicing variant of the p62 protein lacking the KIR domain was identified, which

has the reverse effect of full-length p62. Since it lacks the KIR domain but is still positively regulated by NRF2, with the increased expression of KIR lacking variant, increased ubiquitination of NRF2 has been observed (Kageyama et al., 2018). KEAP1 is also a substrate of p62-mediated autophagy, and aggregation of KEAP1 in an insoluble fraction of autophagy-deficient mice has been reported. Accumulation of p62 has been detected in several disorders, mainly in neurodegenerative diseases and hepatocellular carcinoma (Komatsu et al., 2010).

### *1.12.2 NESTIN*

Nestin is a class IV intermediate filament protein expressed extensively in neural progenitor cells and tumor cells, while its expression is downregulated in differentiated cells (Bernal & Arranz, 2018). Especially on SHH-type medulloblastomas, Nestin is upregulated and shown to interact with SHH transcription factor Gli3, further promoting tumorigenesis (Li et al., 2016). Downregulation of Nestin on neural progenitors has been associated with increased sensitivity to ROS (Sahlgren et al., 2006). Additionally, studies on gastric cancer cell lines showed that the downregulation of Nestin leads to decreased antioxidant enzyme levels, reduced cell viability, and increased apoptosis (Lv et al., 2021).

Unlike p62, Nestin possesses both DLG and ETGE(-like) motifs in the C-terminal region of the protein. The interaction between KEAP1 and Nestin has been found to amplify NRF2 activation, particularly in the context of antioxidant response (Liu et al., 2022). While the precise functional implications of KEAP1-DLG interaction remain to be elucidated, the presence of missense mutation or deletion of ETGE(-like) motif of Nestin disables its function to prevent degradation of NRF2 by occupying the NRF2 binding domain of KEAP1 (Wang et al., 2019).

### *1.12.3 BPTF*

While the direct role of KEAP1 on the regulation of transcriptional regulation via epigenetics is not known, previous studies showed that KEAP1 interacts with Nucleosome Remodeling Factor Subunit, Bromodomain PHD Finger Transcription Factor (BPTF) via yeast two-hybrid screen (Strachan et al., 2004). While BPTF protein is predominantly found in the nucleus, especially on developing or degenerative neurons, localization of BPTF on cytoplasm has been shown. Like other KEAP1 substrates, BPTF

was shown to bind the Kelch domain of KEAP1 protein (Mu et al., 1997; Schoonover et al., 1996).

### 1.13 Aim of the Study

The main goal of this study was to uncover novel chromatin modifiers that drive acquired multi-drug resistance in medulloblastoma. Cohort studies have revealed that several mutated chromatin modifiers are present in multiple subgroups of MB. However, their underlying mechanism remained largely unexplored. Additionally, the impact of WT chromatin modifiers on MB driver genes and drug resistance has not been studied thoroughly. We have established three specific aims for our research to address these gaps.

Firstly, by application of an epigenetic probe library to both parental and drug-resistant MB cells, we validated the effect of inhibition of candidate chromatin modifiers on drug resistance,

Secondly, we performed CRISPR-Cas9-based, epigenome-focused EPIKOL screens on parental cell lines to identify essential chromatin modifiers for MB survival.

Thirdly, by utilizing the EPIKOL screen in the presence and absence of vincristine on drug-resistant MB cell lines, we identified the chromatin modifiers that can be targeted to overcome acquired drug resistance in medulloblastoma.

# 2 MATERIALS AND METHODS

## 2.1 Cell Culture

Human Medulloblastoma cell line Daoy MED (ATCC, HTB-186), Vincristine resistant variants (V1-10, V2-8), and human embryonic kidney cell line 293T (ATCC, CRL-3216) were maintained in DMEM, supplemented with 10% FBS (Biowest/France) and 1% Pen/Strep (Biowest/France), at 37°C and 5% $CO_2$ incubator. Cells were grown in 10 cm or 15 cm petri dishes. Cells were passaged, or medium replenished every 3-4 days, depending on the confluency.

## 2.2 Chemicals and Reagents

Vincristine was purchased from Cayman Chemicals (#11764) and prepared as a main stock solution of 5 mM in DMSO. For cell culture experiments, intermediary stocks of 200 µM intermediary stocks were used for cell culture experiments. ML385 (S8790), Carnosic Acid (S3838), and Nifurtimox (S6459) were purchased from (Selleck Chemicals, United States).

The Bmi1-overexpression plasmid was a gift from Sally Temple (Addgene plasmid # 21577)

## 2.3 Cell Viability Assays

For cell viability assays, 1.5 x $10^3$ cells per well were seeded in triplicates into black 96 well plates for each condition. The next day, cells were treated with respective dilutions of drugs in 200 µl of DMEM. 200 µl of PBS was added to surrounding wells to prevent evaporation. The 72-hour incubation period after the addition of vincristine was used for all cell viability assays.

### *2.3.1 Cell Titer Glo Luminescent Cell Viability Assay*

Cell Titer Glo (CTG) Luminescent Cell Viability assay (Promega, USA) is based on the measurement of ATP molecules from lysed cells, which are then utilized by luciferase enzyme to generate luminescence. Quantification of the Luminescence signal is proportional to the metabolically active cells present in the sample (Gilbert et al., 2011).

After the completion of the incubation period with vincristine, the medium was removed. Cells were incubated with a mixture of 40 µl CTG reagent and 4 µL medium for 10 minutes on the shaker. After incubation, cell rupture was confirmed under a microscope, and luminescence was read from each well by a microplate reader (Synergy H1 Reader, Bio-Tek, USA). Results were analyzed by GraphPad Prism software.

### *2.3.2 MTT Assay*

MTT assay consists of the reduction of soluble tetrazolium salt (3-(4,5-dimethylthiazol-2-yl)-2,5-diphenyl-2H-tetrazolium bromide) by mitochondrial enzymes in metabolically active cells, resulting the formation of insoluble formazan crystals. Measurement of insoluble formazan crystals provides a reliable calorimetric assessment of cell viability (Ghasemi et al., 2021)

3 mg/ml MTT in PBS was prepared for 1/4 of the volume of the initial media in each well of 96-well plates. After 72 hours of incubation, MTT solution was added to each well, and plates were incubated in 37 °C and 5% $CO_2$ incubator for four hours. Afterward, the formation of formazan salt was confirmed under a microscope, and absorbance (570 nm) was read from each well by a microplate reader (Synergy H1 Reader, Biotek, USA).

## 2.4 Establishment of Vincristine-Resistant Cell Lines

Vincristine-resistant cell lines were previously established by Tolga Lokumcu via the dose escalation method (Lokumcu, 2017). Parental Daoy cells were initially treated with 1 nM or 2 nM of vincristine, and then the drug dose was increased gradually through eight months. Ultimately, vincristine-resistant V1-10 (Vincristine 1 nM to 10 nM) and V2-8 (Vincristine 2 nM to 8 nM) cell lines were established. Vincristine-resistant cells showed up to 100-fold resistance to vincristine compared to parental Daoy cells (**Figure 2.1**).

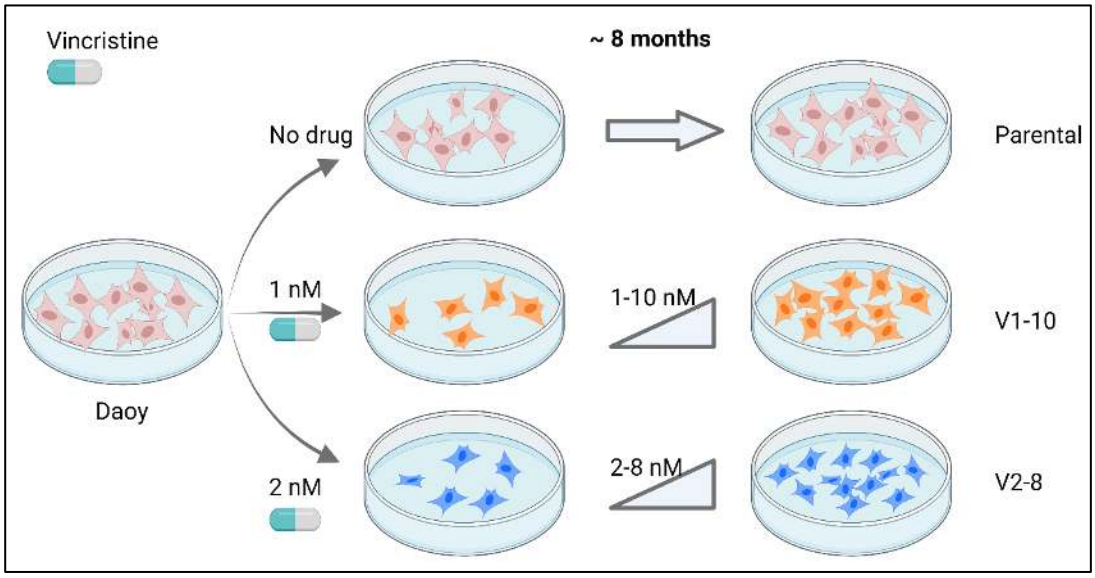


**Figure 2.1: Generation of vincristine resistant cell lines.** Parental Daoy cells were treated with increasing doses of vincristine through 8 months, resulting in V1-10 and V2-8 vincristine-resistant cell lines. Figure created in biorender.com.

## 2.5 Viral Packaging

Lentiviral packaging was used for the transduction of EPIKOL, Cas9, GFP, and sgRNAs. For lentivirus production, 2.5 x $10^6$ 293T cells were seeded per 10 cm petri dish. The next day, 2500 ng of transfer vector was mixed with 2250 ng of psPAX2 and 250 ng of VSVG plasmids in 200 µL serum-free DMEM. Then, this solution was mixed with 200 µL serum-free DMEM containing 15 µL Fugene 6 (Roche, USA). The mixture was incubated for 25 minutes at room temperature and then added to each 10 cm petri dish drop by drop. The medium was replenished after 16 hours, and the lentivirus-containing medium was collected on the 48$^{th}$ and 72$^{nd}$ hours after transfection. Then, to concentrate infectious particles, the collected medium was centrifuged at 1500 rpm, and the supernatant was filtered through 45 µM filters into 1/5$^{th}$ of the initial medium volume of PEG 8000 (P2139, Sigma, USA). The next day, the virus-containing medium was centrifuged at 2500 rpm for 20 minutes at +4 °C. Pellets were dissolved in 1/100$^{th}$ of the collected medium and aliquoted in small amounts for further experiments.

## 2.6 Lentiviral titer calculation

To determine the viral titer, cells were seeded at a density of 1 x $10^5$ cells per well in a six-well plate. The following day, the wells were treated with 1 x $10^0$, 1 x $10^{-1}$, 1 x

$10^{-2,}$ or 1 x $10^{-3}$ µl virus-containing medium supplemented with 8 µg/ml protamine sulfate. Additional wells were used as parental and antibiotic controls.

Subsequently, uninfected cells were selected with relevant antibiotics on the transfer vector's backbone. The cells were trypsinized and counted once the selection process was completed in the antibiotic control well. This cell count was used to calculate the concentration of infection particles per milliliter in the viral stock solution.

## 2.7 Determination of Cas9 Activity

To approximate the time required for achieving knock-out activity in more than 80% of the cells, initially, cells were transduced with plenti-Cas9 with Blasticidin selection at MOI of 1.0. Once the antibiotic selection was completed, cells were further transduced with hGFP using a low MOI of 0.3, following the EPIKOL screening strategy.

Subsequently, stable Cas9 and hGFP-expressing cells were transduced with either pLentiGuide_T1 (sgRNA targeting GFP) or plentiGuide_NT1 (non-targeting control sgRNA) and subjected to puromycin selection.

Starting from the selection day, cells were trypsinized every three days, and 1/10$^{th}$ of the cell suspension was analyzed on flow cytometry for GFP+ cells percentage in the population compared to NT1 transduced cells. Cas9 activity was considered complete when the rate of GFP+ cells in the population fell below 20% and remained stable in subsequent measurements.

## 2.8 Determination of Doubling Time

During the EPIKOL screen, doubling time was measured to determine when 14 doubling that has elapsed after the completion of Cas9 activity, marking the completion of the screen. The doubling time was calculated using **Equation 2.1**, where the logarithm of the number of cells collected after trypsinization was divided by the logarithm of the number of cells initially seeded and then normalized by 3.32 ($\log_2 10$). The cumulative doubling time was obtained by summing all the previously calculated doubling times.

$$PD = 3.32 (\log_2 (\text{Collected Cell Count}) - \log_2 (\text{Seeded Cell count})) \quad (2.1)$$

## 2.9 Determination of representation of sgRNAs in EPIKOL

To examine the representation of sgRNAs in EPIKOL, 24 x $10^6$ Daoy cells were seeded in 10 cm plates in 2 x $10^6$ per plate density. The next day, Daoy cells were transduced with previously packaged EPIKOL in pLentiGuide backbone viruses transduced with low MOI and 1000X representation. Following puromycin selection, 8 x $10^6$ cells were collected and further processed, as described below.

## 2.10 EPIKOL Screening Strategy

For all EPIKOL screens, 3 x 24 x $10^6$ cells (3 sets, ~800 target genes, 1000X representation) were transduced with MOI:0.3. Parental Daoy cells were transduced with EPIKOL as described above, similar to the representation assay. After puromycin selection, 8 x $10^6$ cells were collected for gDNA isolation to serve as initial representation reference and called AP (After Puro). Following puromycin selection, cells were passaged, and 8 x $10^6$ cells were seeded per group after every passage. After completion of previously determined Cas9 activity (~12 days after transduction), parental Daoy cells were divided into three groups, as shown in **Table 2.1**. The first group was defined as "essentiality" and treated with the equal DMSO used for drug-treated groups throughout the screen. The second group was named "low dose," treated with 1.25 nM of Vincristine throughout the screen. The third group was defined as "high dose" and treated with 5 nM of vincristine once after completion of Cas9 activity. After three days of Vincristine treatment, the remaining cells were cultured without Vincristine. At the end of the screen, 8 x $10^6$ cells per set per group were collected for gDNA isolation.

**Table 2.1: Treatment groups used for EPIKOL screen on parental Daoy cells.**

| Treatment Groups | Code | Treatment | Genomic DNA Collection Time |
|---|---|---|---|
| After-Puro | AP | - | Collected after Puromycin selection |
| End-Point | EP | DMSO | 14 PD after Cas9 activity |
| Low-Dose | LD | 1.25 nM | 14 PD after Cas9 activity |
| High-Dose | HD | 5 nM | At the same time, LD |

Vincristine-resistant cells were transduced with EPIKOL similarly. After Cas9 activity (~12 days), cells were divided into treatment groups, as shown in **Table 2.2** and **Table 2.3** for V2-8 and V1-10 cells, respectively.

**Table 2.2: Treatment groups used for EPIKOL screen on V2-8 cells.**

| V2-8 Groups | Code | Treatment | Genomic DNA Collection Time |
|---|---|---|---|
| After-Puro | AP | - | Collected after Puromycin selection |
| Endpoint | EP | DMSO | 14 PD after Cas9 activity |
| Maintenance | M | 8 nM | 14 PD after Cas9 activity |
| Low-Dose-1 | 20nM | 20 nM | 14 PD after Cas9 activity |
| Low-Dose-2 | 50nM | 50 nM | 14 PD after Cas9 activity |
| High Dose | HD | 200 nM | At the same time, with 50nM |

**Table 2.3: Treatment groups used for EPIKOL screen on V1-10 cells.**

| V1-10 Groups | Code | Treatment | Genomic DNA Collection Time |
|---|---|---|---|
| After-Puro | AP | - | Collected after Puromycin selection |
| Endpoint | EP | DMSO | 14 PD after Cas9 activity |
| Maintenance | M | 10 nM | 14 PD after Cas9 activity |
| Low-Dose-1 | 25 nM | 25 nM | 14 PD after Cas9 activity |
| Low-Dose-2 | 100 nM | 100 nM | 14 PD after Cas9 activity |
| High Dose | HD | 200 nM | At the same time, with 100nM |

## 2.11 gDNA Isolation and Nested PCR

MN Nucleospin Tissue kit (Macharey-Nagel, Germany) was used for gDNA isolation from collected samples according to the manufacturer's instructions for a high number of cells. Phusion High-Fidelity DNA Polymerase kit (NEB, USA) was used for PCR reactions, according to the manufacturer's instructions. Nested PCR was performed in two rounds. For External PCR, the DNA sequence containing sgRNA was amplified with 250X coverage (13.2 µg, assuming 6.6 pg gDNA per cell). Primers, including NGS (Illumina) adapters and index, read primer sequences, were used for internal PCR. For this step, 5 µl from the combined external PCR round was used as a template for each reaction. External and internal PCR were run in the same settings, as shown in **Table 2.4**.

**Table 2.4: Nested PCR conditions**

| External PCR | Internal PCR | Step | Temperature (˚C) | Time (min) |
|---|---|---|---|---|
| 1x | 1x | Initial Denaturation | 95 | 3:00 |
| 17x | 23x | Denaturation | 95 | 0:25 |
| | | Annealing | 65 | 0:20 |
| | | Elongation | 72 | 0:15 |
| 1x | 1x | Final Extension | 72 | 3:00 |

PCR products were run on 2% agarose gel. Bands around 350 bp were isolated with MN Nucleospin Gel and PCR Clean-up kit (Macherey-Nagel, Germany) according to the manufacturer's instructions. The isolated PCR product was then run on Fragment Analyzer (Agilent, USA) at KUTTAM, Koç University Hospital, Turkey, to confirm PCR product length further. Then, 25 nM PCR product, calculated according to the results obtained from Fragment Analyzer, was sequenced via NGS at GENEWIZ (NJ, USA), targeting greater than 10 million reads/sample.

### 2.12 Analysis of Screen results with MaGeCK

Bioinformatic analysis of the EPIKOL library was done via the MAGeCK (v.0.5.8) algorithm by Ali Cenk Aksu, Ph.D., and Ayşe Derya Cavga, Ph.D. (Li et al., 2014). Three biological replicates of paired-end fastq files obtained from NGS were introduced to the algorithm and normalized to the library size. For sgRNA count analysis, replicates were used as individual input files, while for gene-level analysis, median normalization was used for downstream analysis. $Log_2$ values of sgRNA counts were obtained from Read per Million (RPM) normalization (Breslow et al., 2018; Sanson et al., 2018). $p<0.05$ cut-off value was used to identify depleted genes for each treatment group. sgRNA density plot and PCA analysis were obtained as the output of MaGeCK analysis. CDPs were plotted with the seaborn package on Python, using normalized count values. sgRNA distribution, gene-level waterfall, and LFC / -log(p-value) graphs were plotted on GraphPad software, utilizing MAGeCK output.

### 2.13 Cloning of sgRNAs for validation of selected hits

Two sgRNAs from selected genes and reverse complementary sequences from EPIKOL were ordered with appropriate overhangs compatible with restriction enzyme BsmBI (5': CACCG, 3':CAAA) (Macrogen, South Korea) as listed in **Table 2.5**

First, 10 µl reaction containing 1 µl of top and bottom oligos, 1 µl of T4 ligase buffer with ATP, and 0.5 µl of T4 Polynucleotide Kinase were incubated at 37 ˚C for 30 minutes, 95 ˚C for 5 minutes then ramped down to 25 ˚C (5 ˚C/min).

In the meantime, 2 µg LentiGuide-Puro backbone (#52963, Addgene) was digested with BsmBI for two hours at 55 ˚C, then run on 1% agarose gel. The upper band was extracted using MN Nucleospin Gel and PCR Clean-up kit (Macherey-Nagel, Germany)

after a 2 kb lower band was confirmed on the gel. 1 µg of 1/200 diluted annealed oligos were mixed with 50 µg of digested LentiGuide-Puro backbone and 1 µl T4 ligase in 10 µl total volume. Then, the mixture was incubated at 16 ˚C for 16 hours.

5 µl of ligation product was incubated with 50 µl competent bacteria (Stbl3 *E. coli*) for 15 minutes on ice, then bacteria were heat shocked at 42 ˚C for 30 seconds and transferred back to ice. Next, bacteria were grown at 37 ˚C, 225 rpm for one hour after adding 150 µl of LB without antibiotics. Then, 100 µl of bacteria were spread on Carbenicillin plates. Plates were incubated at 37 ˚C for 16 hours, then single colonies were picked and cultured in LB containing 100 µg/ml Carbenicillin, and bacteria were grown at 37 ˚C, 225 rpm for 16 hours. In the morning, bacteria were centrifuged at 4 ˚C, 2500 rpm for 30 minutes. The supernatant was discarded, and ligated plasmids were isolated via MN mini-prep (Macherey Nagel, Germany). The inserted sgRNA sequence was confirmed via sequencing (Macrogen, EU), and then the protocol described in **2.5** was followed for lentivirus making.

**Table 2.5: Cloned sgRNA Sequences**

| | Forward Oligo (5'-3') | Reverse Oligo (5'-3') |
|---|---|---|
| ABCB1-g1 | CACCGATTGACAGCTATTCGAAGAG | AAACCTCTTCGAATAGCTGTCAATC |
| ABCB1-g2 | CACCGCTAGGTGATATCAATGATAC | AAACGTATCATTGATATCACCTAGC |
| CBP-g1 | CACCGAGCGGCTCTAGTATCAACCC | AAACGGGTTGATACTAGAGCCGCTC |
| CSNK2A1-g1 | CACCGCTAGTTGGTGAGGATAGCCA | AAACTGGCTATCCTCACCAACTAGC |
| CSNK2A1-g2 | CACCGGAACTGACCTGACATCATAT | AAACATATGATGTCAGGTCAGTTCC |
| CSNK2A1-g3 | CACCGGGTAGTCATCTTGATTTCTG | AAACCAGAAATCAAGATGACTACCC |
| KEAP1-g1 | CACCGAGCGTGCCCCGTAACCGCAT | AAACATGCGGTTACGGGGCACGCTC |
| KEAP1-g2 | CACCGCAGCACCGTTCATGACGTGG | AAACCCACGTCATGAACGGTGCTGC |
| KEAP1-g3 | CACCGCCTGGAGGATCATACCAAGC | AAACGCTTGGTATGATCCTCCAGGC |
| KEAP1-g4 | CACCGGCAATGAACACCATCCGAAG | AAACCTTCGGATGGTGTTCATTGCC |
| RPL11-g1 | CACCGCTCACCTTTGGAAAACACAG | AAACCTGTGTTTTCCAAAGGTGAGC |
| RPL11-g2 | CACCGGGATGCGAAGTTCCCGCATG | AAACCATGCGGGAACTTCGCATCCC |
| RPL12-g1 | CACCGGATAACGTACCAGACCCAGG | AAACCCTGGGTCTGGTACGTTATCC |
| RPL12-g2 | CACCGGGATAACGTACCAGACCCAG | AAACCTGGGTCTGGTACGTTATCCC |
| RPL9-g1 | CACCGAGGGCTTCCGTTACAAGATG | AAACCATCTTGTAACGGAAGCCCTC |
| RPL9-g2 | CACCGATGACTACAAATAGTCCGAA | AAACTTCGGACTATTTGTAGTCATC |
| BMI-g1 | CACCGAACGTGTATTGTTCGTTACC | AAACGGTAACGAACAATACACGTTC |
| BMI-g2 | CACCGGATTGATGTCATGTATGAGG | AAACCCTCATACATGACATCAATCC |
| BMI-g3 | CACCGTCCTACCTTATATTCAGTAG | AAACCTACTGAATATAAGGTAGGAC |
| KAT5-g1 | CACCGTCCGCCGCAGCACGGGTAGG | AAACCCTACCCGTGCTGCGGCGGAC |

| | | |
|---|---|---|
| KAT5-g2 | CACCGTGAGACTACGGCCGTACTTG | AAACCAAGTACGGCCGTAGTCTCAC |
| ASH2L | CACCGCCATGACTCACCTCACTATG | AAACCATAGTGAGGTGAGTCATGGC |
| RBBP4 | CACCGTCTTGGAACCCAAATCTCAG | AAACCTGAGATTTGGGTTCCAAGAC |
| PPP4C | CACCGCGATCAGGATAGCGAACCTG | AAACCAGGTTCGCTATCCTGATCGC |
| BRPF1 | CACCGCGACGTGACGTTTGCAGTGA | AAACTCACTGCAAACGTCACGTCGC |
| KAT6B | CACCGTGGCTGTTACAGACCCCACT | AAACAGTGGGGTCTGTAACAGCCAC |
| SUP16H | CACCGCCCATCCTCCTTTACAGCGA | AAACTCGCTGTAAAGGAGGATGGGC |
| YEATS4 | CACCGAGCTATGGCAATCCTTTAAG | AAACCTTAAAGGATTGCCATAGCTC |
| VPS72 | CACCGCATAAGAAGCGGAAGTGCCC | AAACGGGCACTTCCGCTTCTTATGC |
| TOP2A | CACCGATTCAGTACCAAATTTACTG | AAACCAGTAAATTTGGTACTGAATC |
| SFPQ | CACCGATGATCGTGGAAGATCTACA | AAACTGTAGATCTTCCACGATCATC |
| KAT7 | CACCGAGAGCCAAACGATACTCCGC | AAACGCGGAGTATCGTTTGGCTCTC |
| FBL | CACCGACCAACGATGTCAGAGACAT | AAACATGTCTCTGACATCGTTGGTC |
| TRRAP | CACCGCCACTGGGGATCGTTCAGTG | AAACCACTGAACGATCCCCAGTGGC |
| RUVBL1 | CACCGGTGAACAAGTACATCGACCA | AAACTGGTCGATGTACTTGTTCACC |
| HCF | CACCGAGCCACTTACTTATTTCCGA | AAACTCGGAAATAAGTAAGTGGCTC |

## 2.14 Dual color competition assay

To quantitatively validate the effect of selected genes as sensitizers on drug-resistant cells, nuclei of cells were labeled with either PGK-H2BmCherry (Addgene #21217) or PGK-H2BeGFP (Addgene #21210) viruses at high MOI. 4 x $10^4$ labeled, cas9-stable cells were seeded in 12 well-plates. The next day, mChery-expressing cells were transduced with LentiGuide-NT1, while eGFP-expressing cells were transduced with sgRNA targeting selected genes in the EPIKOL library. After overnight incubation, media were changed, and puromycin selection was applied the next day. Following three days of selection, NT1-mCherry cells were mixed with sgRNA-eGFP expressing cells in a 1:1 ratio and re-seeded into 24-well plates in triplicates. The next day, cells with GFP signal were quantified with Citation5 (BioTek, USA). Cells were passaged when they reached 80% confluency. The GFP signal was measured in intervals. Results were normalized to day 0 measurement.

## 2.15 Long-term clonogenic assay

Long-term clonogenic assay was performed to evaluate the impact of target gene downregulation on relative cell fitness and colony formation ability. This assay has been utilized for hits identified from essentiality and low-dose drug screens.

For hits from essentiality screens, cells were transduced with sgRNAs targeting

selected genes, after completion of puromycin selection, a total of 10 x $10^3$ cells per well were seeded in triplicates in 6-well plates. The cells were incubated until visible colony formation was observed in control wells transduced with the NT1 vector.

For hits from low-dose drug screens, two rows of triplicates were seeded in 6-well plates. The same protocol was followed to test candidate hits from low-dose drug screens. Three days post-seeding on 6-well plates, cells on the bottom row were treated with low-dose vincristine for three days, followed by media replenishment and further incubation until visible colony formation was established in the NT1 transduced wells.

To measure colony area/total area ratio, once colony formation was completed, cells were washed with PBS once and then fixed with ice-cold 100% methanol for 5 minutes. After another wash with PBS, the cells were stained with crystal violet for 15 minutes. Subsequently, the excess crystal violet was washed vigorously. The plates were dried overnight and then imaged against a white background to increase contrast with the purple color. The intensity of the purple signal was determined by ColonyArea ImageJ-plugin and normalized to the control group.

### 2.16 RT-qPCR

RNA extraction was done via the NucleoSpin RNA isolation kit (Macherey Nagel, Germany) according to the manufacturer's instructions. Total RNA was quantified on NanoDrop 2000 (Thermo Scientific, USA). For cDNA synthesis, 1000 ng of total RNA, 1 µl of random hexamers (N8080127, Invitrogen, United States), and 2.5 µl of 2 mM dNTP (R0192, Thermo Scientific, United States) were mixed in 16.5 µl final volume and incubated at 65˚C for 5 minutes for RNA melt procedure, then transferred to ice. A mixture of 5 µl of 5x First Strand buffer (18057, Invitrogen, United States), 2 µl of 0.1 M DTT (18057, Invitrogen, United States), and 0.5 µl of RNAsin (N2111, Promega, United States) were added to the tubes. The solution was incubated in RT for 10 minutes. Then, 1 µl of M-MLV Reverse Transcriptase (18080044, Invitrogen, USA) was added to the solution, and the Reverse transcription protocol was run as shown in **Table 2.6**: Reverse Transcription Conditions. Following the reaction, 75 µl Nuclease-free water was added to the cDNA solution.

**Table 2.6: Reverse Transcription Conditions.**

| Step | Temperature | Time (min) |
|---|---|---|
| Reverse Transcription | 37 ˚C | 60:00 |
| Heat Inactivation | 95 ˚C | 15:00 |

Following cDNA synthesis, for each well of RT-qPCR reaction, 10 µl of SYBR-Green Master Mix, 1 µl of 10 µM primer mix (including both Forward and Reverse primers), 2 µl of diluted cDNA and 8 µl of Nuclease-free water was used. RT-qPCR reaction was run on Lightcycler 480 Instrument II (Roche, Switzerland) with the conditions shown in **Table 2.7**: RT-qPCR Conditions. $2^{(-ddcT)}$ method was used for calculations. GAPDH was used as the housekeeping gene. Primers used for RT-qPCR reactions are shown in **Table 2.8.**

**Table 2.7: RT-qPCR Conditions.**

| Cycle | Step | Temperature | Time (min) |
|---|---|---|---|
| 1 | Initial Denaturation | 95 ˚C | 5:00 |
| 40 | Denaturation | 95 ˚C | 0:30 |
| | Annealing | 60 ˚C | 0:30 |
| | Elongation | 72 ˚C | 0:30 |
| 1 | Melt Curve | 95-55 ˚C | 2.2 °C / min |

**Table 2.8: RT-qPCR primer sequences.**

| Transcript | Forward Primer (5'-3') | Reverse Primer (5'-3') |
|---|---|---|
| ABCA4 | TCGGGAACAGTCCCACGGAA | TTGAACACCCTTCACCGCCAA |
| ABCB1 | ACAGAGGGGATGGTCAGTGT | TCACGGCCATAGCGAATGTT |
| BMI1 | GGTACTTCATTGATGCCACAACC | CTGGTCTTGTGAACTTGGACATC |
| CBP | AGCAGCAGCTGGTTCTACTG | GGAGGCAAACAGGACAGTCA |
| GAPDH | AGCCACATCGCTCAGACAC | GCCCAATACGACCAAATCC |
| KAT5 | GGAACTCACCACATTGCCTGTC | CTCATTGCCTGGAGGATGTCGT |
| KEAP1 | CAACTTCGCTGAGCAGATTGGC | TGATGAGGGTCACCAGTTGGCA |
| NRF2 | TCCATTCCTGAGTTACAGTGTCT | TGGCTTCTGGACTTGGAACC |

## 2.17 Western Blot

Cells were seeded in 10 cm plates in 1 x $10^6$ cell/plate density on PT day 6. When they reached 80% confluency, cells were collected via trypsinization and centrifuged at 1500 rpm for 5 minutes. Then, the pellets were washed with PBS, centrifuged again, and

stored at -80 ˚C. For whole-cell protein isolation, cells were dissolved in lysis buffer based on NP-40 (1% NP-40, 150 mM NaCl, 1mM EDTA, 50 mM Tris-HCl (pH 7.8), 1 mM NaF, 1 mM PMSF, and 1X protease inhibitor cocktail (Complete Protease Inhibitor Cocktail Tablets, Roche) and incubated on ice for 30 minutes. Then, the suspension was centrifuged at 14,000 rpm for 10 minutes at 4 ˚C, and protein-containing supernatant was used for further experiments. Protein concentration was determined via the BCA protein Assay Kit (Thermo Scientific, USA) according to the manufacturer's instructions. 50 µg protein per sample was mixed with 4X Laemni sample buffer (Biorad, 1610747, USA) containing 1:10 β-mercaptoethanol and incubated at 95 ˚C for 10 minutes for denaturation. Then, samples were taken to ice and loaded to 4-12 % Mini Protean TGX Precast Gel (Biorad, 456-1044, USA). Next, proteins were transferred to the PVDF membrane via the Biorad Trans-Blot Turbo Transfer System (Biorad, USA). Following this step, membranes were stained with Ponceau-S (PS05, EcoTech, Turkey) and washed with TBS-T before the blocking step. Membranes were incubated with 5 % non-fat dry milk in TBS-T for blocking, then membranes were treated with appropriate antibodies as shown in **Table 2.9** overnight on a shaker at 4 ˚C. After 16 hours, membranes were washed thrice with TBS-T then incubated with appropriate secondary antibody for one hour. Following secondary antibody incubation, membranes were washed with TBS-T thrice. SuperSignal West Femto Maximum Sensitivity Substrate (34095, Thermo Scientific, USA) or Pierce ECL (32209, Thermo Scientific, USA) is used for signal detection.

**Table 2.9: Antibody list used in Western Blot Experiments.**

| Antibody Target | Brand, Catalogue Number | Dilution |
|---|---|---|
| GAPDH | Abcam, #ab9485 | 1:2000 |
| KEAP1 | Cell Signaling, D6B12 | 1:2000 |
| PARP | Abcam, #ab74290 | 1:2000 |
| ABCB1 | Cell Signaling, E1Y7S | 1:1000 |
| 2°Anti - Mouse | Abcam, ab97023 | 1:10000 |
| 2° Anti - Rabbit | Abcam, ab97051 | 1:10000 |

### 2.18 Calcein-AM Assay

Calcein-AM is a cell-permanent, non-fluorescent dye that can assess cell viability for eukaryotic cells. While non-fluorescent hydrophobic Calcein-AM is membrane

permeable and rapidly diffuses through the plasma membrane, intracellular esterases hydrolyze Calcein-AM to highly fluorescent anionic calcein, which is retained in the cytoplasm of live cells. As a substrate of ABCB1 (P-gp), Calcein AM is pumped out of the cell in ABCB1 overexpressing cells (Ansbro et al., 2013). This study used the Calcein-AM assay to examine the effect of ABCB1 expression where ABCB1 overexpressing cells pump Calcein-AM out of the cell. In contrast, low expression of ABCB1 is expected to yield increased fluorescence activity. 5 x $10^4$ cells were seeded into each well of 24 well-plate. The next day, cells were treated with 125 nM Calcein-AM and incubated for 30 minutes at 37°C and 5% $CO_2$ incubator. Then, green fluorescence was detected via imaging with Cytation5 (BioTek, USA). Synergy H1 Plate Reader (Biotek, USA) was used to quantify green fluorescence.

## 2.19 Oxidative Stress

3 x $10^5$ cells were seeded in each well of 6-well plates. The next day, cells were treated with subtoxic doses of drugs and incubated for 24 hours. Then, cells were collected via trypsinization, and the medium was removed after centrifugation. Muse® Oxidative Stress Kit (MCH100111, Luminex) was used to determine the percentage of ROS (+) cells in the population according to the manufacturer's instructions. Muse® Cell Analyzer (Luminex, USA) was used for the measurements.

## 2.20 Annexin V apoptosis assay

Annexin V staining was performed with Muse® Annexin V & Dead Cell Kit (Luminex, MCH100105) according to the manufacturer's instructions. Briefly, MDA-MB-231 cells were collected nine days post-transduction and adjusted to 300-500 cells/µl per gene for the measurements. Cells were centrifuged at 1200 rpm for 5 minutes. The supernatant was removed, and the pellet was resuspended in 500 µl of cold PBS with 1% FBS. The cell suspension was centrifuged again, resuspended in 75 µl of cold PBS with 1% FBS, and mixed with 75 µl of Annexin V & Dead Cell Reagent. Samples were incubated at room temperature for 20 minutes and analyzed with Muse Cell Analyzer (Merck, Darmstadt, Germany) with 5000 events per sample. Gates were determined according to parental cells.

### 2.21 Live cell microscopy

Experiments involving live cell microscopy were conducted utilizing Leica DM18 inverted microscope equipped with 10X air objective. Cells were incubated in a chamber at 37˚C and 5% $CO_2$. Time-lapse images were captured per 30 minutes for a total of 32 hours. Cells in each frame were counted and normalized to the initial count using Image J, analyzing at least three randomly selected frames at the time point. Live cell assays were performed by Fidan Şeker-Polat, Ph.D.

### 2.22 Immunofluorescence

For immunofluorescence staining, 2x $10^4$ cells were seeded on coverslips in each well of a 24-well plate. After treatment, cells were washed with PBS and fixed with methanol for 20 minutes. Following fixation, cells were washed with PBS twice, then treated with 0.1% Triton-X-100 containing PBS for 15 min at room temperature, and then washed once more with PBS. Following that, cells were blocked with IF Blocking Solution for 15 min at room temperature, then rinsed with PBS once more.

Slides were incubated with diluted 1° antibody for 1 hour at room temperature, then washed again with PBS twice. Finally, coverslips were incubated with respective 2° antibodies for one hour at room temperature in the dark and mounted with DAPI (Abcam, USA). Imaging was conducted with Zeiss Axio Imager M1 at 40 X magnification.

**Table 2.10: List of antibodies used in immunofluorescence staining.**

| Antibody Target | Brand/ Catalogue Number | Dilution |
|---|---|---|
| α-tubulin | Cell Signaling (DM1A) | 1:10000 |
| Alexa Fluor® 488 Anti-IgG | Invitrogen | 1:500 |

### 2.23 YO-PRO apoptosis assay

To analyze apoptotic cells upon combination treatment, cells were seeded in a density of 5 x $10^4$ cells per well. The next day, cells were treated with a combination of vincristine and 1 µM of SGC-CBP30 for 72 hours. Then, cells were stained with 1 µM of YO-PRO-1 reagent (Invitrogen Cat. No: Y3603, Thermo Fisher) and 1 µg/ml PI for 15 minutes at 37 ˚C in a dark environment. Stained cells were then imaged using Nikon

Eclipse TS100 Inverted Fluorescence Microscope. Image J software was utilized for the quantification of the acquired images. YO-PRO assay was performed by Ezgi Özyerli-Göknar, Ph.D.

### 2.24 ChIP-qPCR

ChIP-qPCR assay was performed to examine the H3K27ac mark and p300 occupation on the promoter of selected ABC and SLC transporters. Cells were collected as a suspension, and then 2 x $10^6$ cells were centrifuged at 1500 rpm for 5 minutes. The pellet was dissolved in 1 % formaldehyde and incubated at room temperature for 10 minutes. Then, the reaction was stopped by incubation in glycine for 5 minutes (final concentration: 0.125 M). The supernatant was removed after centrifugation at 1500 rpm for 5 minutes. The pellet was washed with ice-cold PBS twice.

For lysis, the pellet was dissolved in 100 µl ChIP Lysis buffer (1% SDS, 10 mM EDTA, 50 mM Tris-HCl, protease inhibitors, pH:8.1) and then sonicated with Biorupter. Sonicated samples were centrifuged at top speed for 10 minutes to remove the debris, then the supernatant was 1:10 diluted in ChIP dilution buffer (0.01% SDS, 1.1% Triton-X 100, 1.2 mM EDTA, 16.7 mM Tris-HCl, 167 mM NaCl, pH 8.1). 10% of the diluted sample was used as input control.

Cells were incubated overnight with 5 µg target antibody (Anti-H3K27ac, Anti-p300, or non-specific IgG) at +4°C. 108 µl of protein A/G slurry was added to 900 µl of supernatant and incubated for 2 hours at room temperature. Then, the supernatant was removed, and beads were collected with a magnetic rack. Following this step, beads were washed with Low Salt Buffer (1% Triton-X-100, 2 mM EDTA, 0.1 % SDS, 20 mM Tris-HCL, 140 mM NaCl, pH 8.1), High Salt Buffer ( 1% Triton-X-100, 0.1 % SDS, 2 mM EDTA, 500 mM NaCl, 20 mM, Tris- HCL, pH 8.1), LiCl buffer (0.25 M LiCl, 1% IGEPAL-CA 630, 1% deoxycholic acid, 10 mM Tris, 1mM EDTA, pH 8.1) and Tris-EDTA solution respectively. Finally, elution buffer containing 1% SDS and 0.1 M $NaHCO_3$ was utilized to remove beads. Reverse crosslinking was applied with 0.2 M NaCl overnight at 65°C, and DNA was purified with a Qiagen PCR purification kit according to the manufacturer's instructions. RT-qPCR protocol followed with the designed primers, targeting promoter region. ChIP-qPCR experiments were conducted by Ali Cenk Aksu, Ph.D.

**Table 2.11: List of ChIP-qPCR primers**

| Transcript | Forward Primer (5'-3') | Reverse Primer (5'-3') |
|---|---|---|
| ChIP_ABCA4 | CATCTGAGACGCTGCACTAAC | TCTTCCAGCTACCAAACCCTTC |
| ChIP_ABCC3 | TCTACCTTCCCTCTTGGCGT | CCAGACTGCTACCACAAGGA |
| ChIP_SLC14A1 | GAGGCACTTGGAGGAAGGATG | CCTGCTTGGATGTGCAGATAG |

## 2.25 RNAseq and transcriptome analysis

Total RNA isolation was done via MN Nucleospin RNA isolation kit (Macherey Nagel, Germany) as described above. Library preparation and sequencing were performed at the University of Oxford (Oxford, UK) with Illumina Next Seq 500 sequencer using Next Seq 500/550 High Output kit V2.5. The average read length was 41 bp. Outputs from different Lanes were merged before analysis. MultiQC analysis was applied for Quality Control analysis. Obtained paired-end fastq files were aligned to reference human transcriptome (GRCh38) utilizing the STAR algorithm. The SALMON algorithm was used based on Transcripts per Million (TPM) to quantify transcripts. For the identification of differentially expressed genes, the DeSeq2 algorithm was used. KEAP1-g1 and KEAP1-g2 samples were compared to the NT1 group separately. For the identification of Differentially expressed genes (DEGs), LFC<-1 for downregulated and LFC>1 for upregulated parameters were used. False Discovery Rate (FDR) <0.05 was used for statistical analysis for all cases.

Obtained DEGs were utilized as input for Gene Set Enrichment Analysis (GSEA). A default rank-ordered algorithm was used on GSEA software with all available current gene sets (Subramanian et al., 2007)

## 2.26 Statistical Analysis

All experiments were run as triplicates, and statistical analysis was performed using GraphPad Prism version 7.0. The student's t-test was used to compare two groups, while two-way ANOVA was used to compare more than two groups for parametric variables. * $p<0.05$, ** $p<0.01$, *** $p<0.001$.

# 3 RESULTS

## 3.1 Epigenetic Drug Screen in Medulloblastoma

### *3.1.1 Generation and validation of vincristine-resistant medulloblastoma cell lines*

Vincristine-resistant cell lines were previously established by TBO lab alumnus Tolga Lokumcu, Ph.D., via the dose escalation method. Starting from the IC50 of parental Daoy cells, the vincristine dose was increased slowly through eight months, and the IC50 value of vincristine-treated and age-matching parental cells was monitored throughout the experiment. Established vincristine-resistant cell lines were named according to the initial dose and final dose of the vincristine dose they received (**Figure 3.1 A**). Drug resistance of vincristine-resistant cell lines was further confirmed via CTG assay, and up to ~100-fold resistance against was shown compared to the parental Daoy cell line. A slight decrease in the growth rate of vincristine-resistant cell lines was also observed (**Figure 3.1 B-C).**

To validate the vincristine resistance of V2-8 cells compared to parental Daoy cells, several experiments have been conducted. Firstly, via live-cell imaging, the depletion of parental cells in the presence of vincristine was shown. Similarly, when GFP-expressing V2-8 cells were co-cultured with parental cells, a slight increase in the percentage of parental cells at the end of 72 hours was observed, further validating the slower growth rate of V2-8 cells. However, in the presence of vincristine, dramatic depletion of parental cells was observed **(Figure 3.1 D-E**). Similarly, in the presence of vincristine, disruption of the microtubule network was observed in parental cells, while vincristine-resistant V2-8 cells were unaffected (**Figure 3.1 F**).

Moreover, when both V2-8 cells and Daoy cells were treated with vincristine, it was observed that, while V2-8 cells were not affected by 10 nM of vincristine, late apoptotic cell percentage was significantly increased on Daoy cells (**Figure 3.1 G**) Supporting this finding, low dose vincristine treatment (1 nM) induced PARP cleavage on parental Daoy cells. While V2-8 cells remained unaffected from 1 nM of vincristine treatment, 50 nM of vincristine treatment induced PARP cleavage in those cells.

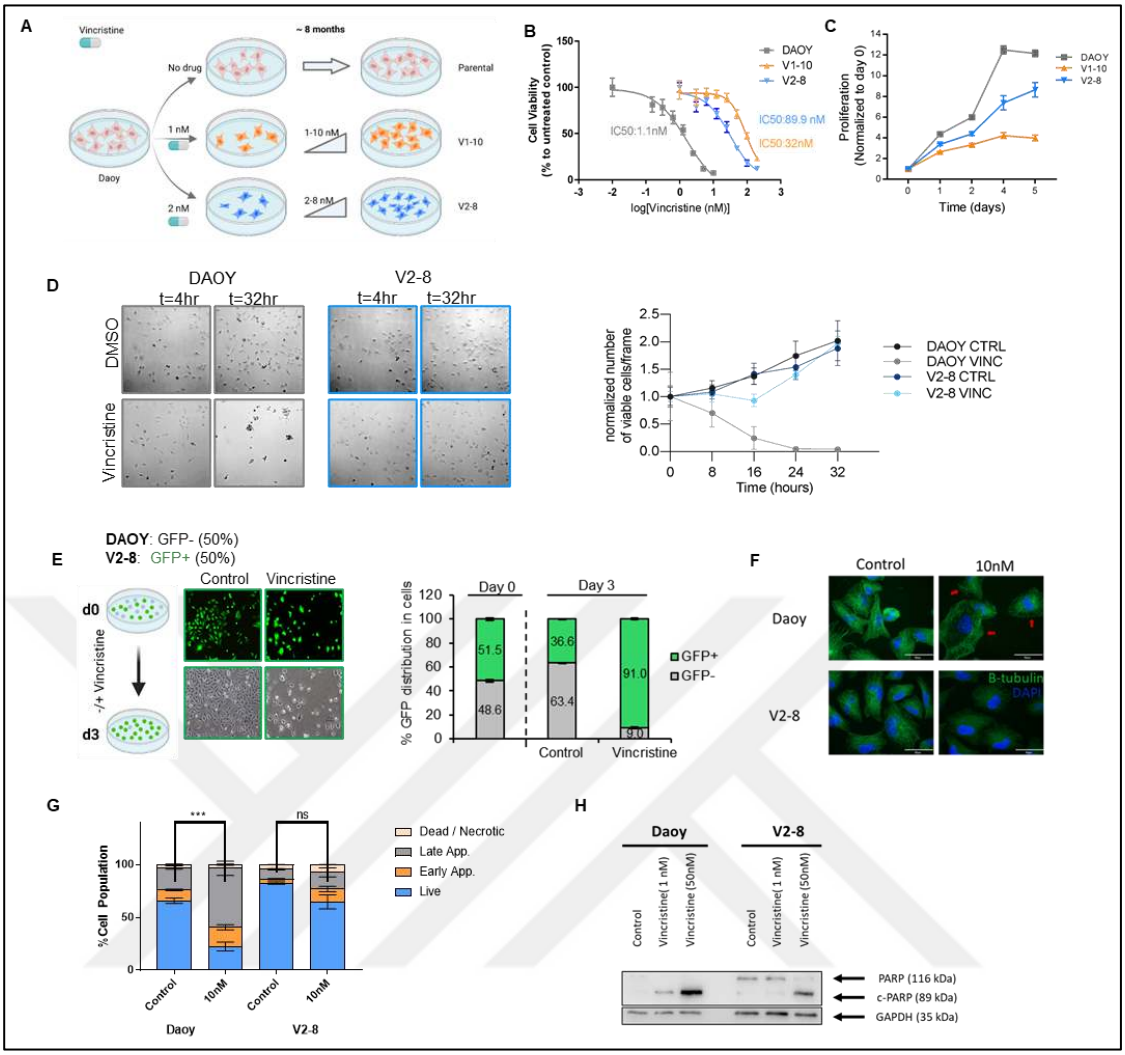


**Figure 3.1: Validation of vincristine resistance on paired cell line model.** A. Generation of V1-10 and V2-8 cell lines via dose escalation method. B. Determination of IC50 values of parental and resistant cell lines. C. Growth curve of parental and vincristine-resistant cells D. Live cell imaging and quantification of Daoy and V2-8 cell lines in the presence and absence of vincristine for 32 hours. E. Competition assay and quantification of co-cultured parental and GFP+ V2-8 cells in the presence and absence of vincristine. F. Immunofluorescence imaging of parental and V2-8 cell line in the presence and absence of Vincristine, stained with β-tubulin antibody and DAPI. G. Annexin V/Dead cell assay in the presence and absence of vincristine. H. Western blot analysis of the parental and V2-8 cells for c-PARP and GAPDH as a loading control (*Karabiyik, Lokumcu, Senbabaoglu, et al., unpublished).*

### *3.1.2 Epigenetic Drug Screen on Parental and Resistant Cell lines*

To identify epigenetic vulnerabilities of parental and vincristine-resistant cells in the presence or absence of vincristine, a chemical probe library consisting of 89 inhibitors targeting epigenetic regulators was utilized by Tolga Lokumcu, Ph.D. Cells were incubated in the presence of vincristine (with their own IC50 value in 96 well plate

setting) or the absence of vincristine (**Figure 3.2 A-C**). While several epigenetic regulators were identified as hits for each screen, bromodomain inhibitors were specifically identified as sensitizers for vincristine resistant V2-8 cell line. Combination of bromodomain inhibitors (SGC-CBP30, I-CBP112, PFI-4, OF-1, NVS-CECR2) with vincristine, significantly decreased cell viability, specifically on the V2-8 cell line (**Figure 3.2 D**).

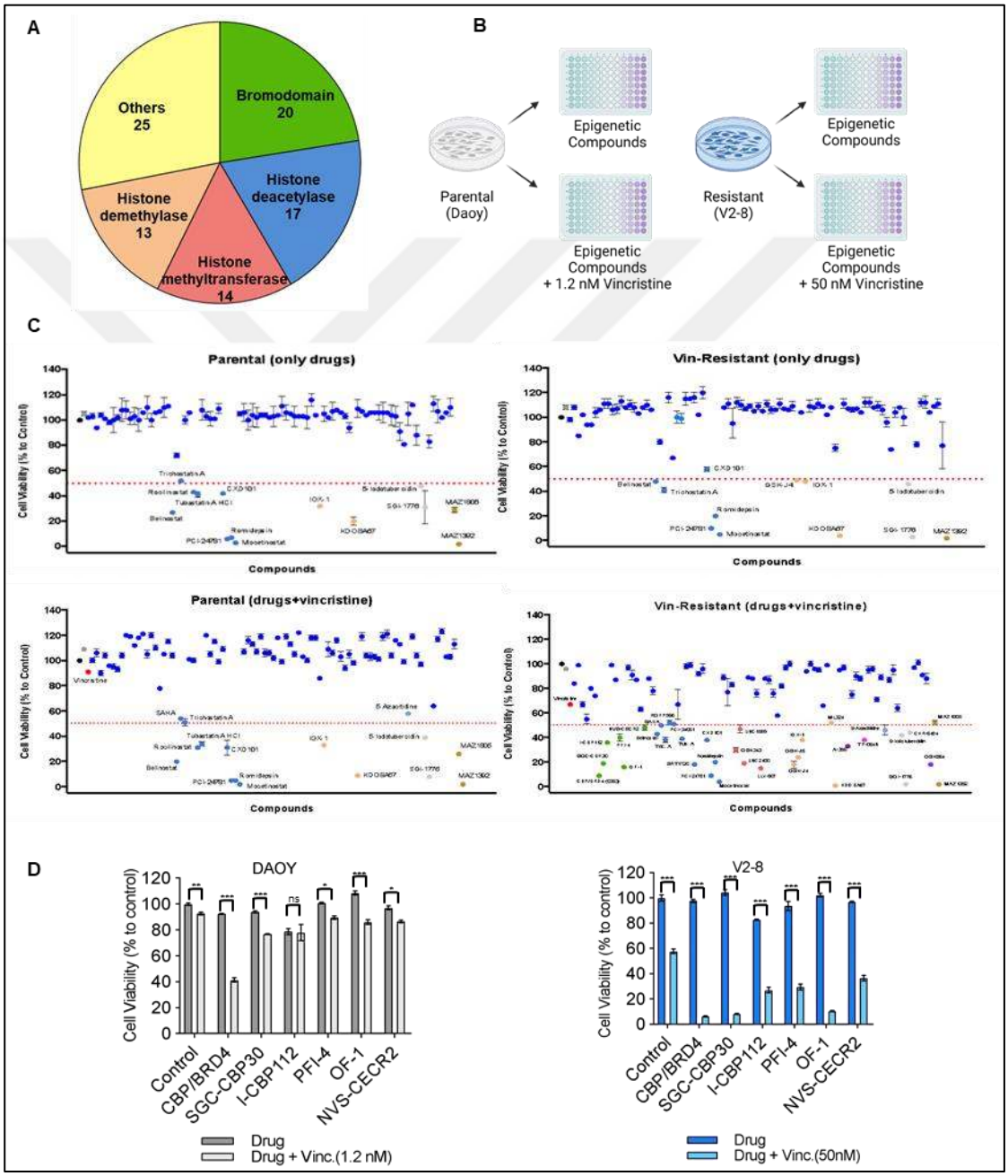


**Figure 3.2: Chemical probe library screen on parental and V2-8 cell lines.** A. Pie chart of the content of the probe library. B. Screening strategy including treatment groups and dosage. C. Screen results normalized to untreated control for each treatment group. (Up: Parental and resistant cell line, epigenetic probe only; Bottom: Parental and resistant

cell lines, in the presence of vincristine.). Color code for hits follow the library content figure. D. Validation of identified Bromodomain inhibitors as sensitizers for V2-8 vincristine resistant cell line (*Karabiyik, Lokumcu, Senbabaoglu, et al., unpublished).*

### *3.1.3 Validation of the sensitizing effect of SGC-CBP30*

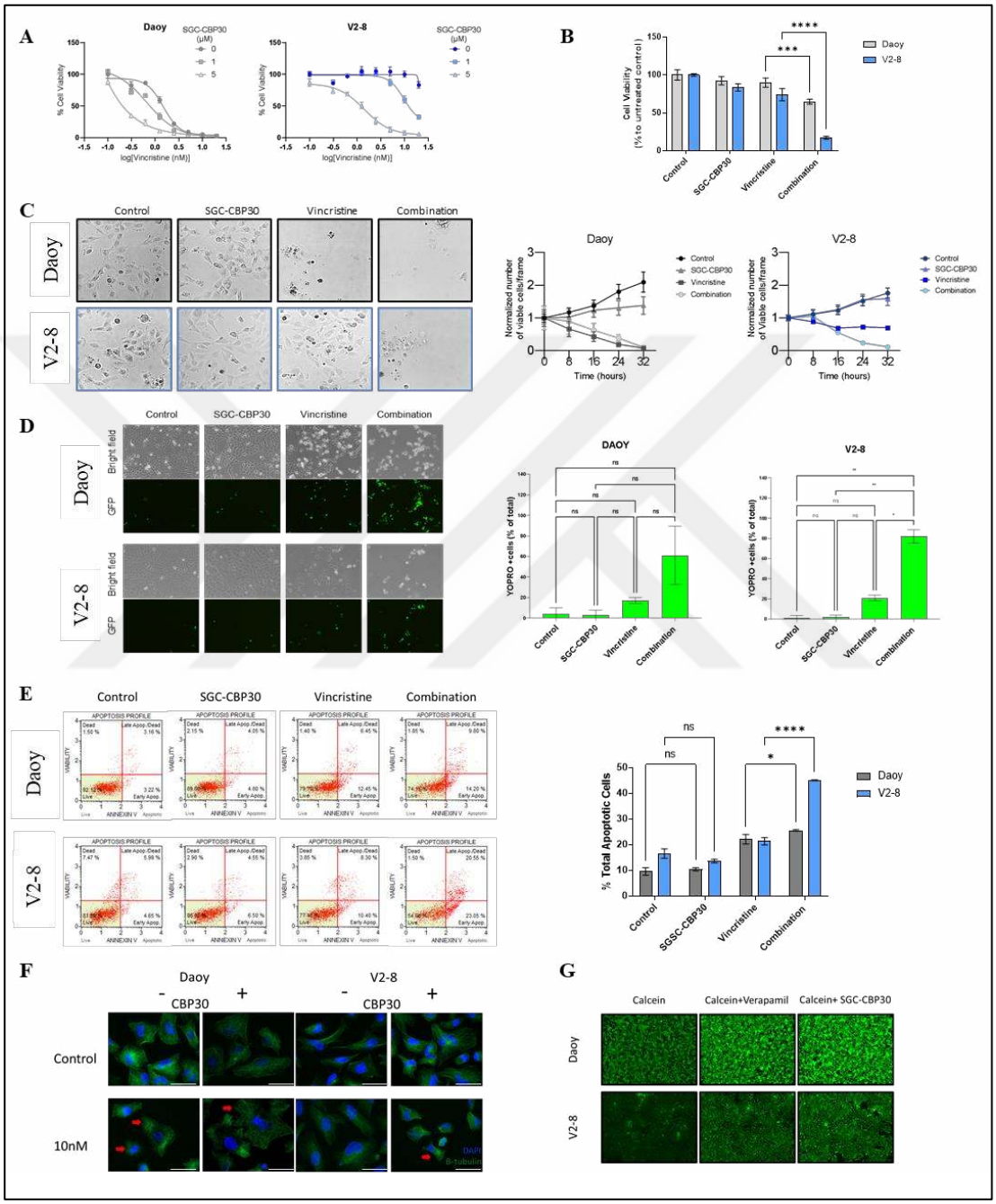


**Figure 3.3. Characterization of the chemo-sensitizing effect of SGC-CBP30.** A. Effect of increasing doses of SGC-CBP30 on parental and resistant cell line for 72 hours of treatment. B. Combination treatment sensitizes V2-8 cells compared to parental cell lines. C. Live-cell imaging of parental and V2-8 cells treated with the combination of SGC-CBP30 and vincristine. D. YO-PRO assay upon combination treatment. E. Annexin V/Dead cell assay upon combination treatment. F. Immunofluorescence imaging on parental and V2-8 cells upon combination treatment, stained with β-tubulin antibody and

DAPI. G. Representative images of Calcein assay on Daoy and V2-8 cells. (*Karabiyik, Lokumcu, Senbabaoglu, et al., unpublished).*

SGC-CBP30, one of the bromodomain inhibitors identified as a sensitizer for the vincristine-resistant V2-8 cell line, was selected for further validation. Increasing doses of SGC-CBP30 were shown to sensitize V2-8 cells further, while incubation with a combination of 1 µM SGC-CBP30 with vincristine was shown to sensitize V2-8 cells significantly (**Figure 3.3 A, B**). Similarly, live-cell imaging showed that SGC-CBP30-treated V2-8 cells are depleted, similar to vincristine-treated parental cells, while only vincristine treatment only did not cause significant depletion in V2-8 cells (**Figure 3.3 C**). YO-PRO assay also confirmed that combination treatment with SGC-CBP30 significantly increased apoptotic cell percentage in V2-8 cells, which was further confirmed with Annexin V/Dead assay in a similar setting (**Figure 3.3 D, E**). Furthermore, disruption of microtubules in the presence of vincristine on V2-8 cells with combination treatment was shown, while vincristine-only treatment did not affect microtubule formation (**Figure 3.3 F**).

### *3.1.4 Transcriptomic Analysis on inhibition of CBP/p300*

Parental and V2-8 cells were treated with 1 µM SGC-CBP30 for 72 hours and then collected for RNA sequencing to examine transcriptomic changes upon chemical inhibition of CBP/p300. PCA showed that, while SGC-CBP30 treated samples were separated on PC2 (Variance-explained: 15%), parental and V2-8 cells were separated on PC1 (Variance-explained: 71%) (**Figure 3.4 A**). Compared to the parental cell line, 423 genes were significantly upregulated on the V2-8 cell line, while 468 genes were downregulated. Upon SGC-CBP30 treatment, mainly downregulation has been observed on both parental and V2-8 cell lines (**Figure 3.4 B, C**). 66 genes were commonly upregulated in V2-8 vs. Daoy comparison and downregulated on V2-8 cells when treated with SGC-CBP30. ABC and SLC family drug transporters, such as *ABCA4*, *ABCC3*, *SLC8A1*, and *SLC4A4,* were also within this identified gene set (**Figure 3.4 D, E**). GSEA showed that the KEGG ABC transporters gene set was one of the top enriched gene sets, while downregulation of ABC transporters has been identified with the treatment of SGC-CBP30 on the V2-8 cell line (**Figure 3.4 F, G**). Upregulation of several ABC transporters was detected on V2-8 cells compared to the parental cell line, and genes such as *ABCC3*, *ABCC4*, *ABCA4*, and *ABCA5* were downregulated to the parental level upon treatment

with SGC-CBP30.

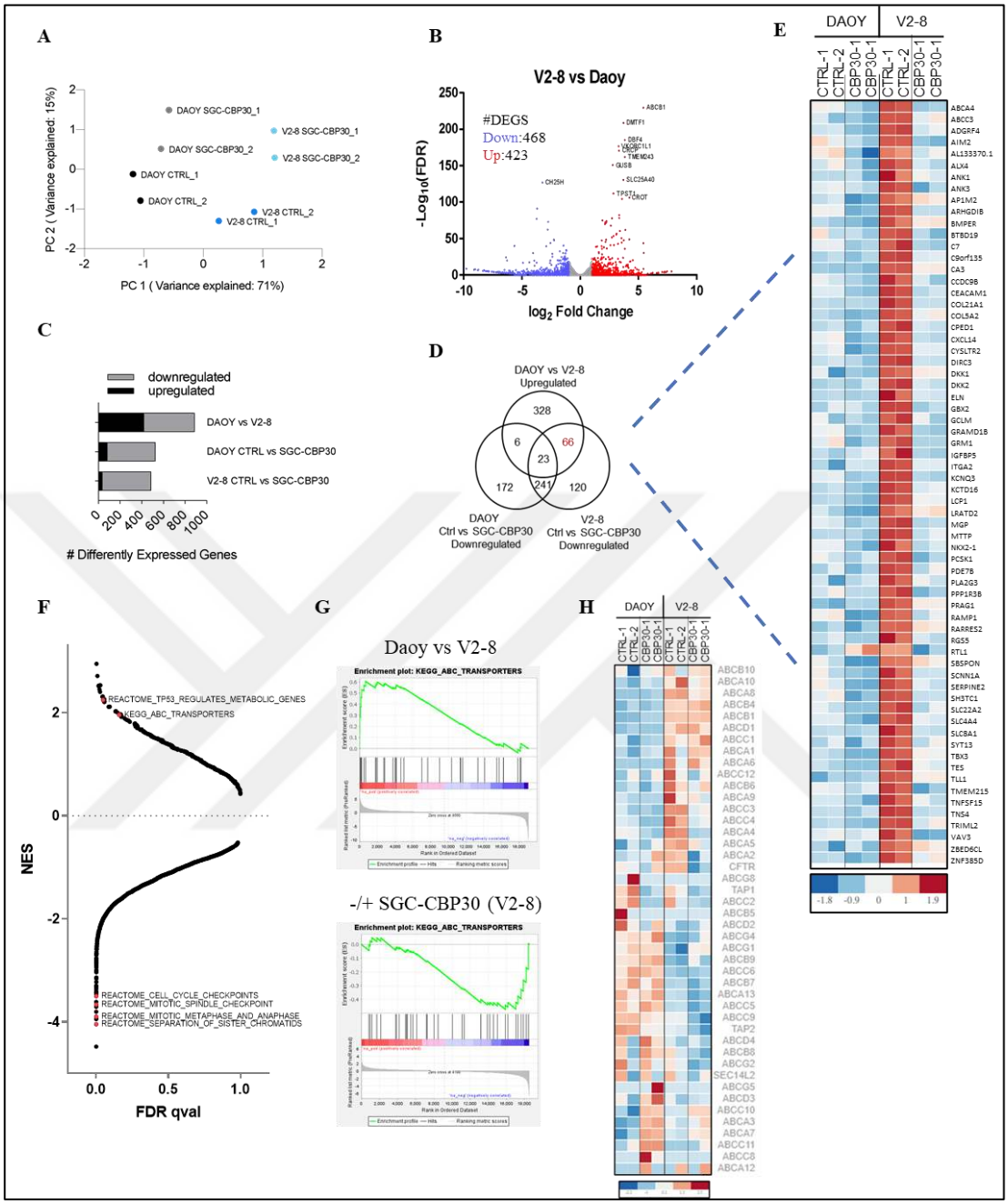


**Figure 3.4. Transcriptome analysis upon inhibition of CBP/p300.** A.PCA on RNAseq results for parental and V2-8 cell line with or without SGC-CBP30 treatment. B. Volcano plot of differentially expressed genes on V2-8 cells compared to parental cell line. C. Number of differentially expressed genes in each comparison. D. Number of genes that were commonly differentially expressed in multiple comparisons. E. Heatmap of 66 genes upregulated in V2-8 compared to Daoy and downregulated upon SGC-CBP30 treatment. F. GSEA analysis showing positively and negatively enriched gene sets on the V2-8 cell line compared to the parental cell line. G. Enrichment plots for KEGG ABC transporters gene set on V2-8 vs. Daoy and V2-8-SGC-CBP30 vs. V2-8 comparison. H. Heatmap of ABC transporters' expression level in each group. (*Karabiyik, Lokumcu, Senbabaoglu, et al., unpublished).*

### *3.1.5 Effect of SGC-CBP30 on regulation of ABCC3 and ABCA4*

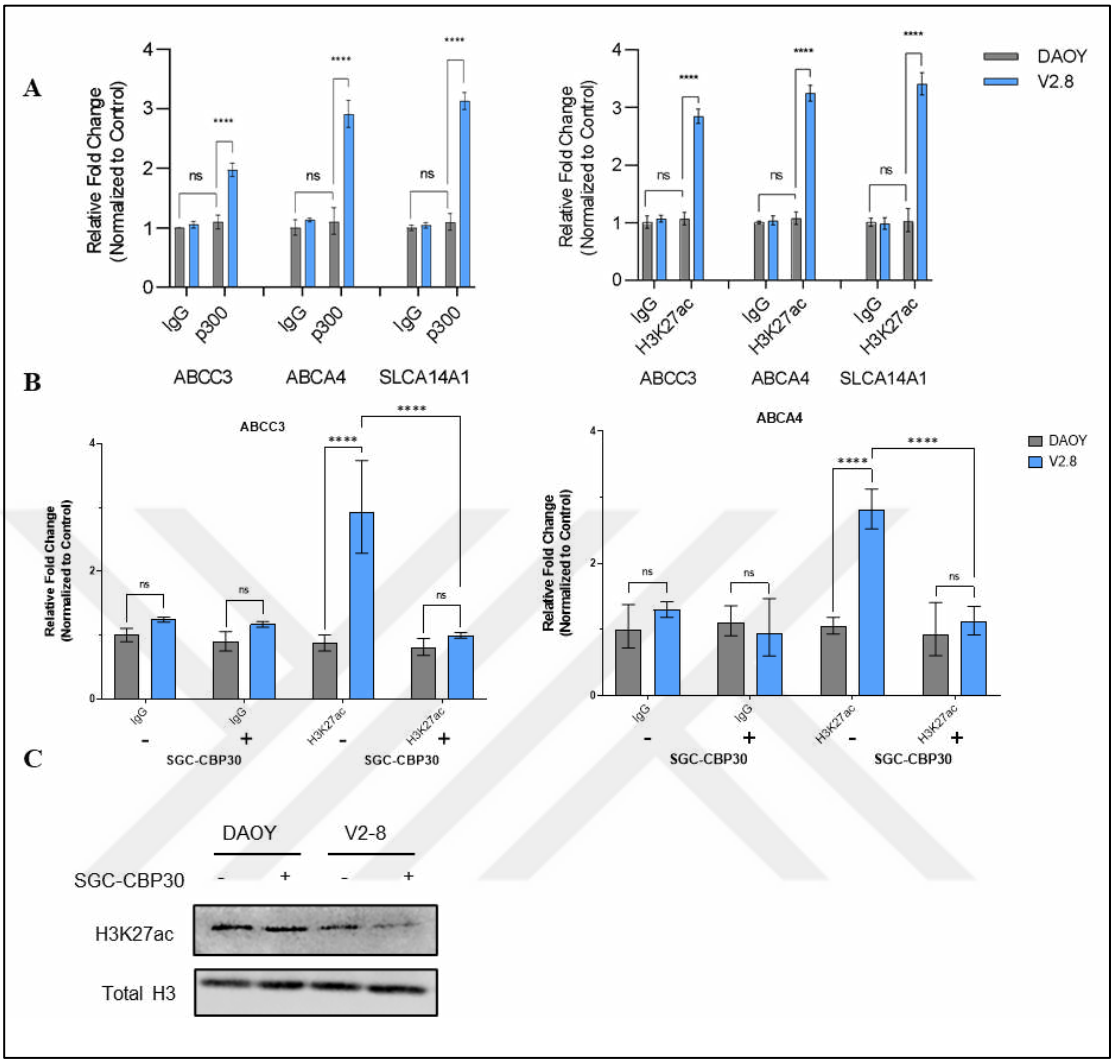


**Figure 3.5. Effect of SGC-CBP30 regulation of H3K27ac mark and p300 occupation on selected promoters.** A. CHIP-qPCR analysis on parental and V2-8 cells with p300 and H3K27ac marks on ABCC3, ABCA4, and SLCA14A1. B. CHIP-qPCR analysis on SGC-CBP30 treated parental and V2-8 cells for H3K27ac mark on ABCC3 and ABCA4. C. Western blot analysis of the parental and V2-8 cells for the H3K27ac mark. H3 was used as a loading control. (*Karabiyik, Lokumcu, Senbabaoglu, et al., unpublished).*

CHIP-qPCR assay on V2-8 cells compared to parental cell lines showed that p300 and H3K27ac occupation on *ABCC3, ABCA4*, and *SLC14A1* promoters significantly increased compared to IgG control on V2-8 cells. The same phenotype was not observed in the parental cell line (**Figure 3.5 A**). Treatment with SGC-CBP30 reversed the deposition of the H3K27ac mark on promoters of two of the ABC transporters, which were identified to be upregulated on V-8 cells and downregulated upon treatment with SGC-CBP30, *ABCC3*, *ABCA4* (**Figure 3.5 B**). In parallel, a decrease

in total H3K27ac acetylation has been observed in V2-8 cells upon drug treatment (**Figure 3.5 C**).

## 3.2 EPIKOL Screen in Parental Medulloblastoma Cell Line

To investigate epigenetic vulnerabilities of medulloblastoma, the Daoy cell line was used by utilizing the CRISPR/Cas9-based sgRNA library EPIKOL. Preliminary experiments were conducted to improve the yield and reliability of EPIKOL screens on medulloblastoma cell lines, as described below.

### *3.2.1 Determination of Cas9 activity on parental Daoy cells*

To examine the efficacy of Cas9, previously Cas9 transduced Daoy cells were further transduced with hGFP vector with low MOI and selected with Hygromycin. Afterward, cells were transduced with non-targeting (NT1) or targeting (T1) pLentiGuide vectors. Every third day after transduction, cells were trypsinized, and GFP percentage was measured with flow cytometry using only Cas9 transduced cells as negative control and hGFP transduced cells as positive control. After PT Day 12, the percentage of GFP-positive cells in the population went under 20 % on cells transduced with the T1 vector compared to NT1 transduced cells. Following PT Day 15, the percentage of GFP-positive cells in the population was stabilized, and PT Day 12 was designated as the completion of Cas9 activity after transduction for further experiments (**Figure 3.6**).

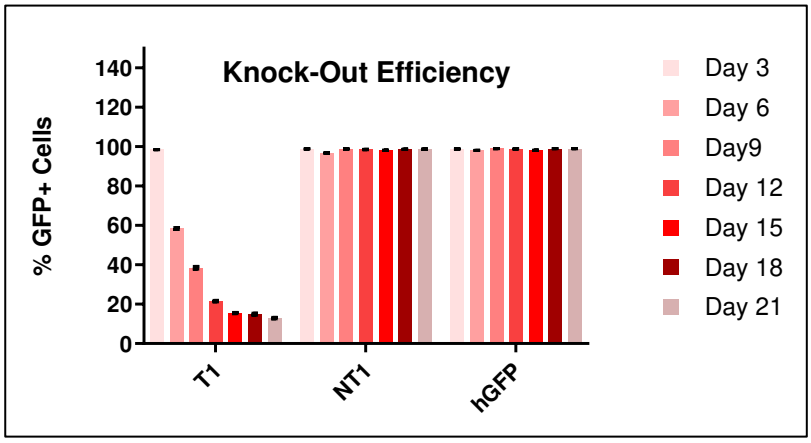


**Figure 3.6: Cas9 Activity of parental Daoy cells.** GFP % of sgT1 transduced cells was measured in the population. Cas9 stable V2-8 cells were used as a negative control, and hGFP cells were used as a positive control for gating.

### *3.2.2 Representation analysis of EPIKOL on parental Daoy cells*

To demonstrate the distribution of sgRNAs on packaged viral vectors, parental Daoy cells were transduced with LentiGuide_EPIKOL vector with low MOI and 1000X representation. Then, cells were collected after antibiotic selection, and the region containing sgRNA was amplified with nested PCR. The PCR product was run on a particle analyzer, and as expected, the average PCR product length was determined to be around 358 bp, as shown in **Figure 3.7**. Following particle analysis, PCR products were sequenced as described. The normal distribution of sgRNAs on the viral vector was demonstrated in **Figure 3.8**.

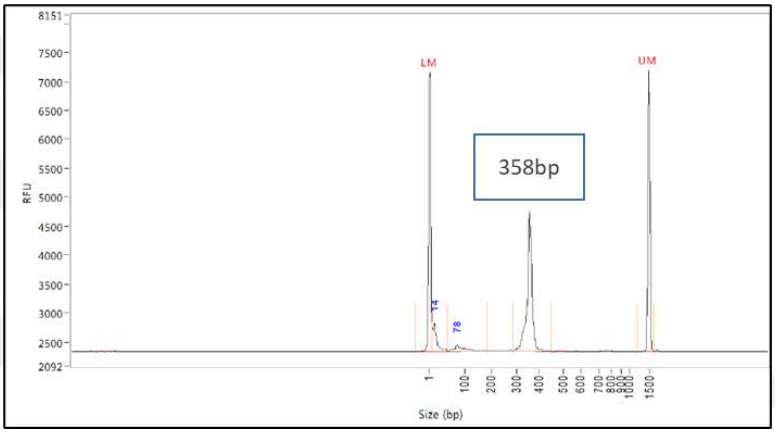


**Figure 3.7: Particle Analyzer results.** Nested PCR products were run on the Particle analyzer. LM: lower marker, UM: Upper marker.

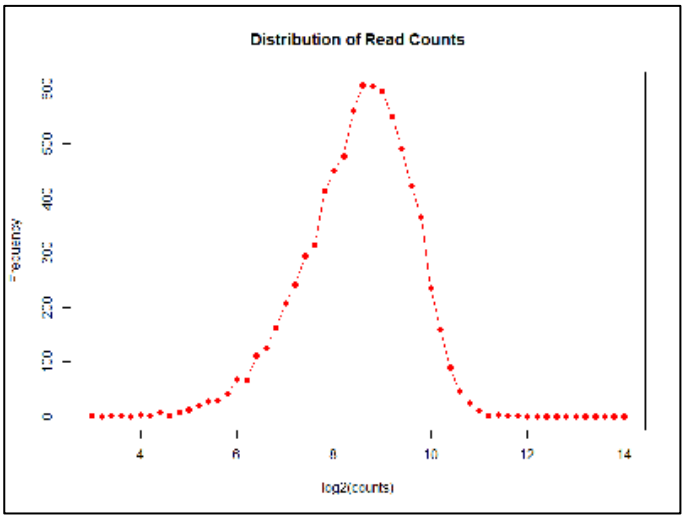


**Figure 3.8: Density plot for sgRNA distribution on Daoy cells transduced with pLentiGuide EPIKOL for representation assay.** Count data were analyzed with the MaGECK algorithm.

### *3.2.3 In vitro EPIKOL screen on parental cell line*

To reveal epigenetic vulnerabilities of medulloblastoma, parental Daoy cells were screened with EPIKOL in triplicates with low MOI to prevent synthetic lethality caused by multiple sgRNA insertions and 1000X representation to prevent bias during screening. After-Puro (AP) samples were collected after puromycin selection, similar to the representation assay (**Figure 3.10**).

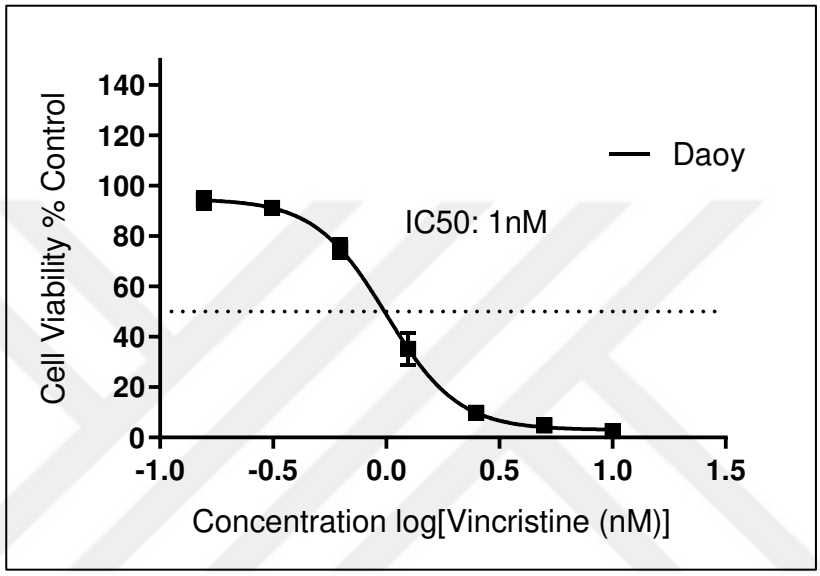


**Figure 3.9: Determination of IC 50 value for parental Daoy Cell line.** IC50 value of Daoy cell line was determined via CTG assay.

After completion of Cas9 activity, cells were separated into End-point (EP), Low-dose (LD), and High-dose (HD) groups and then passaged in the presence or absence of vincristine throughout the screen. A previously determined IC50 value of 1nM of vincristine was used for LD treatment (**Figure 3.9**). A slight lagging on cumulative population doubling was observed in the LD group compared to the EP group (**Figure 3.11**). Cells were collected at the end of the screen after completion of 16 doubling times. After amplification of the region containing the sgRNA coding sequence via nested PCR, PCR products were sequenced with NGS.

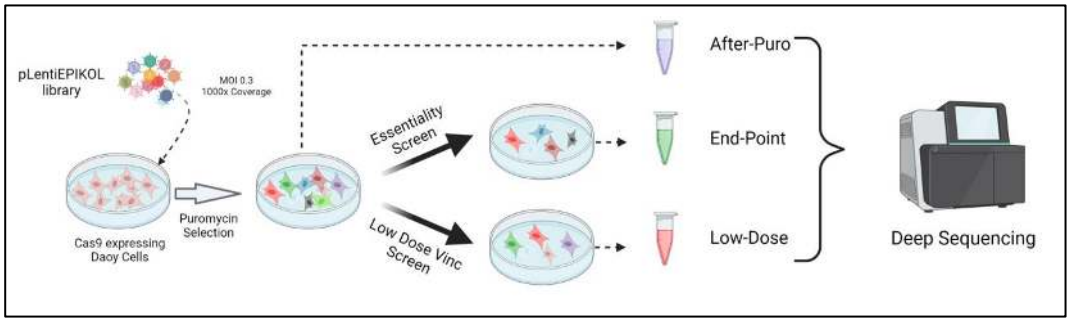


**Figure 3.10: EPIKOL Screening strategy on parental Daoy cell line**. Figure Created in biorender.com (*Karabiyik et al., unpublished).*

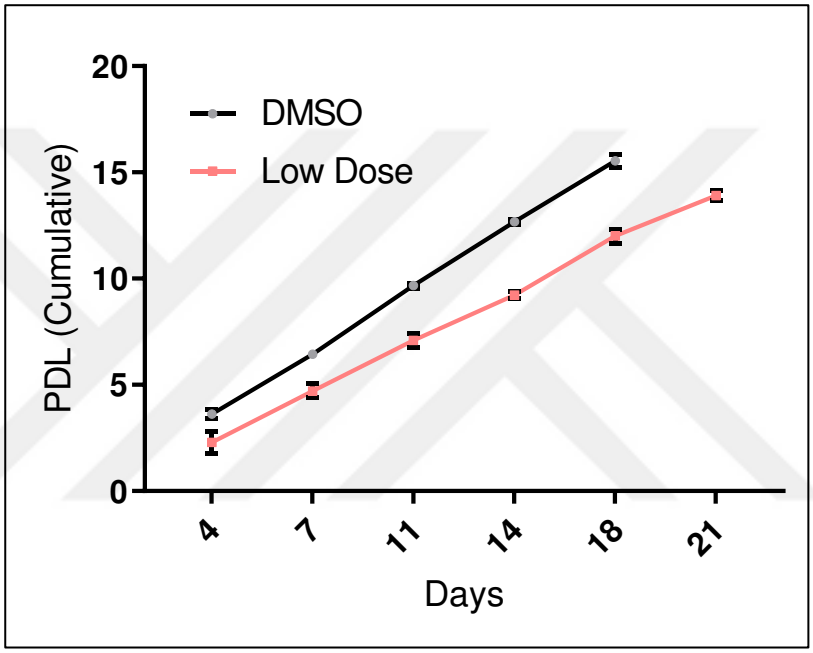


**Figure 3.11: Cumulative Population Doubling Time during EPIKOL screen on parental Daoy cells.** Cells were counted after each passage after the completion of Cas9 activity.

The MaGeCK algorithm was used to analyze the screen results. Initial quality control analysis showed that the distribution of sgRNAs in the AP group was similar to the distribution of sgRNAs in the representation assay. A shift toward the right was observed on LD samples, while a shift toward the left was observed on EP and HD samples (**Figure 3.12**).

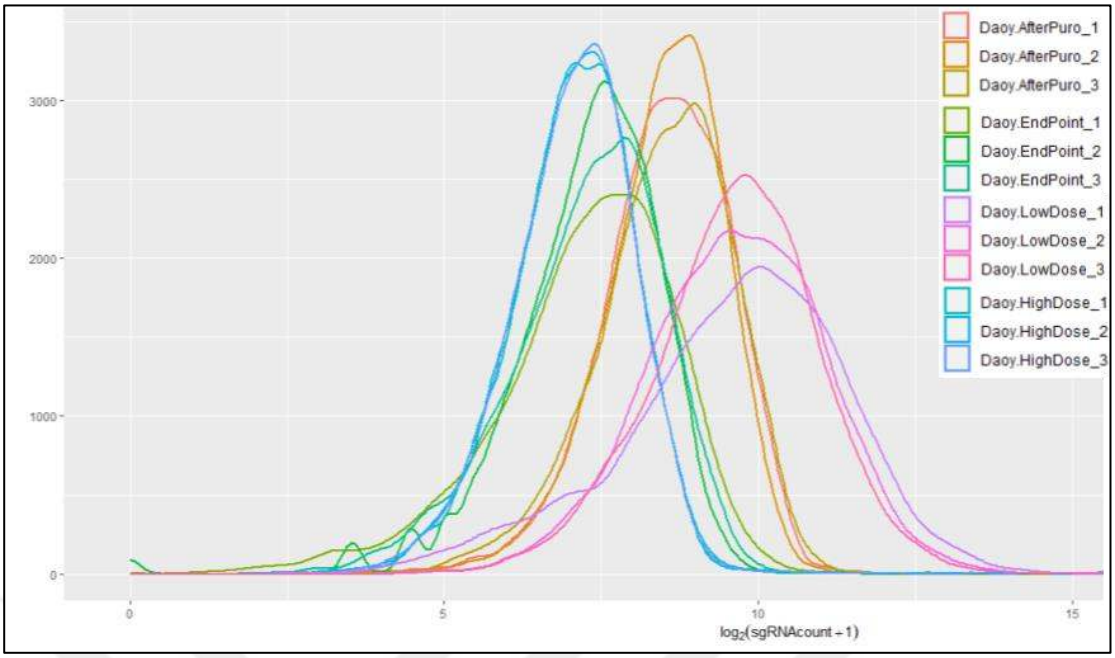


**Figure 3.12: sgRNA density plot for each treatment group of Daoy cells after completion of EPIKOL screen.**

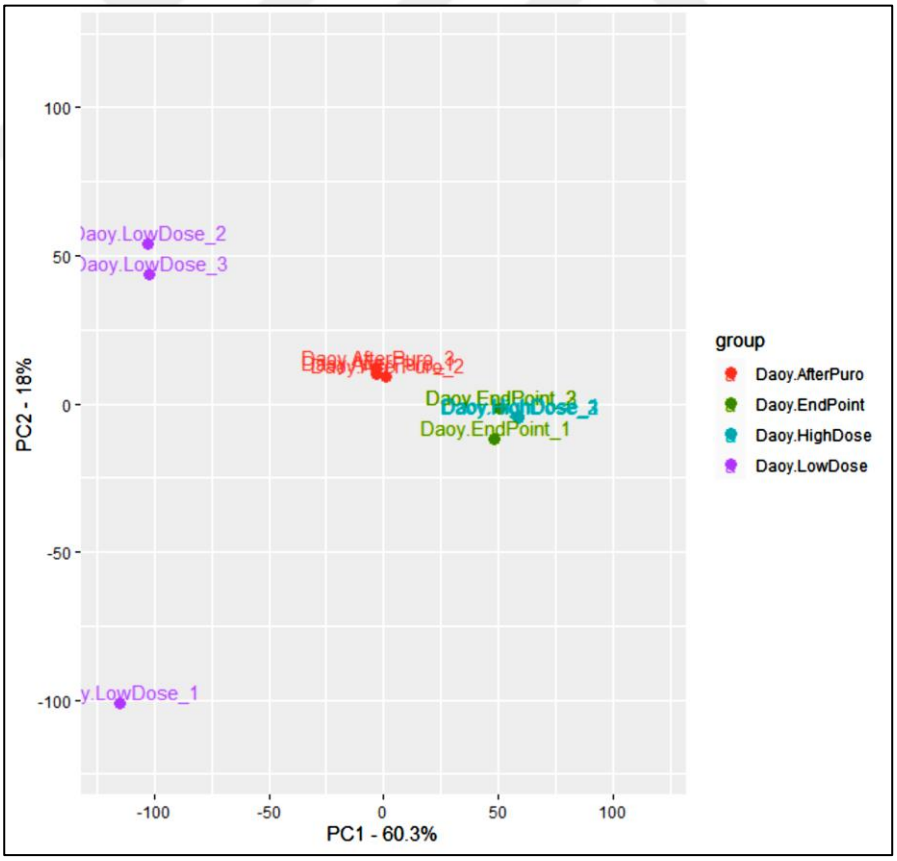


**Figure 3.13: PCA graph for AP, EP, LD, and HD samples.**

The separation of different treatment groups from AP samples was observed via Principal Component Analysis (PCA). While HD and EP groups were localized together, similar to the sgRNA density plot, the LD group was separated from all other treatment groups, especially on PC1. Separation of one set of LD groups from the additional two biological replicates was observed on PC2. However, the variance explained by PC2 is higher than PC1 (**Figure 3.13**).

### *3.2.4 Analysis of EPIKOL screen results on parental cell line.*

Following the initial quality control analysis, $log_2$ transformed sgRNA count values of the AP group were compared to each treatment group. Non-targeting sgRNAs were used as negative controls on the EPIKOL screening strategy and expectedly found around the diagonal line, showing that their representation in the population did not change between AP and treatment groups (EP and LD) since they were not expected to exhibit any effect on the cells. In contrast, sgRNAs targeting essential genes were included in the EPIKOL library as positive controls. They were expected to be depleted at the end of the screen since those sgRNAs target essential genes (**Figure 1.5**). Conceivably, sgRNAs targeting essential genes were found under the diagonal line for each comparison, showing apparent depletion of those sgRNAs in the population, thus increasing the reliability of the EPIKOL screen on both EP and LD groups (**Figure 3.14**).

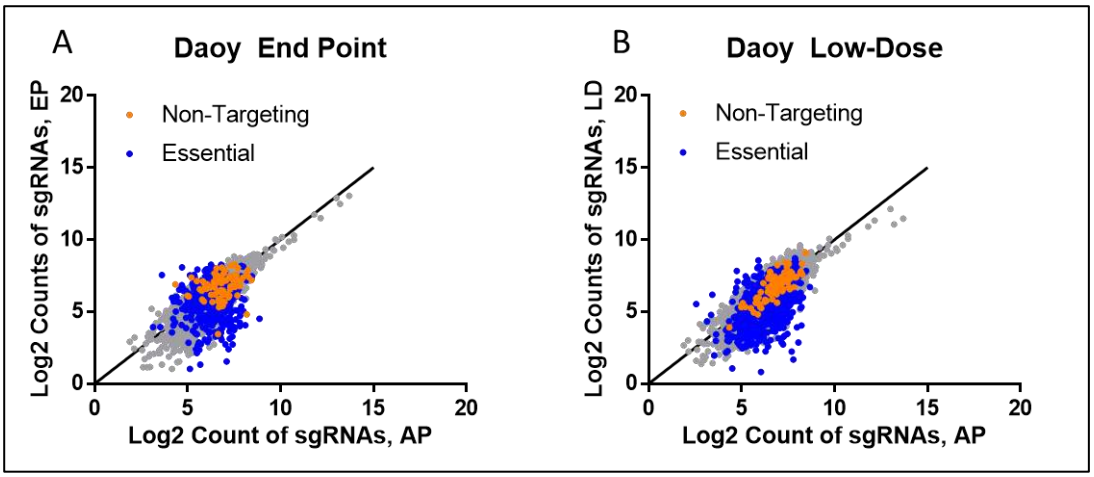


**Figure 3.14: sgRNA distribution of EPIKOL screen on parental Daoy cell line.** A. sgRNA distribution of EP group compared to AP group. B) sgRNA distribution of the LD group compared to the AP group.

Depletion of genes targeted by sgRNAs was also examined following sgRNA distribution analysis. This analysis used median normalization to identify gene-level depletions within treatment groups. Similar to the sgRNA distribution shown above, gene-level depletion of essential genes was observed on almost all genes for both treatment groups. Nontargeting sgRNAs were grouped and represented as one gene, thus represented with one data point on gene level analysis, and they were shown to be not changing in both treatment groups (**Figure 3.15**). For gene level analysis, the LD group was compared to the EP group, thus representing depleted genes compared to EP versus AP. Therefore, the depletion of essential genes in this waterfall plot is not expected.

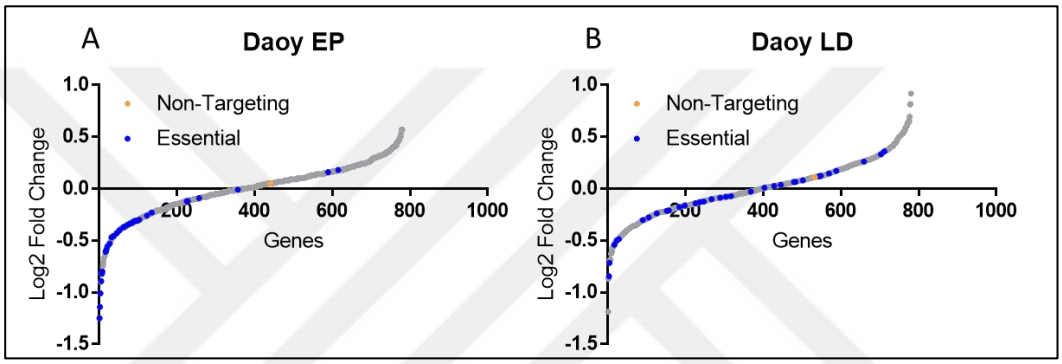


**Figure 3.15: Waterfall plots demonstrating gene level depletion on Daoy cells** A. End-Point / AP comparison, B. Low Dose / EP comparison. A normalized median count of sgRNAs from three replicates was used as input.

Genes targeted by depleted sgRNAs in the population for EP vs. AP and LD vs. EP are shown below. While most of the essential genes used as positive controls in EPIKOL showed depletion on EP vs. AP comparison, LFC scores were low. Several promising candidate genes were identified on the essentiality screen. Cutoff criteria of LFC<-0.5 and p-value<0.05 parameters were applied (**Figure 3.11**) for validation. Subsequently, relevant studies highlighting depleted genes were reviewed with a focus on factors such as identified mutations and differential expression within the context of MB.

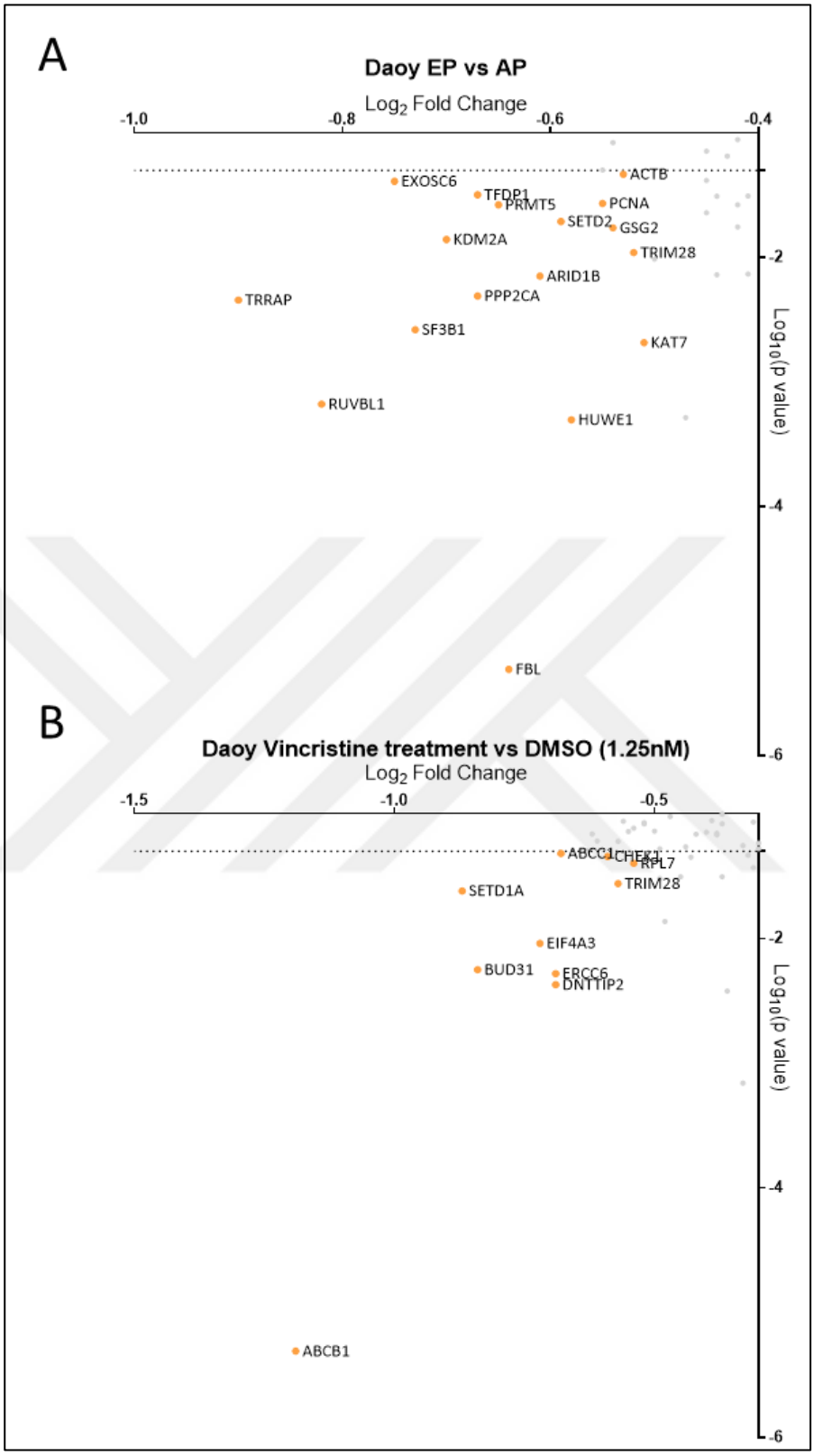


**Figure 3.16: Results of the EPIKOL screens with parental Daoy cells** (A. EP vs. AP, B LD vs. EP). Volcano plots represent $log_2$Fold Changes of genes with corresponding $log_{10}$(p-value) targeted by sgRNAs in EPIKOL.

### 3.2.5 Validation of EPIKOL screen on parental Daoy cell line

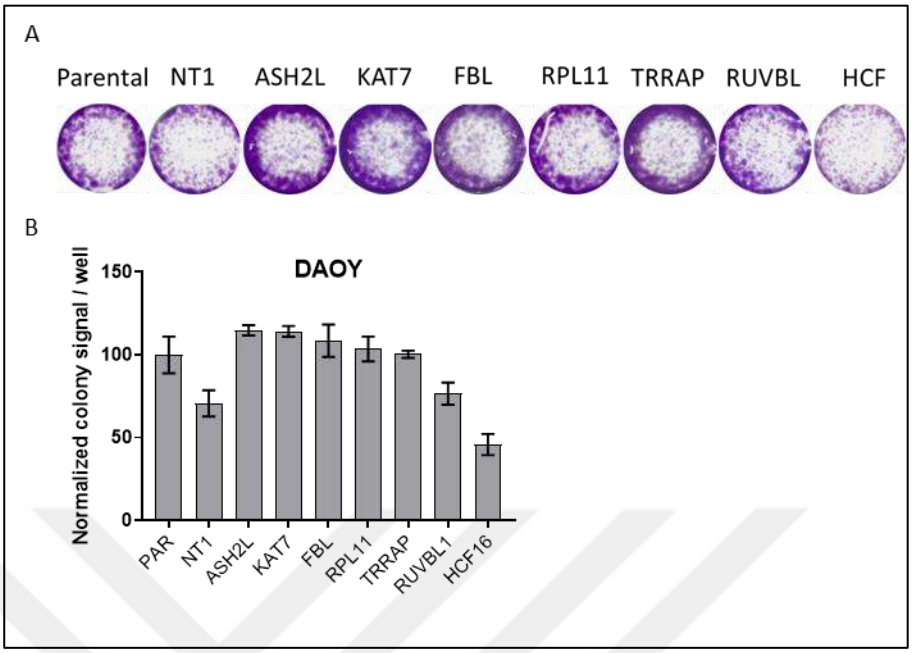


**Figure 3.17: Long term clonogenic assay results of selected hits from EPIKOL screen on parental Daoy cells.** A. Representative images from each group transduced with sgRNA targeting selected gene. B. Quantification of long-term clonogenic assay (n=3).

To validate hits identified in the EPIKOL essentiality screen on the parental Daoy cell line, sgRNAs targeting selected genes were individually cloned into the pLentiGuide backbone. Daoy cells were transduced with sgRNA of interest, and a long-term clonogenic assay was conducted. In this assay, cells transduced with individual sgRNAs were seeded equally for clonogenic assay seven days post-transduction and cultured for an additional seven days. Compared to parental and NT1 transduced cells, only cells transduced with HCF sgRNA grew less (**Figure 3.17**).

In low-dose drug screens, notably higher depletion scores were observed compared to EP vs. AP comparison. Specifically, a significant depletion of sgRNAs targeting the *ABCB1* gene was observed with high $Log_2$ Fold Change (LFC). This finding strongly supports the accuracy of the EPIKOL screen conducted on Daoy cells with a low dose of vincristine. It is an interesting outcome, as the parental cells would not activate ABCB1 at the basal level. However, since these cells were consistently exposed to a low dose of vincristine throughout the screen, a possible induction of *ABCB1* and, thereby, exporting vincristine from the cell might have been eliminated by the ablation of the

*ABCB1* gene in the screen. Similarly, *ABCC1* was identified as a hit, also responsible for vincristine efflux.

## 3.3 EPIKOL Screen on Vincristine-Resistant Medulloblastoma Cell Lines

### *3.3.1 Screening strategy for vincristine-resistant medulloblastoma cell lines*

To identify epigenetic vulnerabilities and possible genes that can be targeted to sensitize vincristine-resistant cell lines, EPIKOL screening was utilized with 1000X representation and MOI:0.3 in three sets, similar to previous EPIKOL screens described above in the presence or absence of vincristine. Four vincristine treatment groups were included, consisting of three low-dose vincristine treatment groups and one high-dose vincristine treatment group.

For each vincristine-resistant cell line, the initial analysis was focused on EP vs. AP sgRNA comparison, which revealed candidate epigenetic vulnerabilities specific to vincristine-resistant cell lines. This comparison highlighted candidate genes that can be targeted to decrease cell growth in vincristine-resistant cell lines. Subsequently, the sgRNA content of low-dose treatment groups was compared to the EP group to identify potential targets for sensitizing the resistant cells to vincristine.

All findings were compared to previous comparisons, including the EPIKOL screen conducted on parental Daoy cells, a screen conducted by Ezgi Yağmur Kala, a member of the TBO lab, using astrocytes as a normal cell line, and the DepMap database (DepMap, 2023) for general essential genes in cancer cells. To identify unique and specific targets for LD vs. EP comparison, common findings were excluded in the latter comparison. For example, genes commonly identified as hits in both EP vs. AP and LD vs. EP comparisons were only reported on EP vs. AP analysis.

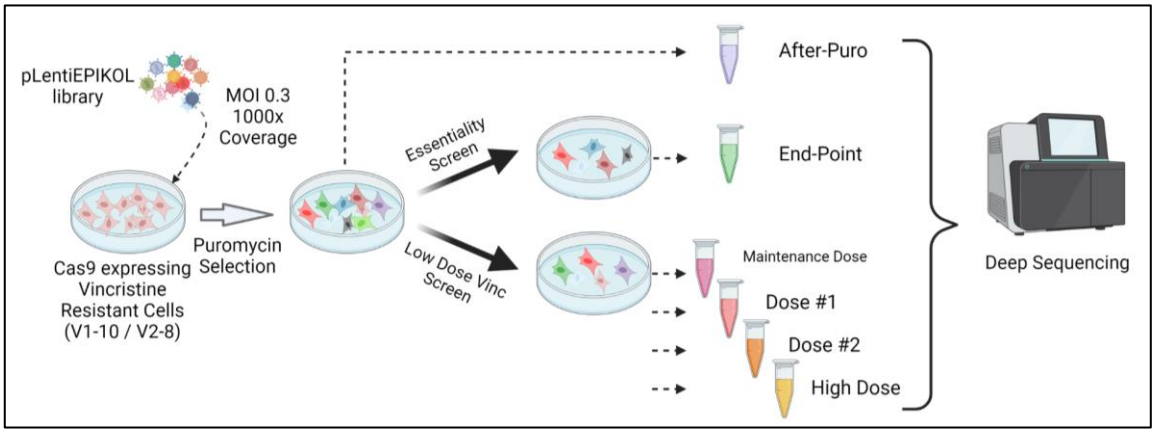


**Figure 3.18: EPIKOL screening strategy on Vincristine resistant cell lines.** Figure created in biorender.com (*Karabiyik et al., unpublished).*

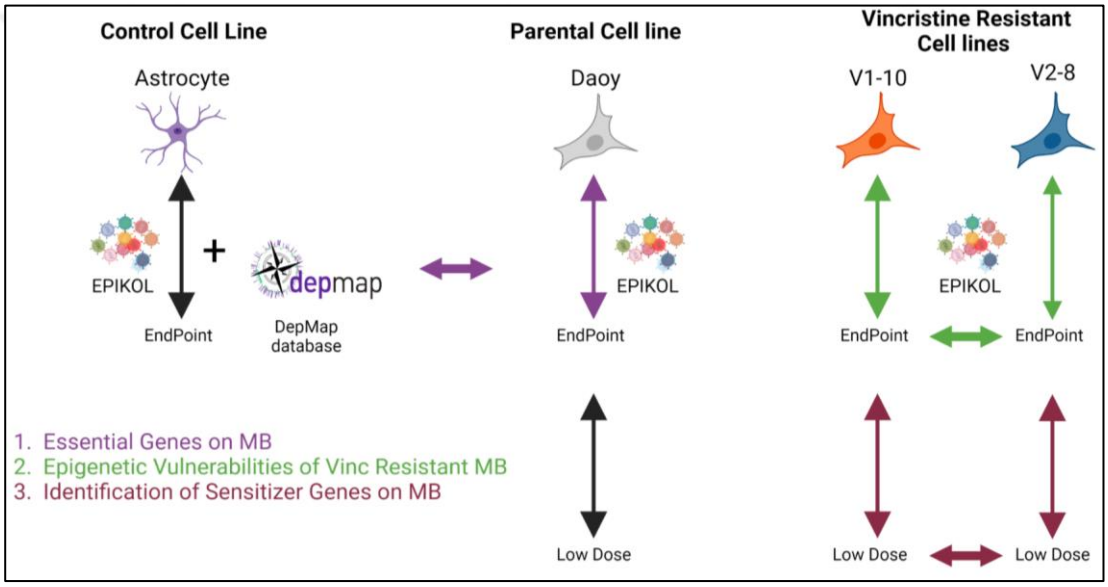


**Figure 3.19: Analysis strategy of EPIKOL Screen on Vincristine Resistant Cell lines.** Figure Created in biorender.com (*Karabiyik et al., unpublished).*

### *3.3.2 EPIKOL Screening on V1-10 Vincristine Resistant Cell Line*

The doubling time of V1-10 cells in different treatment groups was examined throughout the screen. While no significant difference was observed between EP, maintenance dose (M, 10 nM), and 25 nM treatment groups, the 100 nM treatment group was affected by treatment and finalized three days after the other treatment groups.

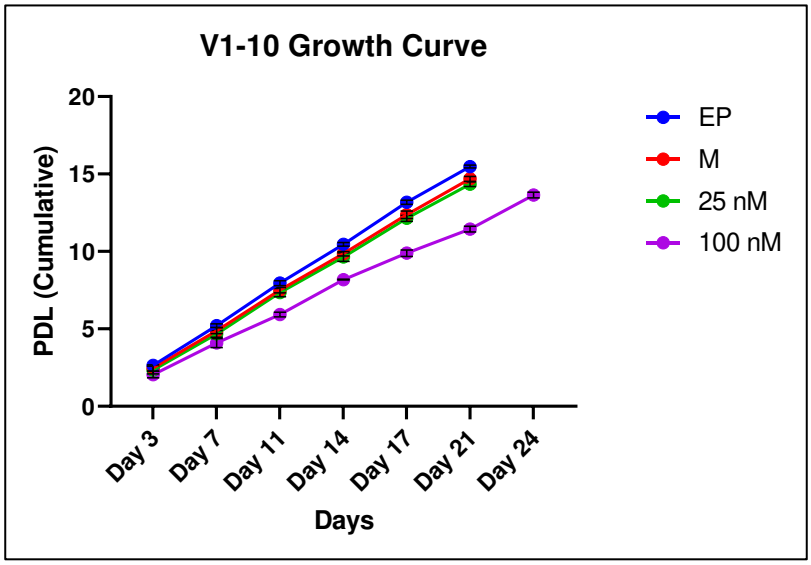


**Figure 3.20 PDL for EPIKOL screen on V1-10 vincristine resistant cell line.** Each set was counted separately after passaging in confluency between 60-80%. (*Karabiyik et al., unpublished).*

Similar to sgRNA distribution in a parental cell line, non-targeting sgRNAs were also observed around the diagonal line in all groups compared to the AP group. Most positive control sgRNAs were also depleted in V1-10 treatment groups (**Figure 3.21).** In the same way, Cumulative distribution plots (CDP) also show depletion of essential sgRNAs in all treatment groups compared to AP (**Figure 3.22**).

Depletion of genes targeted by essential sgRNAs can also be seen at the gene level. Compared to the EPIKOL screen on the parental cell line, higher depletion, thus a higher LFC score, has been observed in AP comparison (**Figure 3.23**).

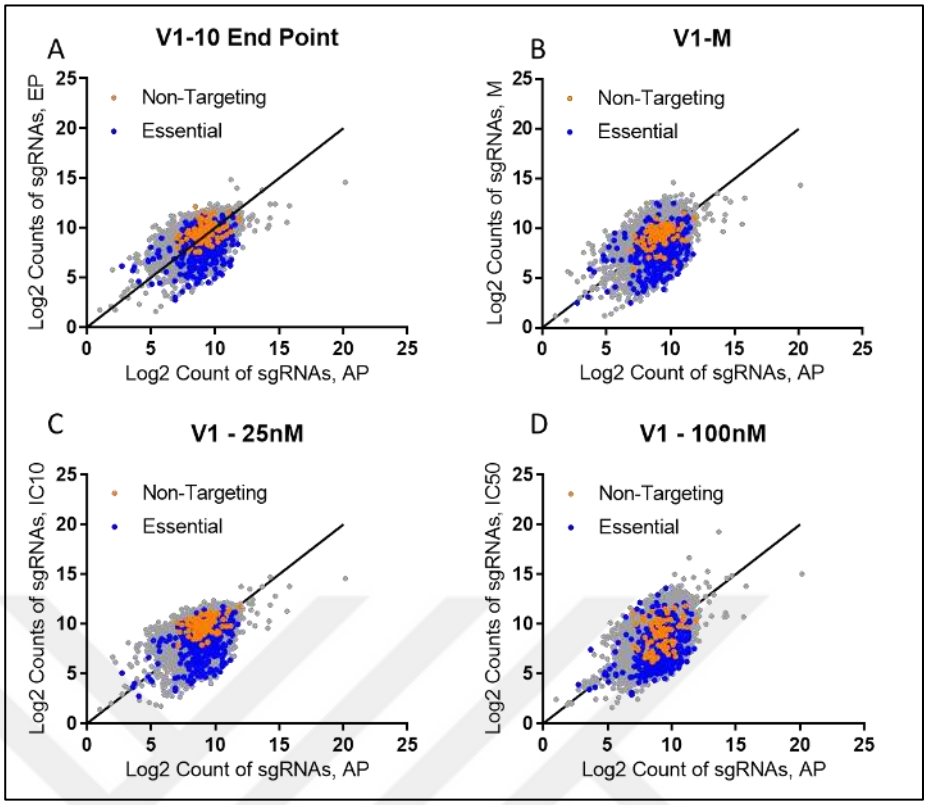


**Figure 3.21: sgRNA distribution of EPIKOL screen on parental V1-10 cell line compared to After-Puro samples.** A. End-Point, B. Maintenance dose (10 nM), C. 20 nM vincristine treatment group, D.100 nM vincristine treatment group. (*Karabiyik et al., unpublished).*

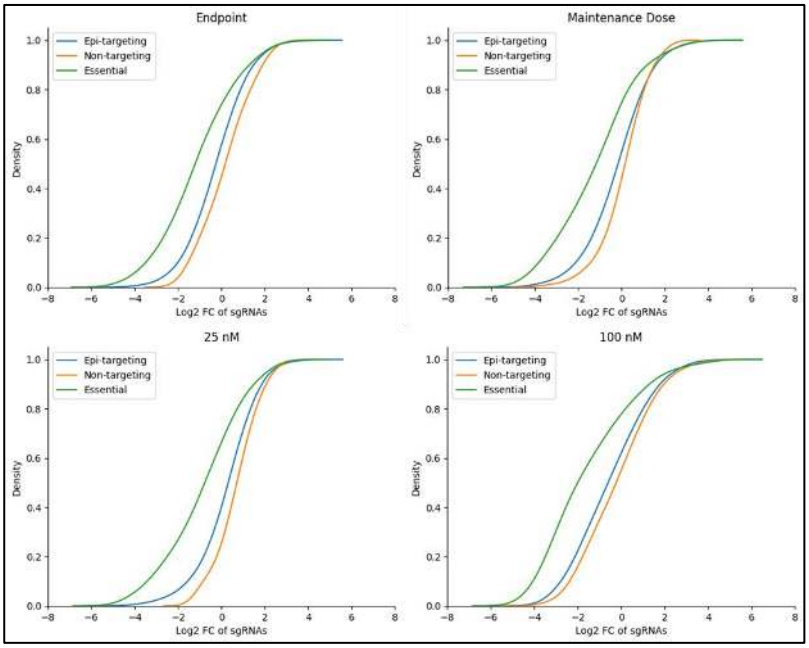


**Figure 3.22: Cumulative Distribution Plots of read counts compared to initial representation for V1-10 EPIKOL Screen.** A. End-Point, B. Maintenance dose (10 nM), C. 20 nM vincristine treatment group, D.100 nM vincristine treatment group (*Karabiyik et al., unpublished).*

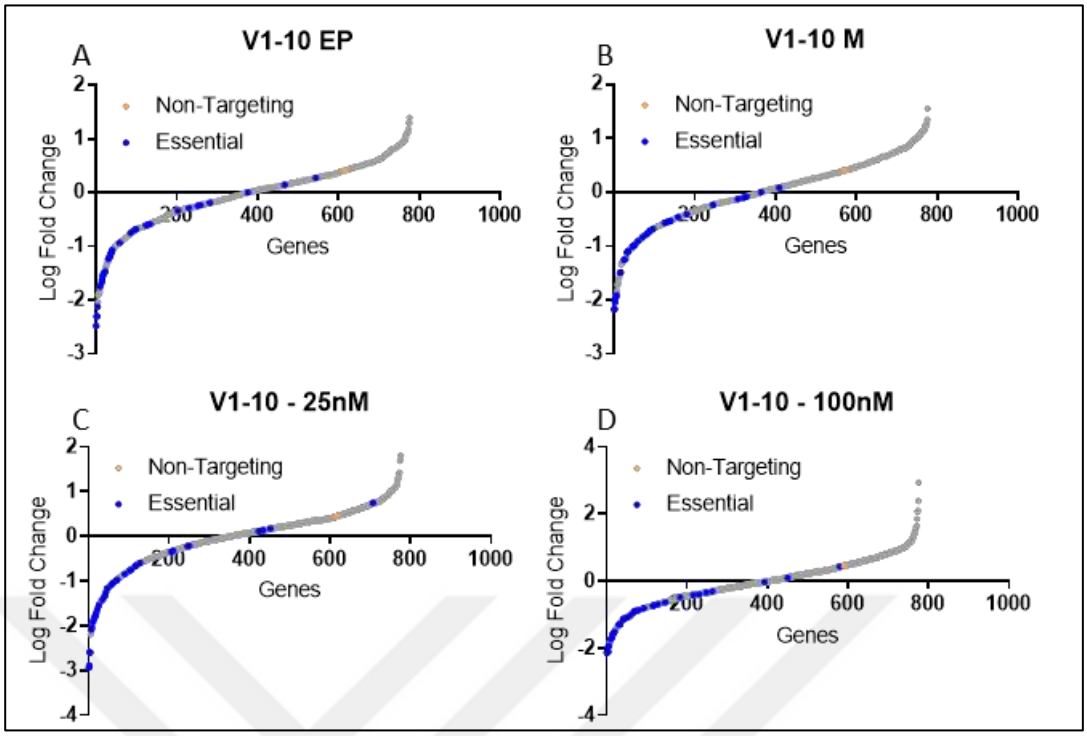


**Figure 3.23: Waterfall plots demonstrating of gene level depletion on V1-10 cells in comparison to AP** A. End-Point, B. Maintenance dose (10 nM), C. 25 nM vincristine treatment group, D.100 nM vincristine treatment group (*Karabiyik et al., unpublished).*

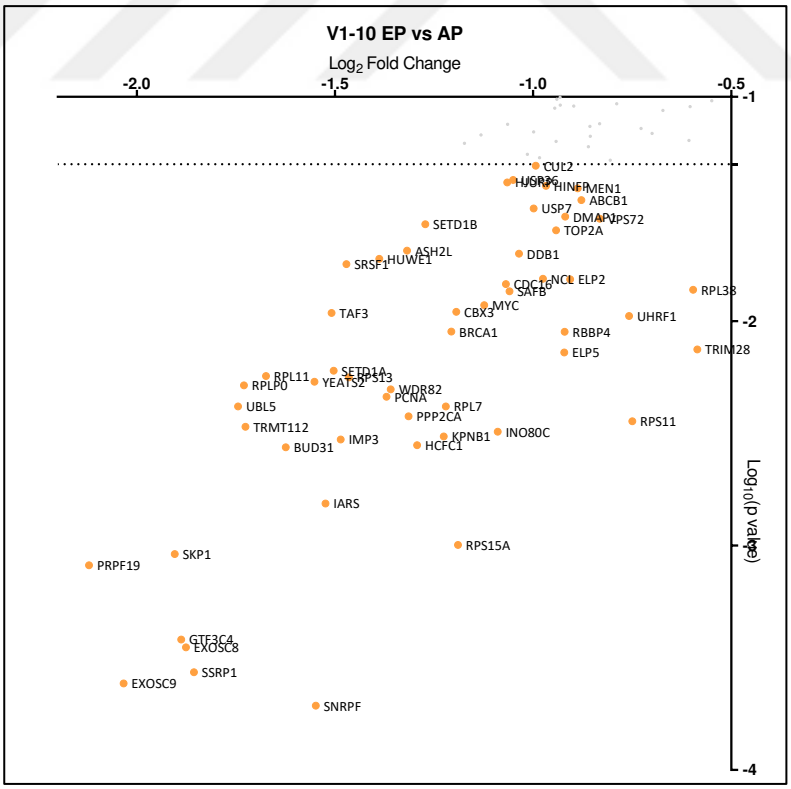


**Figure 3.24 Volcano plot showing EPIKOL screen results on V1-10 cells EP vs. AP comparison.** Only genes with $Log_2FC<-0.5$ and p-value <0.5 are shown. (*Karabiyik et al., unpublished).*

**Table 3.1: neg|score, neg|lfc and neg|p-value values of candidate essential genes for EPIKOL screen conducted on vincristine resistant V1-10 cell line.**

| MB | DepMap | Gene | Complex | neg\| score | neg\|p-value | neg\|lfc | neg\| goodsgrna |
|---|---|---|---|---|---|---|---|
| NO | + | DMAP1 | NuA4 | 0.0058 | 0.029 | -0.92 | 7 |
| NO | + | VPS72 | NuA4 | 0.0056 | 0.029 | -0.83 | 5 |
| NO | | ASH2L | CHD8, COMPASS | 0.0038 | 0.021 | -1.32 | 6 |
| Mutated | + | HCFC1 | CHD8, COMPASS | 0.0004 | 0.003 | -1.29 | 9 |
| NO | | MEN1 | CHD8, COMPASS | 0.0081 | 0.039 | -0.89 | 7 |
| NO | | INO80C | CHD8,Ino80 | 0.0005 | 0.003 | -1.09 | 7 |
| NO | | SETD1A | COMPASS | 0.0010 | 0.006 | -1.50 | 8 |
| NO | | SETD1B | COMPASS | 0.0052 | 0.027 | -1.27 | 6 |
| Mutated | + | WDR82 | COMPASS | 0.0008 | 0.005 | -1.36 | 8 |
| NO | | SKP1 | BCOR | 0.0001 | 0.001 | -1.90 | 6 |
| YES | | USP7 | BCOR | 0.0064 | 0.032 | -1.00 | 7 |
| DEG | + | BRCA1 | BRCA1,BRCC | 0.0015 | 0.009 | -1.21 | 8 |
| DEG | + | RBBP4 | CAF-1 NuRD, NuRF | 0.0015 | 0.009 | -0.92 | 7 |
| YES | + | SSRP1 | FACT | 0.0000 | 0.000 | -1.86 | 8 |
| DEG | | HUWE1 | MLL2/3 | 0.0035 | 0.019 | -1.39 | 7 |
| DEG | + | GTF3C4 | | 0.0001 | 0.000 | -1.89 | 9 |
| Mutated | + | HJURP | | 0.0088 | 0.042 | -1.07 | 7 |
| YES | + | PCNA | | 0.0007 | 0.005 | -1.37 | 6 |
| YES | + | PPP2CA | | 0.0005 | 0.004 | -1.31 | 8 |
| NO | | TRIM28 | | 0.0012 | 0.007 | -0.59 | 5 |
| DEG | | UHRF1 | | 0.0018 | 0.011 | -0.76 | 5 |

### *3.3.3 Validation of V1-10 fitness genes*

Genes from different epigenetic complexes such as NuA4, COMPASS, CHD8, and BCOR were identified as candidate fitness genes with significant depletion. From those, previously cloned sgRNAs by Özlem Yedier-Bayram, Ph.D., were used for the initial round of validation for the V1-10 essentiality screen. Long term clonogenic assay was used as the primary method for validating fitness genes. Depletion of cells transduced with sgRNAs targeting *ASH2L* and *RBBP4* was observed (**Figure 3.25**)

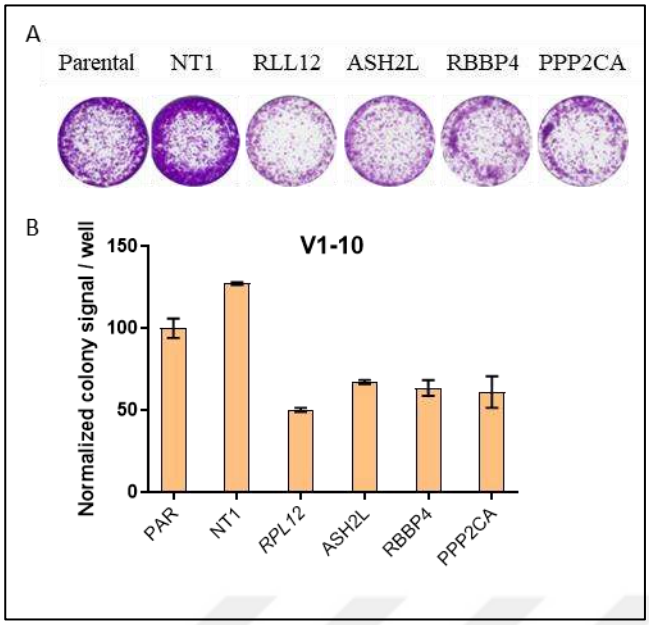


**Figure 3.25: Long term clonogenic assay results of selected hits from V1-10 Essentiality screen** A. Representative images from each group transduced with sgRNA targeting selected gene. B. Quantification of long-term clonogenic assay (n=3)

### *3.3.4 Validation of vincristine sensitizers on V1-10 cell line*

Low-dose drug treatment groups were compared to the Endpoint group to validate candidate sensitizer genes. This comparison aimed to identify genes depleted explicitly in the drug treatment group, as the depletion of essentiality genes had already been validated in all groups compared to AP samples. As a result, essentiality genes (positive controls on EPIKOL) were not marked in waterfall plots (**Figure 3.26**).

Common candidate sensitizer genes from different treatment groups were compared for further validation. While several candidate hit genes were identified from M, 25nM, and 100 nM drug treatment groups, only eight genes were commonly depleted in the drug treatment groups (**Figure 3.27**). Compared to LFC scores obtained from the EPIKOL screen conducted in the parental Daoy cell line, higher LFC scores were obtained from the EPIKOL screen shown in the V1-10 cell line. Expectedly, ABC transporter genes such as *ABCB1* were identified as sensitizer genes in the 25 nM vincristine treatment group. However, depletion of ABC transporters was not observed commonly in all treatment groups.

Considering biological relevance to literature in MB and drug resistance, *CSNK2A1, BRPF1,* and *CBP*, *KAT6A* were selected for the initial round of validation of

candidate sensitizer genes. Additionally, *RPL12* and *ABCB1* were used as positive controls, while Parental and NT1 transduced cells were used as negative controls for validation experiments.

Both long-term clonogenic assay and dual-color competition assays were utilized to validate sensitizer genes. An apparent reduction of growth of cells transduced with sgRNAs targeting *RPL12* and *ABCB1* was observed in vincristine (+) samples compared to vincristine (-) samples. However, the same level of reduction was not observed for cells transduced by sgRNAs targeting selected candidate sensitizers on both assays.

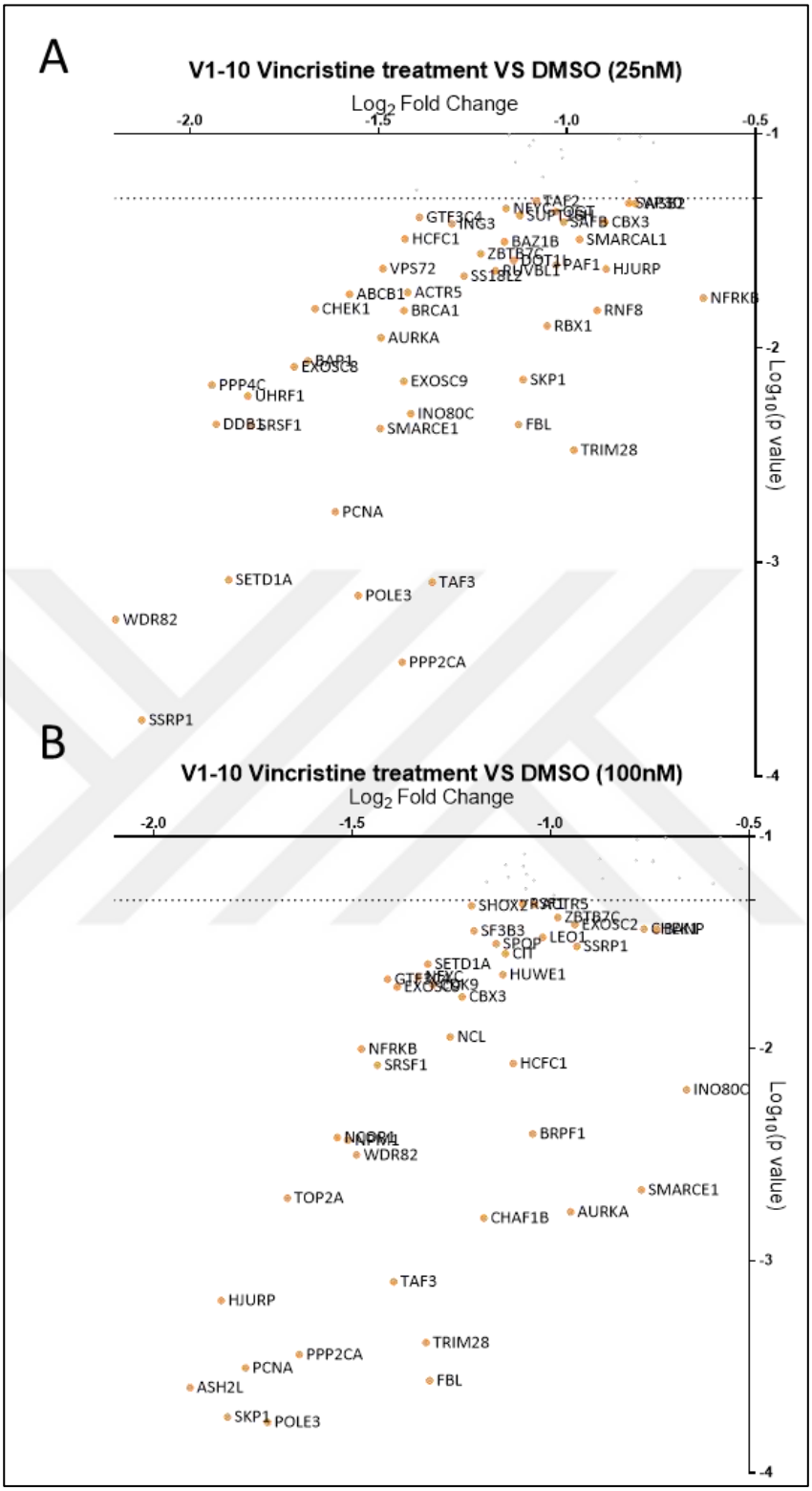


**Figure 3.26: Volcano plot showing genes targeted by significantly depleted sgRNAs on EP-EP comparison on V1-10 EPIKOL screen.** A. 25 nM vincristine treatment group, B. 100 nM vincristine treatment group. Only genes with Log2FC<-0.5 and p-value <0.5 are shown. (*Karabiyik et al., unpublished).*

A

| M | 25 nM | 100 nM |
|---|---|---|
| CBX8 | ABCB1 | ACTR5 |
| CSNK2A1 | APOBEC2 | AR |
| CUL1 | AR | BRPF1 |
| KDM4B | ARID4A | CBX5 |
| MRGBP | CBX7 | CBX8 |
| MTA3 | CBX8 | CDK7 |
| NCOA6 | CHEK1 | CHD8 |
| NR3C1 | CSNK2A1 | CSNK2A1 |
| PELP1 | CXXC1 | EHMT2 |
| PHF2 | EHMT2 | KAT6B |
| PRPF31 | HDAC1 | KEAP1 |
| SAP30 | HDAC6 | MBD2 |
| TEX10 | KDM5C | NR3C1 |
| | PRRX1 | SIRT2 |
| | RNF8 | SMEK1 |
| | SFMBT2 | |
| | SFPQ | |
| | SIRT2 | |
| | SMARCAL1 | |
| | SMYD3 | |
| | SUPT3H | |
| | SUV39H1 | |
| | TAF1L | |
| | TAF9B | |
| | TET3 | |
| | UBR2 | |
| | ZMYND11 | |

B

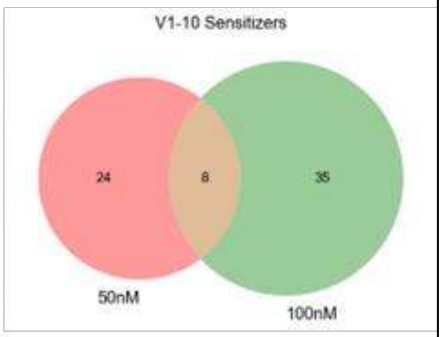


**Figure 3.27: Common hits of EPIKOL screen with low-dose vincristine on V1-10 cells.** A. Genes targeted by depleted sgRNAs in drug treatment groups. B. Number of genes targeted by depleted sgRNAs in 50 nM and 100 nM drug treatment groups. Only genes with $Log_2FC<-0.5$ and p-value <0.5 were included. (*Karabiyik et al., unpublished).*

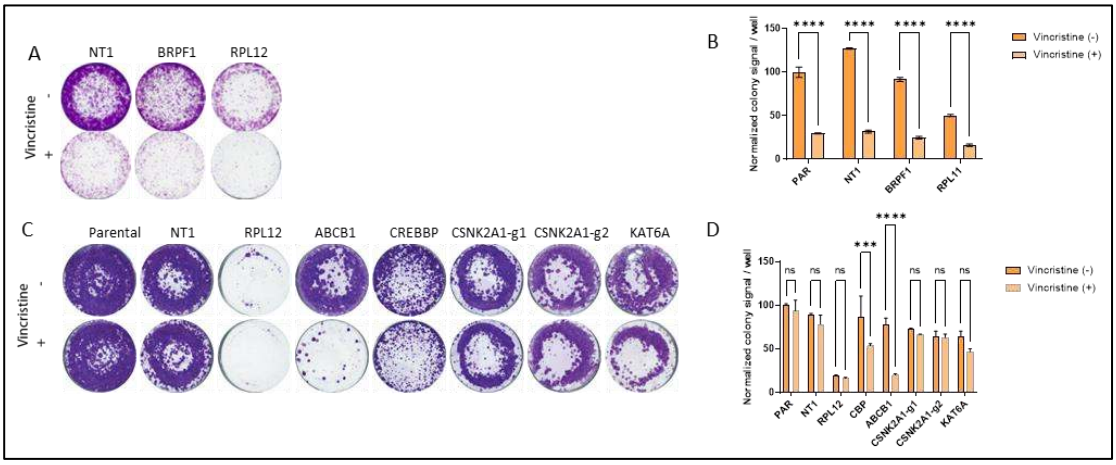


**Figure 3.28: Long term clonogenic assay results of selected hits from V1-10 Low dose Vincristine screen.** The experiment was conducted in two parts. A, B. Results for the experiment for the *BRPF1* gene with its own positive (*RPL12*) and negative (NT1) controls and its quantification. C, D. Results for the experiment for *ABCB1*, *CBP*, *CSNK2A1,* and *KAT6* genes with their own positive (*RPL12*) and negative (NT1) controls. (*Karabiyik et al., unpublished).*

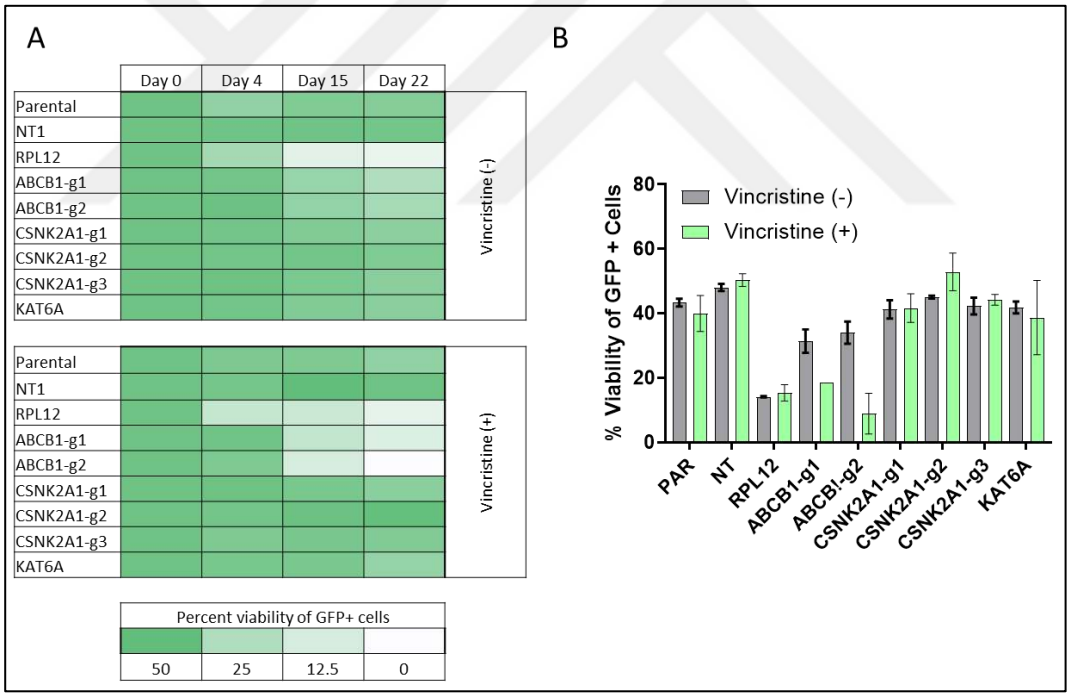


**Figure 3.29: Dual Color Competition Assay.** A. Heatmap of the results with respect to GFP + cell percentage within the population. B. Line graph of the same results, showing depletion of GFP+ cells in the population compared to the control group. (*Karabiyik et al., unpublished).*

### *3.3.5 EPIKOL Screening on V2-8 Vincristine Resistant Cell Line*

Similar to the EPIKOL screen on V1-10 cells, EP, M (8 nM), and 20 nM vincristine treatment groups were used after the completion of Cas9 activity. Doses were selected according to IC10 and IC50 values obtained on a 96-well plate setting. While the EP vs. AP comparison aimed to identify genes essential for the fitness of V2-8 cells in the absence of vincristine, drug treatment groups were compared to the EP group to identify epigenetic modifiers when knocked out reverts resistance against vincristine. EP, M, and 20 nM vincristine treatment groups showed similar population doubling profiles, while 50 nM showed a distinct signature on PDL in the early days after transduction. However, after a week of incubation in 50 nM of vincristine, a similar trend in all treatment groups was observed (**Figure 3.30**).

EPIKOL screen on the V2-8 cell line showed the best sgRNA distribution profile among all EPIKOL screens described within this study. While essential genes were clearly depleted in volcano plots, non-targeting genes were around the diagonal line for all treatment groups (**Figure 3.31**). Also, on CDP, depletion of sgRNAs targeting essential genes was observed compared to non-targeting sgRNAs, especially in Endpoint and low-dose vincristine-treated groups (**Figure 3.32**).

Similar to sgRNA distribution, the apparent depletion of essential genes was also visible in gene-level analysis. Greater LFC scores compared to other EPIKOL screens were also obtained on the EPIKOL screen conducted in the V2-8 cell line in AP comparison. Slight enrichment of the non-targeting group is visible in all groups except the 25 nM Vincristine-treated group (**Figure 3.33**).

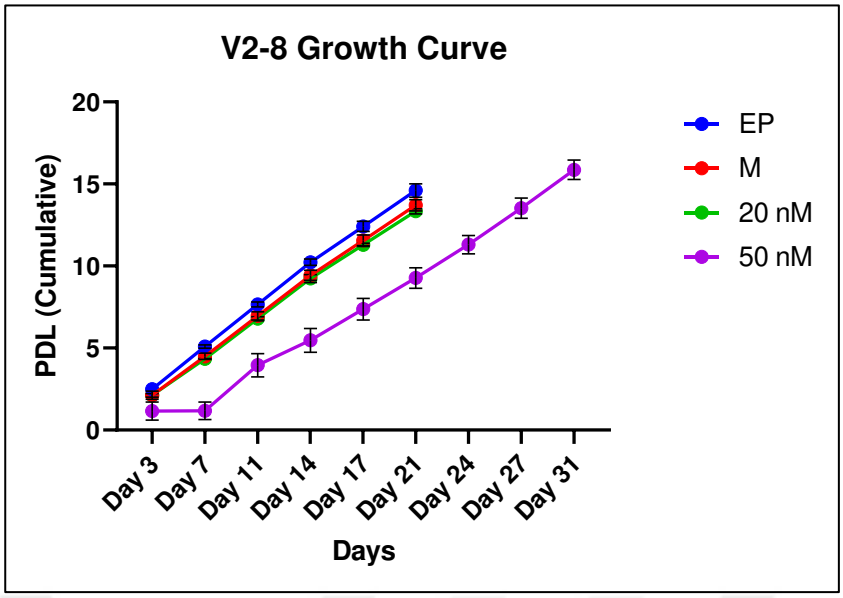


**Figure 3.30: PDL for EPIKOL screen on V2-8 vincristine resistant cell line.** Each set was counted separately after passaging in confluency between 60-80%. (*Karabiyik et al., unpublished).*

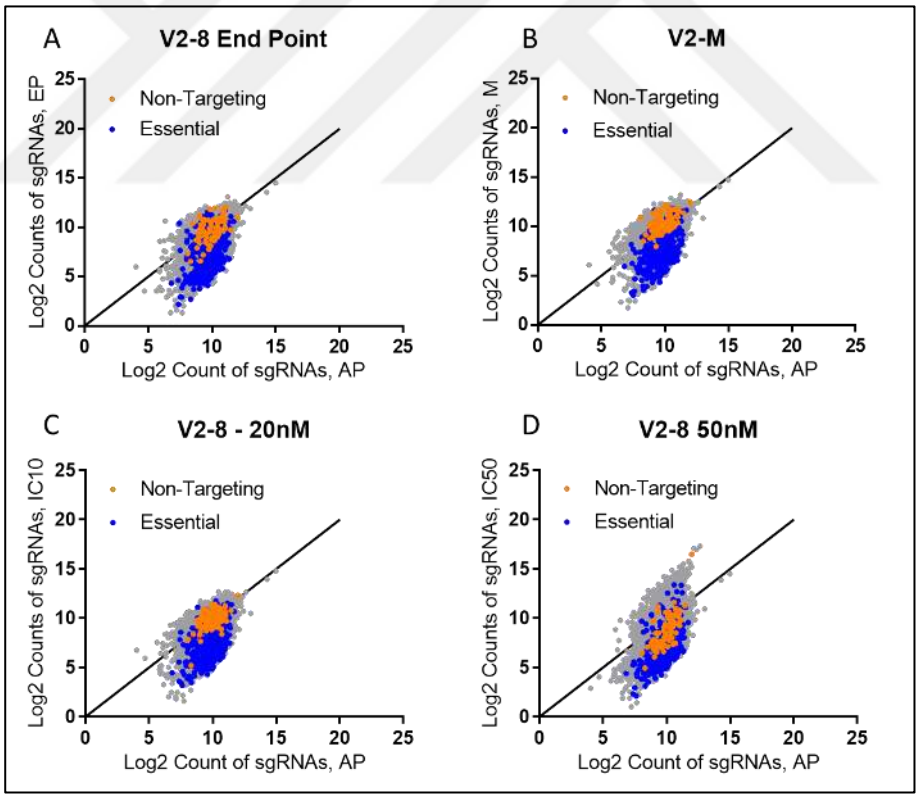


**Figure 3.31: sgRNA distribution of EPIKOL screen on parental V2-8 cell line compared to After-Puro Samples.** A. End-Point, B. Maintenance dose (8 nM), C. 20 nM vincristine treatment group, D.100 nM vincristine treatment group (*Karabiyik et al., unpublished).*

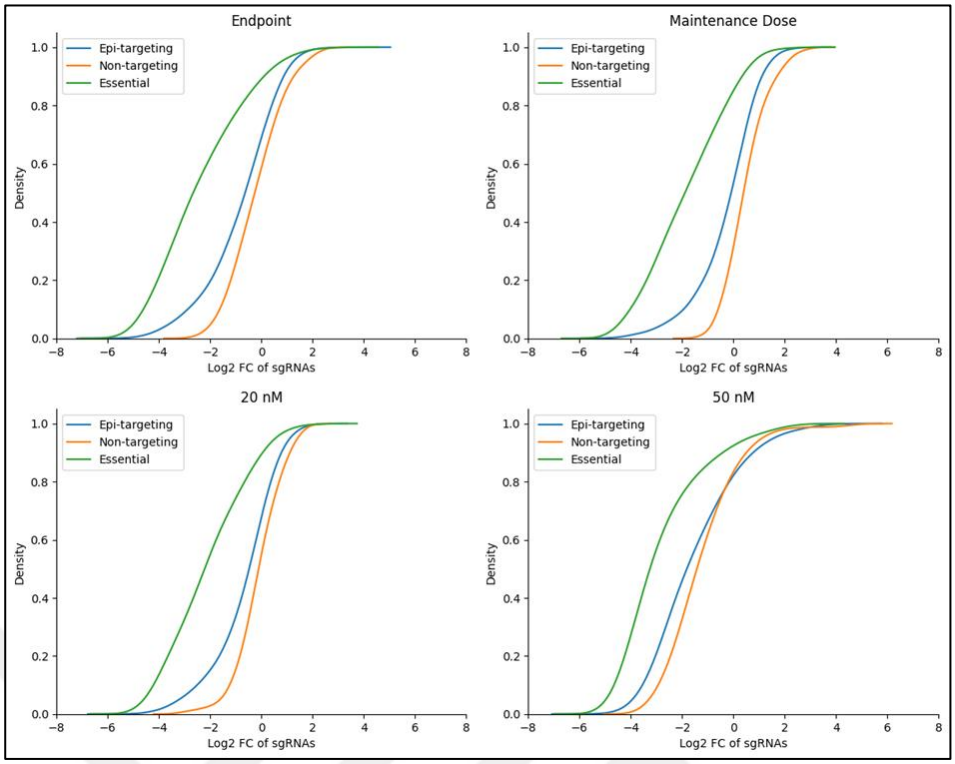


**Figure 3.32 Cumulative Distribution Plots of read counts compared to initial representation for V2-8 EPIKOL Screen.** A. End-Point B. Maintenance dose C. 20 nM vincristine treatment group, D.100 nM vincristine treatment group (*Karabiyik et al., unpublished).*

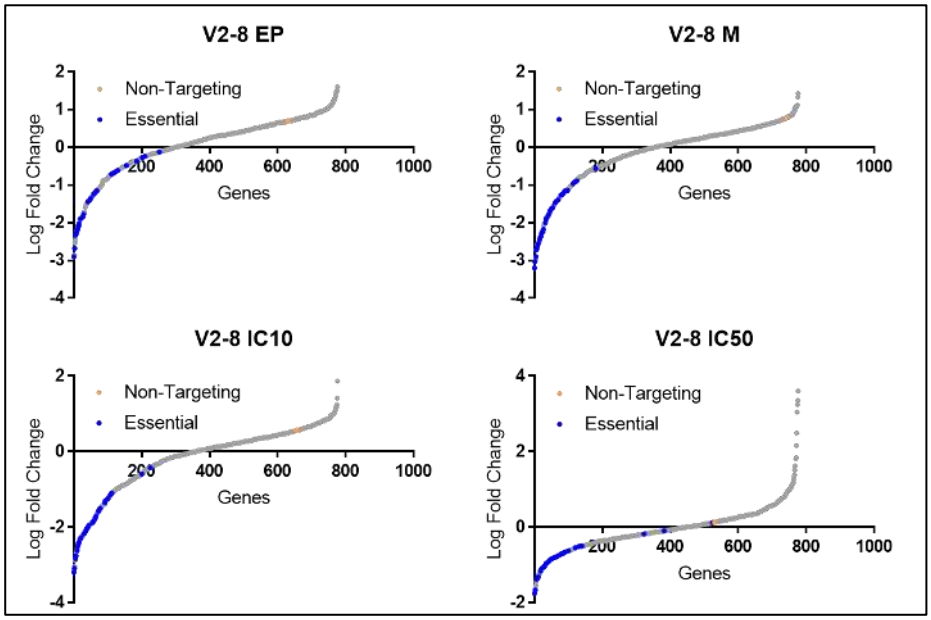


**Figure 3.33: Waterfall plots demonstrating gene level depletion on V2-8 cells compared to AP. A.** End-Point, B. Maintenance dose (8 nM), C. 20 nM vincristine, D. 100 nM Vincristine. (*Karabiyik et al., unpublished).*

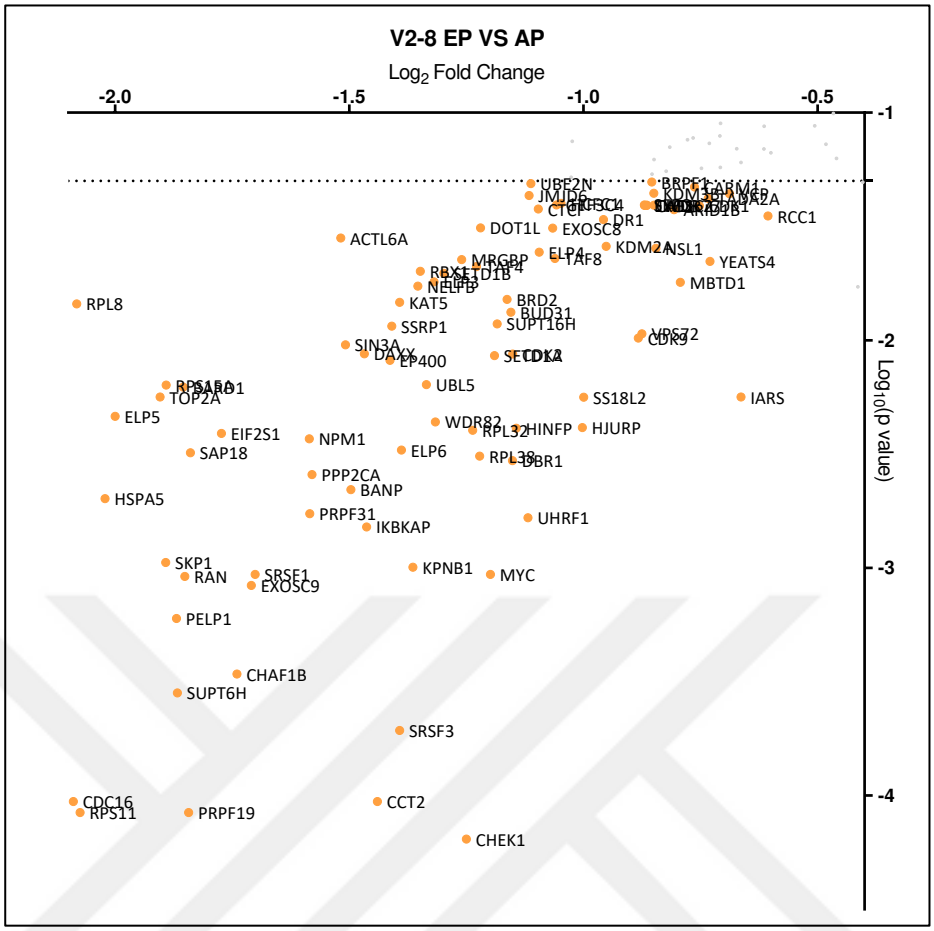


**Figure 3.34: Volcano plot showing EPIKOL screen results on V2-8 cells EP vs. AP comparison.** Only genes with $Log_2FC<-0.5$ and p-value <0.05 are shown. (*Karabiyik et al., unpublished).*

**Table 3.2: neg|score, neg|lfc and neg|p-value values of candidate essential genes for EPIKOL screen conducted on vincristine resistant V2-8 cell line.**

| MB | DepMAp | Gene | Complex | neg\| score | neg\| p-value | neg\|lfc | neg\| goodsgrna |
|---|---|---|---|---|---|---|---|
| NO | | SETD1A | COMPASS | 0.001 | 0.009 | -1.19 | 8 |
| NO | + | SETD1B | COMPASS | 0.004 | 0.020 | -1.30 | 7 |
| NO | + | WDR82 | COMPASS | 0.001 | 0.004 | -1.32 | 8 |
| NO | + | EP400 | NuA4 | 0.001 | 0.008 | -1.41 | 7 |
| DEG | + | KAT5 | NuA4,SWR | 0.003 | 0.015 | -1.39 | 8 |
| NO | | VPS72 | NuA4 | 0.002 | 0.011 | -0.88 | 7 |
| NO | | YEATS4 | Nua4 | 0.004 | 0.022 | -0.73 | 7 |
| DEG | | CHD8 | CHD8, MLL2/3 | 0.008 | 0.039 | -0.87 | 7 |
| Mutated | | TAF1 | CHD8, MLL2/3 | 0.008 | 0.039 | -0.86 | 7 |
| NO | + | TAF4 | CHD8, MLL2/3 | 0.004 | 0.021 | -1.23 | 7 |
| DEG | + | ACTL6A | BAF, INO80 | 0.006 | 0.028 | -1.52 | 6 |
| NO | + | SIN3A | SWI/SNF,mSin3A | 0.002 | 0.010 | -1.51 | 6 |
| NO | + | BARD1 | BRCA1 | 0.001 | 0.006 | -1.85 | 6 |

| | | | | | | | |
|---|---|---|---|---|---|---|---|
| YES | | BRPF1 | Moz/MORF | 0.011 | 0.050 | -0.85 | 6 |
| YES | + | CHAF1B | Winac, CAF-1 | 0.000 | 0.000 | -1.74 | 8 |
| NO | | DOT1L | | 0.006 | 0.031 | -1.22 | 6 |
| YES | + | PPP4C | PPP4C | 0.000 | 0.001 | -2.19 | 7 |
| NO | + | SKP1 | BCOR | 0.000 | 0.001 | -1.89 | 7 |
| NO | + | SRSF1 | | 0.000 | 0.001 | -1.70 | 7 |
| NO | | SS18L2 | CREST-BRG1 | 0.001 | 0.006 | -1.00 | 7 |
| YES | + | SSRP1 | FACT | 0.002 | 0.012 | -1.41 | 7 |
| YES | | SUPT16H | FACT,WINAC | 0.002 | 0.012 | -1.18 | 7 |
| NO | + | SUPT6H | | 0.000 | 0.000 | -1.87 | 9 |
| NO | | TADA2A | PCAF, ATAC | 0.009 | 0.042 | -0.73 | 7 |
| DEG | + | TOP2A | | 0.001 | 0.006 | -1.90 | 8 |
| Mutated | | WDR77 | methylosome | 0.008 | 0.039 | -0.85 | 6 |

### *3.3.6 Validation of V2-8 fitness genes*

For validation of genes essential for V2-8 fitness, the same parameters used for previous EPIKOL screens were utilized. Several genes were significantly depleted, especially from epigenetic complexes such as COMPASS, NuA4, CHD8, and SWI/SNF. Several genes from those complexes were chosen for further validation using similar criteria for choosing genes to be validated. For the initial round of validation, previously cloned sgRNAs by Özlem Yedier Bayram, Ph.D., were used.

Long-term clonogenic assay was utilized for the validation of fitness genes. Parental and NT1 samples were used as negative controls, and *RPL11* was used as a positive control. Especially depletion of cells was observed upon transduction with sgRNAs *TOP2A* and *PPP4C*. In contrast, complex-specific depletion was not observed.

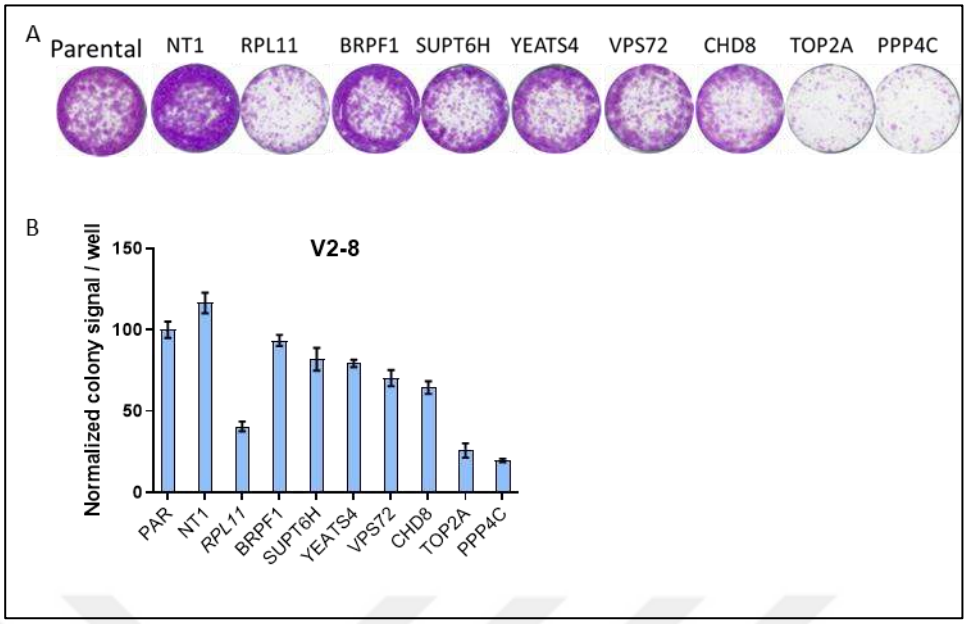


**Figure 3.35: Long term clonogenic assay results of selected hits from V2-8 essentiality screen** A. Representative images from each group transduced with sgRNA targeting selected gene. B. Quantification of long-term clonogenic assay (n=3)

### *3.3.7 Validation of vincristine sensitizers on V2-8 cell line*

Several sgRNAs were depleted in the population in the presence of vincristine compared to the DMSO control. A higher commonality between treatment groups was observed compared to the EPIKOL screen conducted on the V1-10 cell line. Furthermore, depletion of sgRNAs targeting ABC efflux pumps such as *ABCB1*, *ABCC1*, and *ABCG2* was observed in multiple vincristine-treated groups, validating the accuracy of the EPIKOL screen (**Figure 3.36**).

Unlike EP vs. AP comparison, hits obtained for V2-8 low drug screen were not accumulated around certain epigenetic complexes. *KEAP1* was a common hit in all drug-treated groups, and compared to other candidate vincristine sensitizers, KEAP1 was depleted with higher LFC and significance. Because of this reason, in addition to a few other genes relevant to MB and drug resistance in literature, KEAP1 was selected as the initial target of validation rounds (**Figure 3.37**).

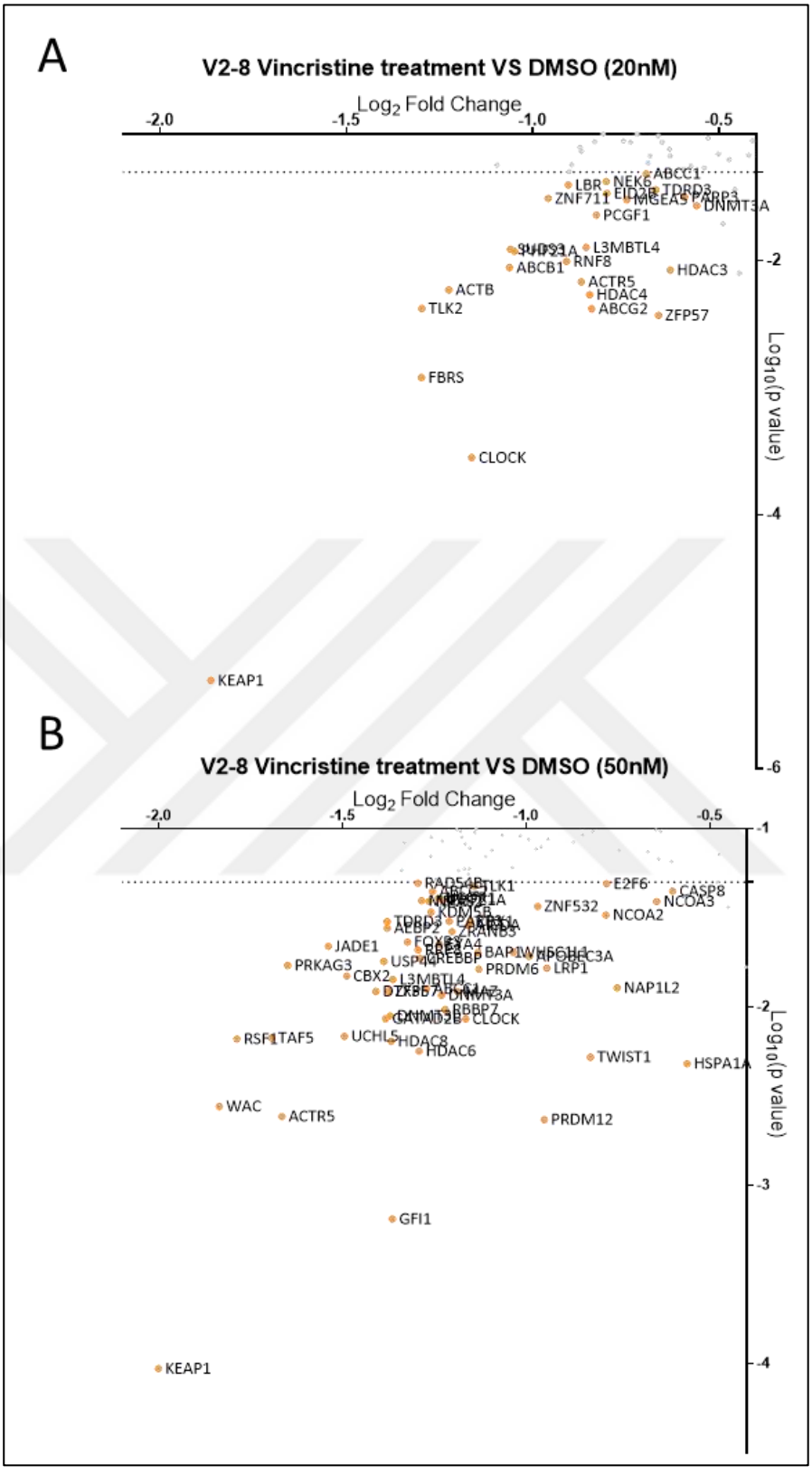


**Figure 3.36: Volcano plot showing EPIKOL screen results on V2-8 cells for treatment groups comparison**. A. 20 nM Vincristine treatment group. B. 50 nM vincristine treatment group. Only genes with $Log_2FC<-0.5$ and p-value <0.5 are shown. (*Karabiyik et al., unpublished).*

A

| M | 20 nM | 50 nM |
|---|---|---|
| ABCB1 | ABCB1 | ABCC1 |
| ACTR5 | ABCC1 | ABCG2 |
| CHD4 | ABCG2 | ACTR5 |
| E2F6 | ACTB | CBX2 |
| HAT1 | ACTR5 | CREBBP |
| HDAC4 | CLOCK | DNMT3A |
| HIF1AN | DNMT3A | DNMT3L |
| HMGB1 | EID2B | DTX3L |
| KDM1A | FBRS | E2F6 |
| KEAP1 | HDAC3 | GFI1 |
| NEK6 | HDAC4 | HDAC6 |
| PHF21A | KEAP1 | HDAC8 |
| PRMT2 | L3MBTL4 | HSPA1A |
| RAD54B | LBR | KDM5B |
| RCOR1 | MGEA5 | KEAP1 |
| RSF1 | NEK6 | PHF21A |
| SFPQ | PARP3 | RAD54B |
| SMARCE1 | PCGF1 | RBBP7 |
| SMYD2 | PHF21A | RSF1 |
| TAF5 | RNF8 | TAF5 |
| UCHL5 | SUDS3 | TDRD3 |
| USP44 | TDRD3 | TWIST1 |
| ZFP57 | TLK2 | UCHL5 |
| | ZFP57 | USP44 |
| | ZNF711 | ZFP57 |

B

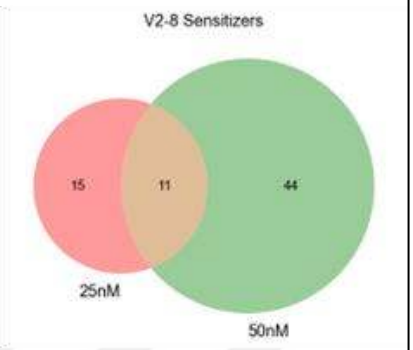


**Figure 3.37: Common hits of EPIKOL screen with low-dose vincristine on V2-8 cells.** Only genes with Log2FC<-0.5 and p-value <0.5 were included. (*Karabiyik et al., unpublished).*

On the first round of validation, cells transduced with sgRNA targeting *SFPQ* were highly depleted even in the absence of vincristine, showing a similar phenotype with positive control *RPL11* **(Figure 3.38 A).** Vincristine treatment showed further depletion of *SFPQ* sgRNA-transduced samples. Similarly, cells transduced with sgRNA targeting *SMARCE4* showed a depletion profile compared to the NT1 group, which was not as clear as positive control *RPL11*.

On the second round of validation, similar to the first round, NT1 and *RPL11* were used as negative and positive controls, respectively. In this round, sgRNAs targeting *ABCB1*, *CBP,* and *KEAP1* were used to validate candidate genes from low-dose drug

screens. Positive control *RPL11* showed better depletion in the second round than in the first round (**Figure 3.38 B**). While colonies were not distributed individually, an apparent reduction in all cells targeting sgRNAs was observed. *ABCB1* was also a significant control for this part of the study since vincristine is mainly transported from cytosol via *ABCB1*; depletion of both *CBP* and *KEAP1* samples, compared to NT1 sample similar to *ABCB1,* is a promising development. Similarly, on dual color competition assay, *ABCB1* and *RPL11* showed similar depletion profiles. Even though the depletion of *KEAP1* and *CBP* KO samples was not as aberrant as positive controls, apparent depletion was observed compared to the NT1 sample **(Figure 3.39)**.

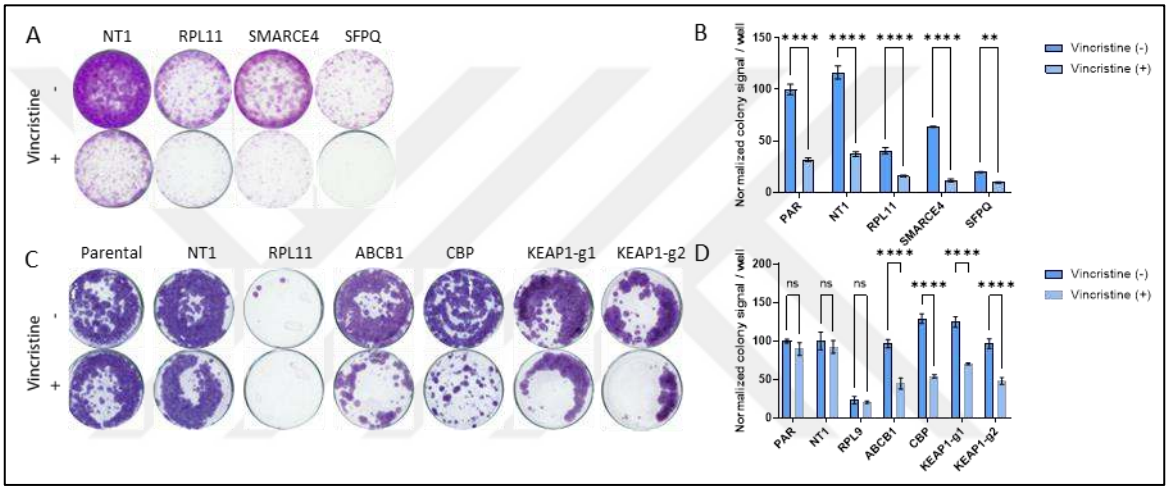


**Figure 3.38: Long term clonogenic assay results of selected hits from V2-8 Low dose Vincristine screen.** A, B. Results of the first round of validation for *SMARCE4* and *SFPQ*. C, D. Results of the second round of validation for *ABCB1*, *CBP*, and *KEAP1*. NT1 sgRNA was used as a negative control, while *RPL11* sgRNA was used as a positive control for both experiments. (*Karabiyik et al., unpublished).*

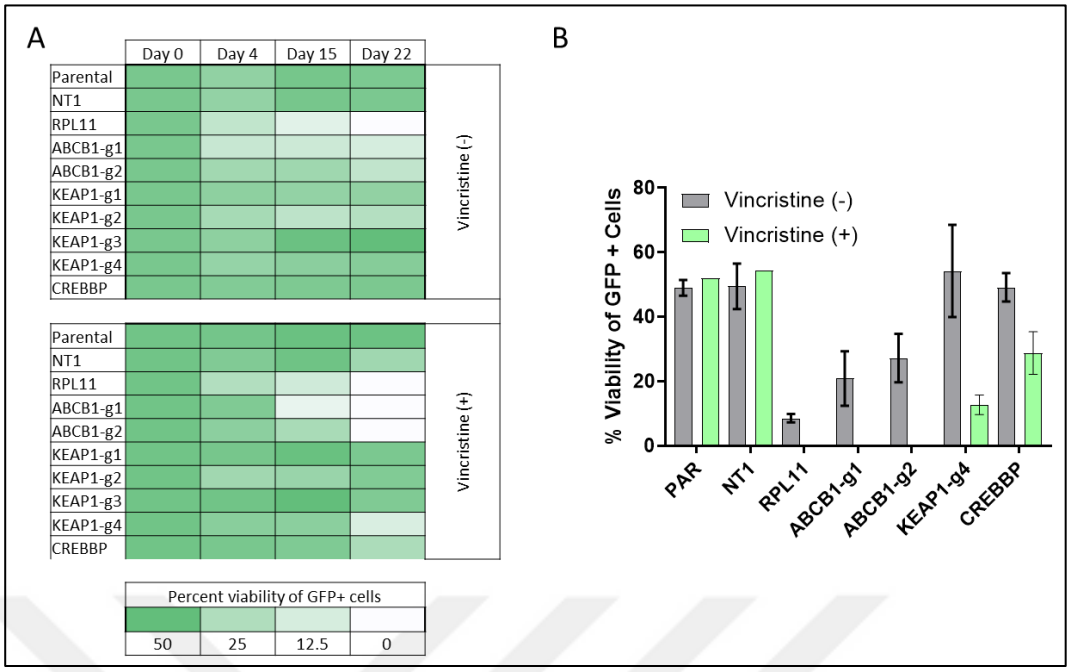


**Figure 3.39: Dual- Color Competition Assay.** A. Heatmap of the results with respect to GFP + cell percentage within the population. B. Bar graph of the day 22 showing depletion of GFP+ cells in the population compared to the control group (*Karabiyik et al., unpublished).*

## 3.4 Characterization of KEAP1 Knockout

To understand the cellular pathways regulated by KEAP1, we first examined RNA sequencing on cells that are either parental or resistant (V2-8). When compared with Daoy cells, significant difference in NRF2 target genes were observed in V2-8 cells (**Figure 3.40**). While NRF2 targets such as *SOD3*, *SOD2*, *HIF1A,* and *SLC7A11* were downregulated on the V2-8 cell line, other NRF2 targets such as *ABCC3*, *NES*, *NQO1* were upregulated compared to parental Daoy cell line. In addition, NRF2 expressing gene *NFEL2* was slightly downregulated, and *KEAP1* was upregulated on the V2-8 cell line, suggesting KEAP1/NRF2 dependent differential gene regulation on the V2-8 cell line (**Figure 3.40**).

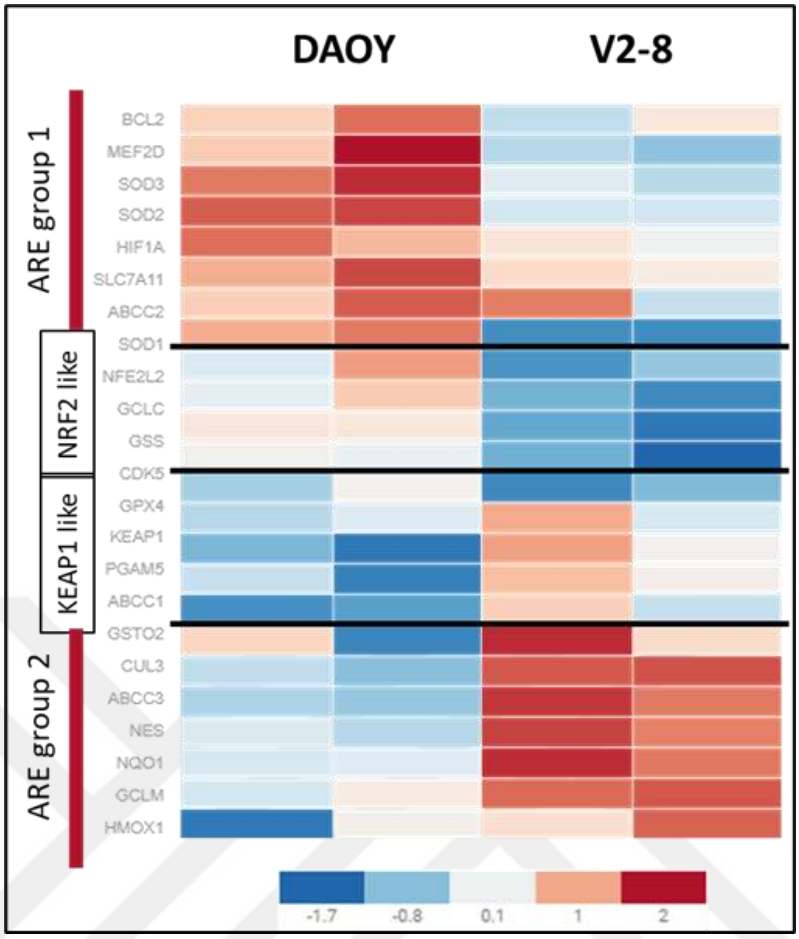


**Figure 3.40: Heatmap of RNAseq results of genes affected by KEAP1-NRF2 pathway (***Karabiyik et al., unpublished).*

### *3.4.1 Validation of the effect of KEAP1 Knockout on V2-8 cell line*

To further analyze the chemo-resistance regulation by KEAP1, we focused on V2-8 cells, and *KEAP1* and *ABCB1* KO cells were generated utilizing two sgRNAs from the EPIKOL library. On both RNA (**Figure** 3.41) and protein (**Figure 3.42)** levels, efficient KO of *KEAP1* and *ABCB1* has been shown. In addition, decreased *ABCA4* RNA expression, one of the top-upregulated ABC transporters, was also observed in *KEAP1* KO cells.

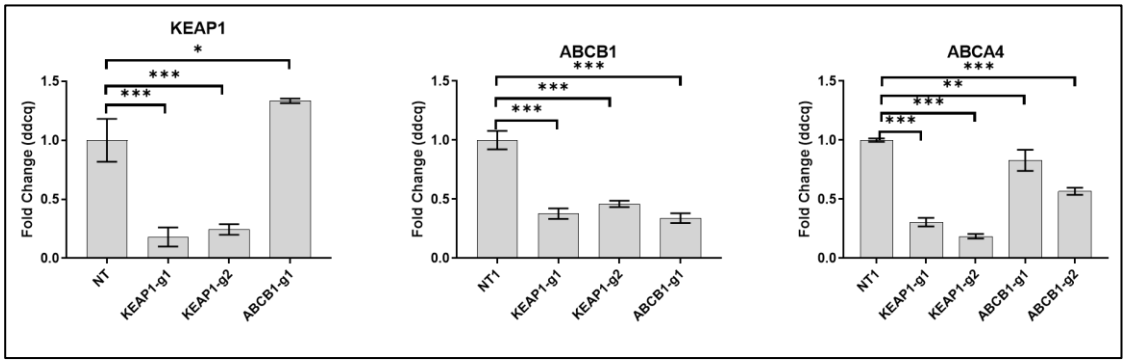


**Figure 3.41: KEAP1, ABCB1, and ABCA4 mRNA expression levels upon KEAP1 or ABCB1 KO.** Fold change was normalized to NT1 transduced samples. (*Karabiyik et al., unpublished).*

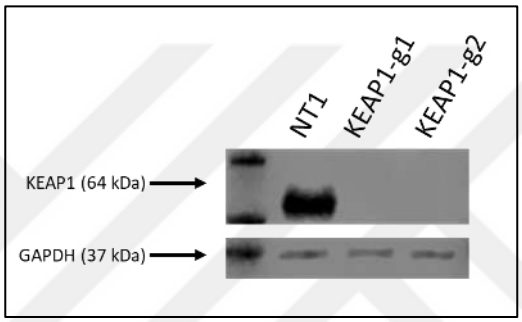


**Figure 3.42: Evaluation of KEAP1 protein expression on KEAP1 KO cells. (***Karabiyik et al., unpublished).*

Similarly, a significant decrease in cell viability on *KEAP1* KO cells compared to NT cells in the presence of vincristine was shown with MTT and long-term clonogenic assays (**Figure 3.43**). While on parental Daoy cells, *KEAP1* KO does not affect cell viability in comparison to control, on V2-8 cells, *KEAP1* KO showed a similar viability phenotype with *ABCB1* KO on around IC50 value (50 nM). Furthermore, a similar phenotype has been observed in the long-term clonogenic assay.

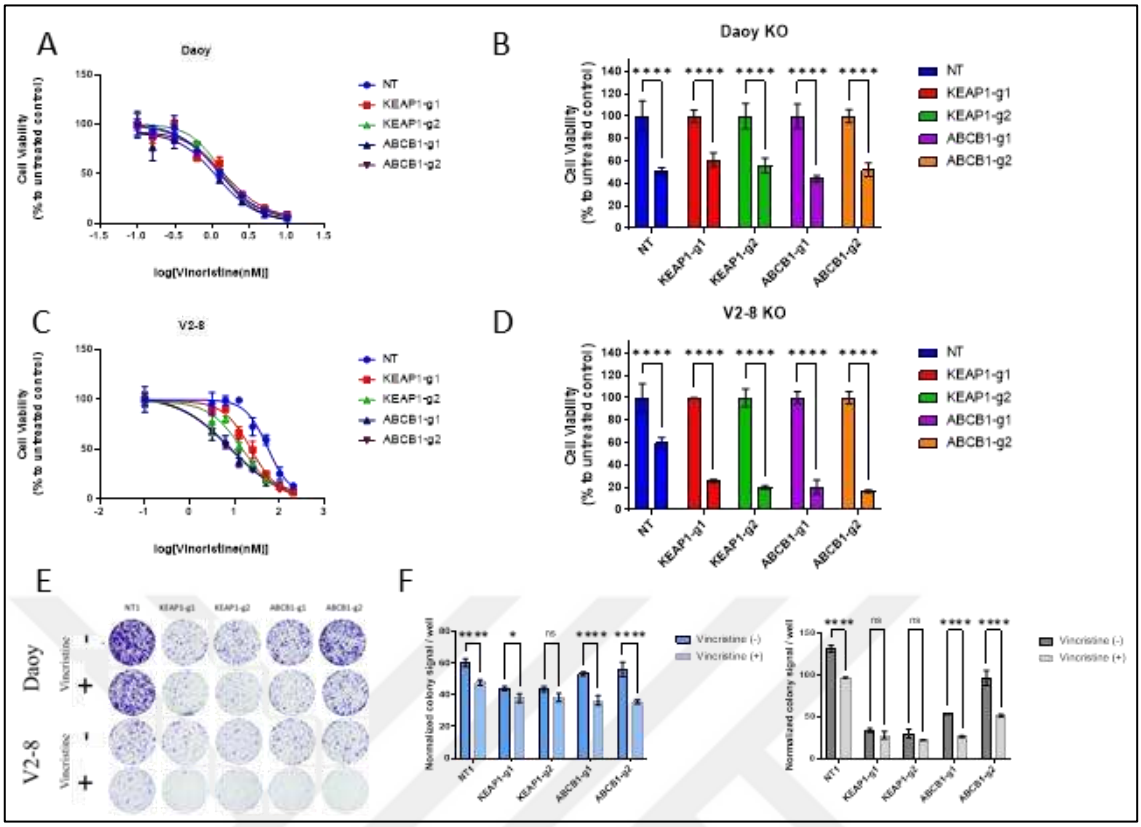


**Figure 3.43: Effect of KEAP1 KO on viability when treated with Vincristine.** A. IC50 curve of parental Daoy Cell line transduced with sgRNAs targeting NT1, KEAP1, or ABCB1. B. Simplified bar graph, comparing IC50 value of parental cell line (1 nM) to DMSO control. C. IC50 curve of vincristine resistant V2-8 cell line transduced with sgRNAs targeting NT1, KEAP1, or ABCB1. D. Simplified bar graph, comparing IC50 value of vincristine resistant V2-8 cell line (~50nM) to DMSO control. E. Long-term clonogenic assay for KEAP1 and ABCB1 knockout cells in response to vincristine. F. Quantification of long-term clonogenic assay (*Karabiyik et al., unpublished).*

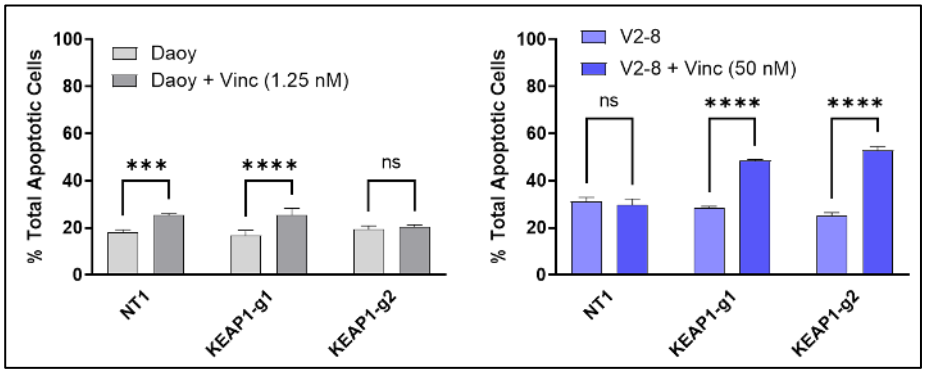


**Figure 3.44: Annexin V – Cell death assay on cells transduced with sgRNAs targeting KEAP1 showing increased early and late apoptotic cells on KEAP1-KO V2-8 cells.** A. Results of cell death assay on parental Daoy cell. B. Results of cell death assay on V2-8 cell line. (*Karabiyik et al., unpublished).*

Similarly, increased total apoptotic cell percentage on *KEAP1* KO V2-8 cells in response to vincristine was observed compared to NT1 transduced cells after 24 hours of incubation for both sgRNAs. No significant change was observed in *KEAP1* KO parental Daoy cells compared to their control cells on 24 hours of vincristine treatment (**Figure 3.44**).

### *3.4.2 Transcriptome analysis upon KEAP1 loss*

To investigate the impact of *KEAP1* on transcriptomic changes in the absence of *KEAP1*, Cas9-stable V2-8 cells were transduced with NT1, KEAP1-g1, or KEAP1-g2 sgRNAs in triplicates. RNA sequencing was performed on collected cells on PT Day 9 (Oxford, UK). Comparative analysis was conducted between KEAP1-g1 and NT1 as well as between KEAP1-g2 and NT1 samples.

PCA analysis revealed distinct clustering patterns among KEAP1 and NT samples, indicating distinct gene expression profile changes. Specifically, the KEAP1-g1 samples showed a close accumulation compared to the KEAP1-g2 samples, suggesting a higher similarity within this group. However, no complete separation was observed between the KEAP1-g1 and KEAP1-g2 samples on any principal components, indicating similarity between these groups.

In contrast, KEAP1-KO samples exhibited clear separation from the samples transduced with a non-targeting vector on PC1, which has a higher power of explaining variance, suggesting a distinct gene expression profile associated with KEAP1 KO.

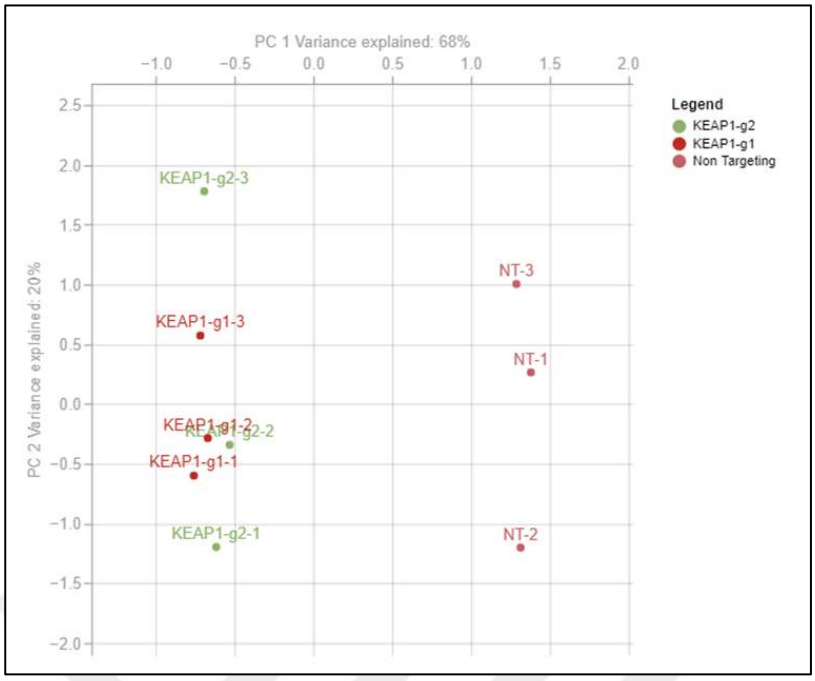


**Figure 3.45: Principal Component Analysis plot for RNAseq experiment on NT1, KEAP1-g1, or KEAP1-g2 transduced cells.**

Analysis showed that 1224 genes were significantly upregulated, and 1291 genes were significantly downregulated on KEAP1-g1 transduced cells, while 1248 genes were significantly upregulated, and 1234 genes were significantly downregulated on KEAP1-g2 transduced cells with cutoffs LFC<-1 and FDR<0.05. Of those, 996 were commonly upregulated, while 895 were commonly downregulated (**Figure 3.46**). *KEAP1* and *ABCB1* were significantly downregulated for both KO groups, similar to previous experiments and also as an internal control in the RNAseq experiment.

Moreover, several genes regulated by NRF2 were significantly upregulated compared to the control group, which was an expected result since KEAP1 is the negative regulator of NRF2, and in the absence of proteasomal degradation guided by KEAP1, NRF2 was expected to localize in the nucleus and activate transcription of genes with ARE elements in their regulatory regions (**Figure 3.47**).

GSEA report showed that 83 gene sets from all were significantly positively enriched with p value<1%, while 156 gene sets were significantly negatively enriched. Expectedly, the top positively enriched gene sets included genes that were regulated by NRF2 were positively enriched (**Figure 3.48**).

Similarly, several negatively enriched pathways were identified. Due to the downregulation of several histone variants, multiple negatively enriched gene sets were identified including GO genets GOMF_monocarboxylic_acid_binding, GOBP_cellular_ketone_metabolic_process, GOBP_xenobiotic_metabolic_process, in addition to Reactome gene-sets REACTOME_nuclear_events_mediated_by_nfe2l2, REACTOME_cellular_response_to_chemical_stress, REACTOME_keap1_nfe2l2_pathway.

Several negatively enriched gene sets included significantly downregulated histone variants such as GOCC_DNA_packaging_complex, GOCC_nucleosome, and GOCC_protein_DNA_complex (**Figure 3.49**). While several histone variants were identified as significantly downregulated, no change in the growth rate was observed.

Gene sets that had the highest negative enrichment scores were bmi1_dn_mel18_dn.v1_dn and mel18_dn.v1_dn, which were C6: Oncogenic Signature gene sets resulted from RNAi studies conducted on Daoy cells. Both gene sets were obtained by a study where BMI1 and PCGF2 genes were knocked down via RNAi.

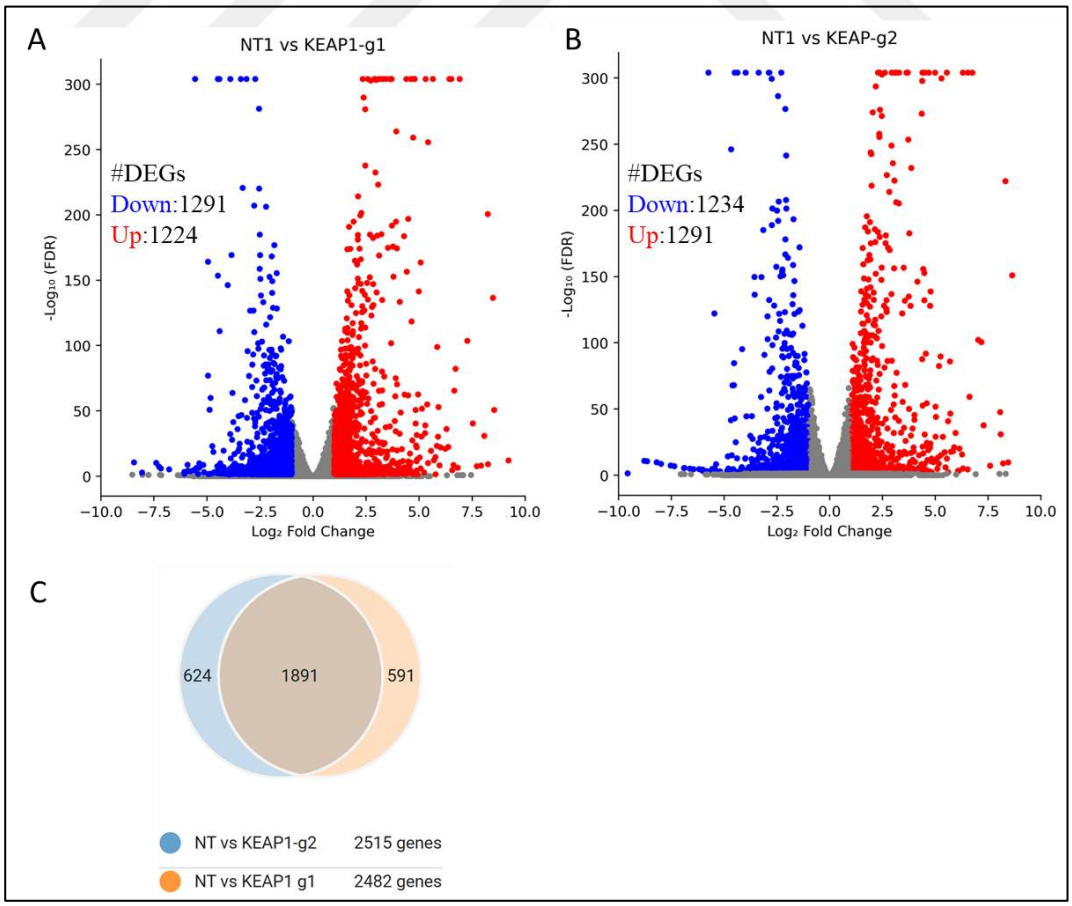

**Figure 3.46: RNA-seq analysis of KEAP1 KO compared to NT.** A. Volcano plot showing DEGS in KEAP1 KO with KEAP1-g1. B. Volcano plot showing DEGS in KEAP1 KO with KEAP1-g2. C. Common DEGs identified with both KEAP1-g1 and KEAP1-g2. D. Top 10 gene sets enriched in downregulated gene sets upon KEAP1 Knockout. (*Karabiyik et al., unpublished).*

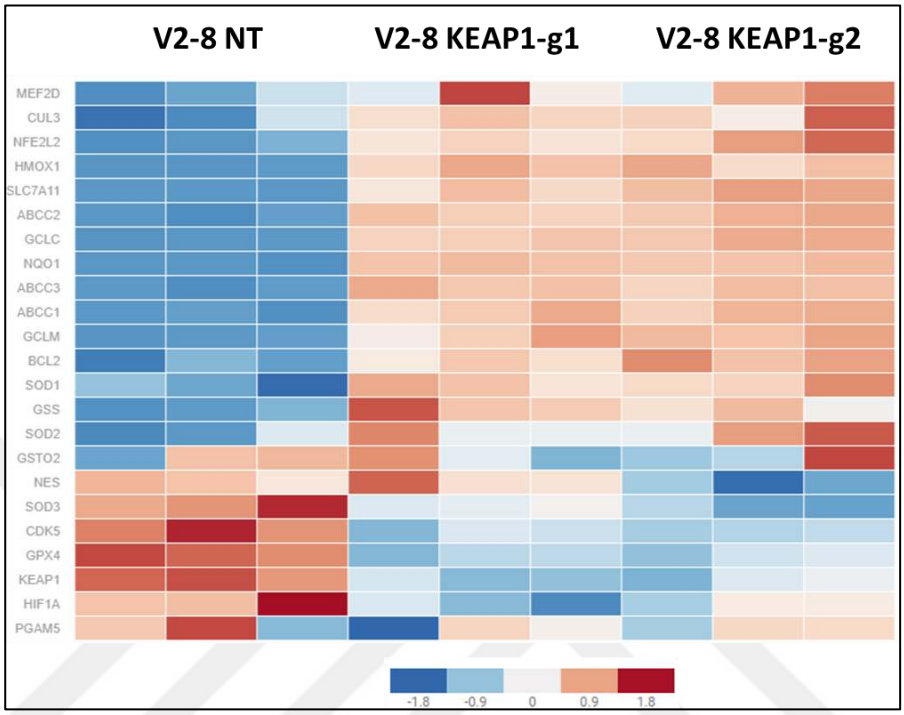


**Figure 3.47 Heatmap of RNAseq results of NRF2 targets on KEAP1 KO V2-8 cells.**

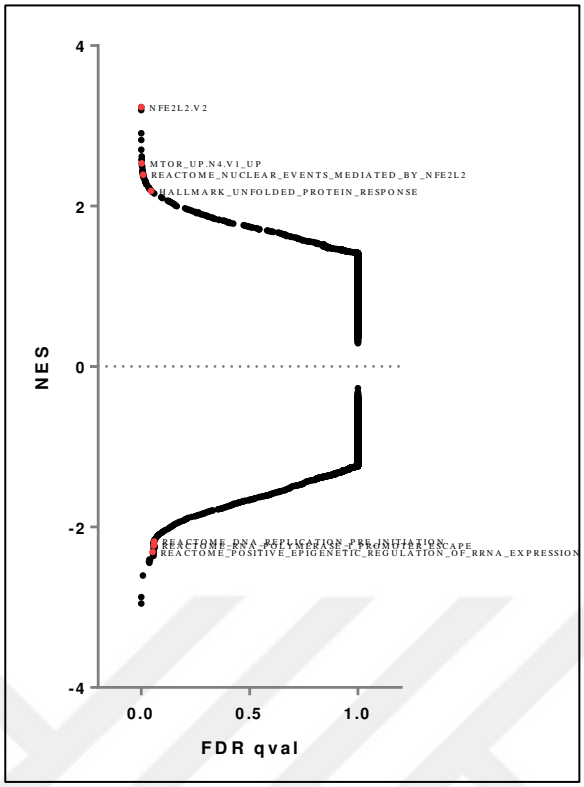


**Figure 3.48: NES score and FDR-qval values of GSEA analysis** in all differentially expressed genes for all gene sets available in MSigDB v 7.5. Relevant enriched genesets in both upregulated and downregulated populations were highlighted. (*Karabiyik et al., unpublished).*

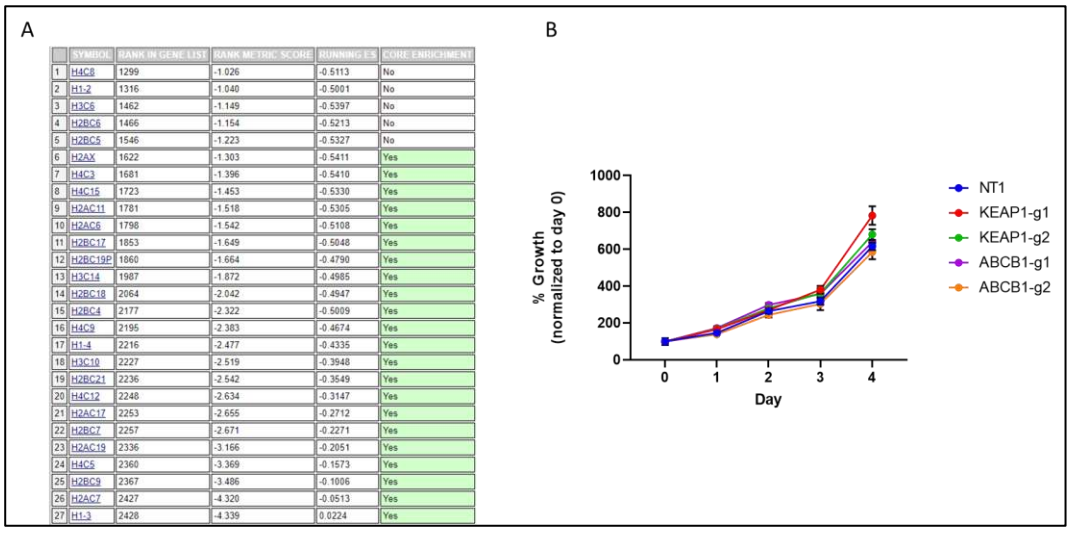


| | SYMBOL | RANK IN GENE LIST | RANK METRIC SCORE | RUNNING ES | CORE ENRICHMENT |
|---|---|---|---|---|---|
| 1 | H4C8 | 1299 | -1.026 | -0.5113 | No |
| 2 | H1-2 | 1316 | -1.040 | -0.5001 | No |
| 3 | H3C6 | 1462 | -1.149 | -0.5397 | No |
| 4 | H2BC6 | 1466 | -1.154 | -0.5213 | No |
| 5 | H2BC5 | 1546 | -1.223 | -0.5327 | No |
| 6 | H2AX | 1622 | -1.303 | -0.5411 | Yes |
| 7 | H4C3 | 1681 | -1.396 | -0.5410 | Yes |
| 8 | H4C15 | 1723 | -1.453 | -0.5330 | Yes |
| 9 | H2AC11 | 1781 | -1.518 | -0.5305 | Yes |
| 10 | H2AC6 | 1798 | -1.542 | -0.5108 | Yes |
| 11 | H2BC17 | 1853 | -1.649 | -0.5048 | Yes |
| 12 | H2BC19P | 1860 | -1.664 | -0.4790 | Yes |
| 13 | H3C14 | 1987 | -1.872 | -0.4985 | Yes |
| 14 | H2BC18 | 2064 | -2.042 | -0.4947 | Yes |
| 15 | H2BC4 | 2177 | -2.322 | -0.5009 | Yes |
| 16 | H4C9 | 2195 | -2.383 | -0.4674 | Yes |
| 17 | H1-4 | 2216 | -2.477 | -0.4335 | Yes |
| 18 | H3C10 | 2227 | -2.519 | -0.3948 | Yes |
| 19 | H2BC21 | 2236 | -2.542 | -0.3549 | Yes |
| 20 | H4C12 | 2248 | -2.634 | -0.3147 | Yes |
| 21 | H2AC17 | 2253 | -2.655 | -0.2712 | Yes |
| 22 | H2BC7 | 2257 | -2.671 | -0.2271 | Yes |
| 23 | H2AC19 | 2336 | -3.166 | -0.2051 | Yes |
| 24 | H4C5 | 2360 | -3.369 | -0.1573 | Yes |
| 25 | H2BC9 | 2367 | -3.486 | -0.1006 | Yes |
| 26 | H2AC7 | 2427 | -4.320 | -0.0513 | Yes |
| 27 | H1-3 | 2428 | -4.339 | 0.0224 | Yes |

**Figure 3.49: Negative enrichment of GO genesets including histone variants.** A. GSEA result of GOCC_DNA_Packaging_Complex geneset on KEAP1 KO V2-8 cells compared to NT1 transduced cells. B. Growth curve of KEAP1 and ABCB1 KO cells compared to NT1 transduced cells. (*Karabiyik et al., unpublished).*

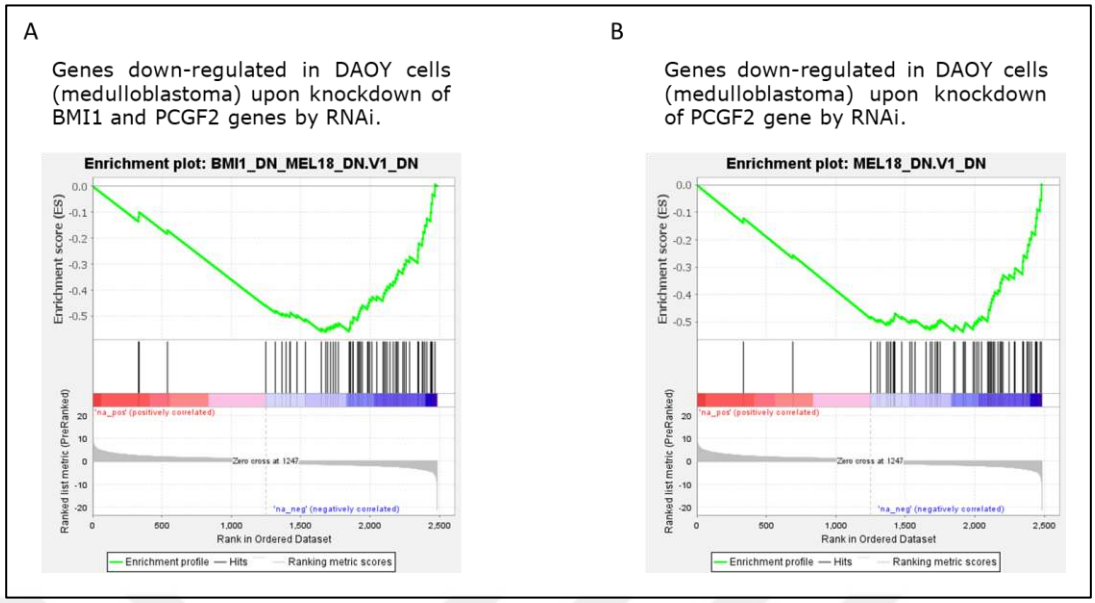


**Figure 3.50: GSEA Enrichment plots of top negatively enriched genesets.** A. BMI1_DN_MEL18_DN.V1_DN, B. MEL18_DN.V1_DN.

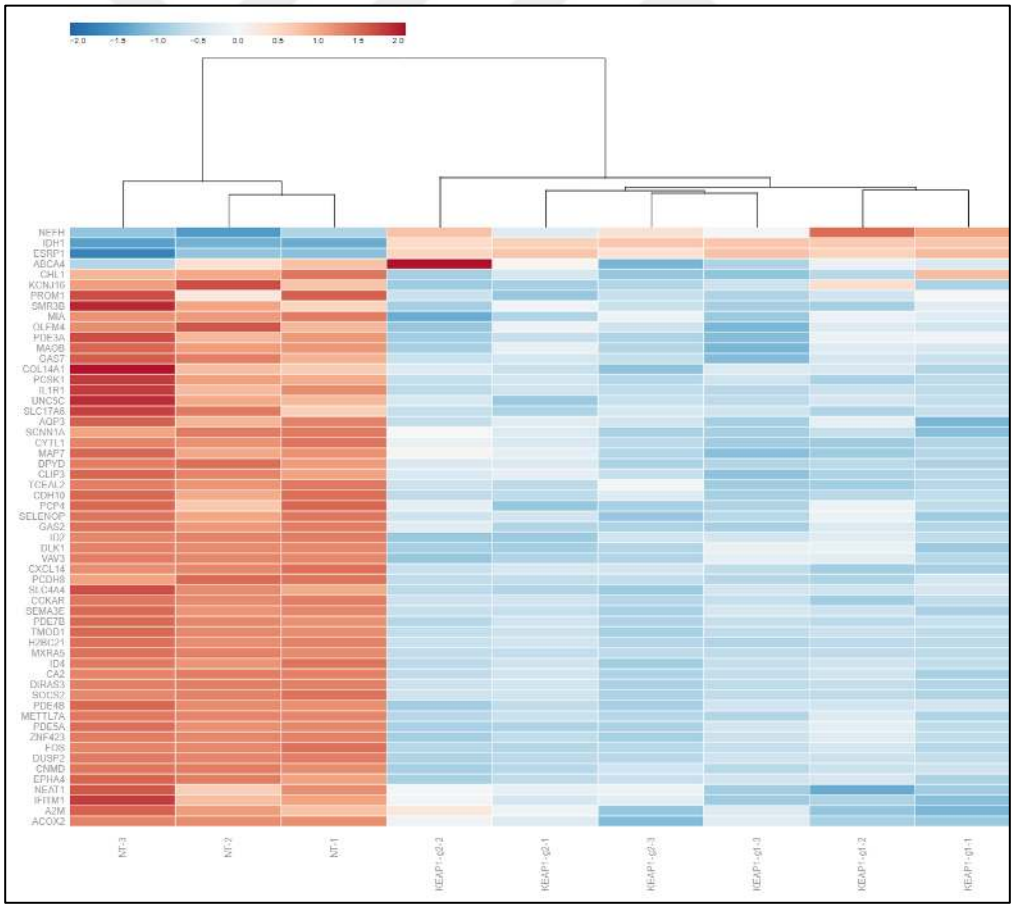

**Figure 3.51: Heatmap showing expression of genes within BMI_DN_MEL18_DN. V1_DN geneset.**

### 3.4.3 Effect of BMI1 on regulation of ABCB1

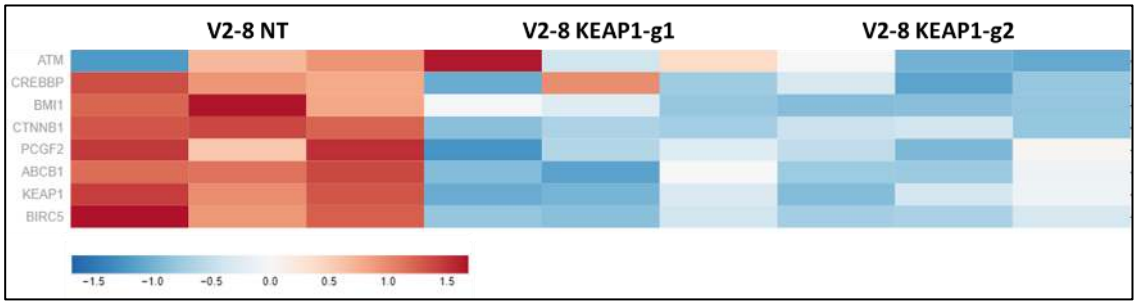


**Figure 3.52: Expression of selected genes related to BMI1 on KEAP1 KO V2-8 cell line.**

Expression of genes previously related downstream of *BMI1* was examined on KEAP1 KO V2-8 cells compared to NT1 transduced cells. Downregulation of genes such as *ATM*, *BIRC5*, and also proteins that were known to interact with BMI1 on the regulation of *ABCB1*, such as CBP, was shown. Furthermore, CTNNB1, which encodes β-Catenin and regulates BMI1 expression, was also downregulated on KEAP1 KO samples compared to NT1 transduced cells.

To better understand the relationship between BMI1 and KEAP1 on the regulation of *ABCB1*, *ABCB1* levels in *BMI1* knockout cells were examined. Two sgRNAs targeting *BMI1* from the EPIKOL library were used for the experiment. While BMI1-g2 was not able to significantly downregulate the expression of *BMI1*, significant downregulation of *BMI1* was observed on samples transduced with BMI1-g1. Similarly, a significant decrease in *ABCB1* levels was observed in the BMI1-g1 sample, while the same depletion was not observed in the BMI1-g2 sample.

To elucidate previous findings, the effect of BMI1 overexpression on KEAP1 knockout cells compared to control cells was examined in the presence of vincristine. Lenti_BMI1 vector was transduced into KEAP1 KO V2-8 cells, and cell viability in the presence of vincristine compared to NT1-BM1-OE was measured via CTG assay. A small but significant increase in survival was observed in the KEAP1-KO – BMI-OE sample compared to the control group. Suggesting

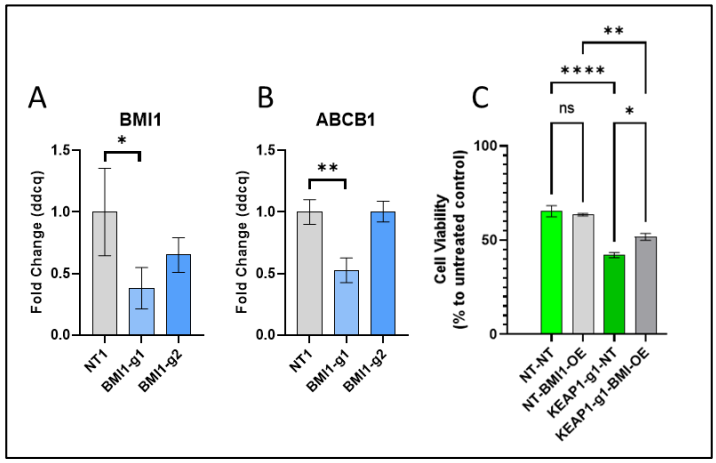


**Figure 3.53: Effect of BMI1 on downstream of KEAP1 regulating ABCB1 expression.** A, B. mRNA expression of *BMI1* and *ABCB1* upon *BMI1* Knockout. C. Cell viability of *KEAP1* KO cells with BMI overexpression. (*Karabiyik et al., unpublished).*

# 4 DISCUSSION

Medulloblastoma is the most common childhood brain tumor, accounting for approximately 20% of all cases, with the highest occurrence between ages 6 and 8. Recent cohort studies have identified four major subtypes of MB, each with distinct transcriptome and epigenome signatures mainly caused by disruptions in developmental pathways such as WNT and SHH. Patients exhibit diverse mutation patterns within subtypes with mutations in at least one chromatin modifier found in most cases, possibly influencing driver mutations on specific subtypes of MB.

While the 5-year survival rate for most MB subtypes exceeds 50%, more than 30% of the patients experience relapse. Furthermore, relapsed patients often develop acquired-drug resistance, posing a challenge for the application of traditional therapy approaches, resulting in a survival rate drop to 25%. Especially for patients with acquired drug resistance, understanding the mechanism of drug resistance and identifying novel targets to overcome drug resistance is crucial to developing new, targeted approaches for MB treatment.

In this thesis, we ultimately aimed to identify novel chromatin modifiers that can be targeted to sensitize vincristine-resistant medulloblastoma. To achieve this, we first utilized a chemical probe library to identify chromatin modifiers that can be targeted in combination with vincristine to induce cell death. We also identified bromodomain inhibitors to be adequate for this end. In a similar approach, we conducted CRISPR/Cas9-based epigenome-wide EPIKOL screens on vincristine resistant medulloblastoma cell lines compared to parental cell line. We identified KEAP1 as a novel target to overcome acquired drug resistance in medulloblastoma.

**Vincristine-resistant medulloblastoma cell lines show multidrug resistance characteristics.**

Drug resistance, especially in relapsed MB patients, has been commonly observed. To develop high-level laboratory models for drug-resistant MB for the study, the dose incrementation method was utilized on the medulloblastoma cell line Daoy cell line (McDermott et al., 2014). Vincristine, as the most commonly used chemotherapeutic

agent for most, if not all regimens, was chosen to establish drug-resistant models. Two vincristine-resistant cell lines, namely V1-10 and V2-8, were generated according to the initial and final doses of vincristine they received. Compared to the parental cell line, decreased growth rate and up to a hundred-fold resistance were observed via viability assays.

Resistance to vincristine was further confirmed with several functional assays and transcriptomic analyses. Compared to parental control, almost a thousand genes were differentially regulated, from this, *ABCB1*, the main efflux pump for vincristine, was one of the most significantly upregulated genes (Taylor et al., 2023). Additionally, the upregulation of several genes from ABC and SLC transporter families was observed, which was also confirmed with GSEA analysis.

Furthermore, negative enrichment on Reactome gene sets such as Cell cycle checkpoints and mitotic spindle checkpoints was observed on vincristine resistant V2-8 cells compared to parental cells. Since vincristine promotes apoptosis through M phase arrest, alteration of checkpoints on cell cycle progression could be advantageous for the progression of mitosis in a vincristine-resistant cell line (Visconti et al., 2016)

**Epigenetic probe screen on drug-resistant medulloblastoma cell line identified bromodomain inhibitors as sensitizers to vincristine.**

To identify epigenetic vulnerabilities and sensitizers of vincristine-resistant medulloblastoma, we conducted an epigenetic probe library screen on Daoy and V2-8 cells in the presence and absence of vincristine. We revealed distinct classes of hits for each comparison. HDACs, histone demethylases, and kinase inhibitors were identified as hits that induce cell death for both parental and resistant cell lines in the absence of vincristine. In contrast, bromodomain inhibitors and methyltransferase inhibitors were only found to be sensitizing drug-resistant V2-8 cell line to vincristine, as reported previously (Lokumcu, 2017).

Identified bromodomain inhibitors (SGC-CBP30, I-CBP112, PFI-4, OF-1, and NVS-CECR2) were further validated in combination with vincristine, showing apparent sensitization effect, specifically on vincristine-resistant V2-8 and V1-10 cells without adversely impacting cell viability when administered alone. Additionally, no significant

toxicity when administered alone or in combination with vincristine was observed on the parental cell line compared to untreated control. Specifically, SGC-CBP30 and I-CBP112 target bromodomains of two highly homologous transcriptional co-activators with active HAT domains, CBP and p300, also named KAT3A and KAT3B, respectively (Conery et al., 2016). While bromodomains are functional domains that recognize acetylated histone residues, they were shown to regulate the HAT activity of the CBP and p300 by facilitating protein-protein interaction (Chekler et al., 2015; Ghosh et al., 2016). Changes in the expression or regulation of these proteins have been reported to be linked with the development and advancement of hematological malignancies (Zhu et al., 2023). Similarly, CBP mutations have been detected in patients with SHH MB. However, the functional effect of those mutations in relation to driver mutations of MB has not been identified yet (Merk et al., 2018; Northcott et al., 2017). Moreover, Bromodomain and BET inhibitors targeting BRD4 were previously shown to affect SHH and Group 3 MB, where inhibition of BRD4 was shown to inhibit downstream signaling of SHH and MYC pathways (Henssen et al., 2013; Tang et al., 2014).

Inhibition of CBP/p300 bromodomain with SGC-CBP30 sensitized V2-8 cells to vincristine, which was confirmed with various viability and apoptosis assays. Furthermore, inhibition of bromodomain of CBP/p300 via SGC-CBP30 caused downregulation of sixty-six genes that were specifically upregulated on V2-8 cells compared to parental cells, including several ABC and SLC family transporters such as *ABCA4*, *ABCC3*, *SLC4A4*, and *SLC14A1* which was further confirmed with negative enrichment of KEGG ABC transporters upon SGC-CBP30 treatment. However, significant *ABCB1* downregulation was not observed in V2-8 cells. Despite that, inhibition of SGC-CBP30 administration on V2-8 cells showed a similar effect with verapamil, an MDR inhibitor, on the Calcein-AM assay. Finally, Knockout of *CBP* or *ABCB1* showed a similar sensitization effect with the long-term clonogenic assay.

In a recent study, I-CBP112, a chemical inhibitor targeting CBP/p300, was utilized in triple-negative breast cancer, lung cancer, and hepatic cancer cell lines and shown to significantly downregulate ABC transporters, particularly *ABCC1* and *ABCC10* compared to the untreated group. When combined with chemotherapeutic agents like doxorubicin, etoposide, and cisplatin, inhibition of CBP/p300 demonstrated synthetic lethality. They proposed that I-CBP112 works via enhanced acetylation and inhibition of

recruitment of *LSD1* (Strachowska et al., 2021). Our study identified increased H3K27ac and p300 occupation on promoters of upregulated transporters ABCC3, ABCA4, and SLCA14A1 via ChIP-qPCR. Unlike I-CBP112, SGC-CBP30 was shown to not increase acetylation levels in the targeted domain (Zucconi et al., 2016). Similarly, our study showed that administration of SGC-CBP30 decreased total H3K27ac levels on the V2-8 cell line. In contrast to the I-CBP112 treatment, we showed that the sensitization effect was specific to vincristine-resistant cell lines, while the parental cell line was unaffected. Furthermore, the H3K27ac mark is significantly reduced to the parental level on ABCC3 and ABCA4 shown with ChIP-qPCR.

Since the introduction of JQ1, the pioneering inhibitor targeting the bromodomain and extra-terminal domain, Bromodomain and BET inhibitors have been studied thoroughly due to their identified functions in several human diseases (Kulikowski et al., 2021; Nicodeme et al., 2010). More recently, with the notable success of pre-clinical studies involving BET inhibitors, more than 20 clinical trials have been conducted with probes targeting BET for multiple solid and hematological cancer types. However, a lack of complete understanding of the mechanism of action, alongside challenges related to optimal dosing, has surfaced as limiting factors (Ameratunga et al., 2020; Shorstova et al., 2021).

Additionally, given the complexity of the chemical compounds used in the studies, it is essential to investigate off-target interactions extensively. A recent study, which utilized a chemical probe library in combination with diverse anticancer compounds, identified a direct interaction of one of the bromodomain inhibitors, PFI-4, with ABGG2. This interaction, not the inhibition of the bromodomain by PFI-4, potentiated the effectiveness of the anticancer agent. Similarly, a deeper exploration of the off-target effects of SGC-CBP30 should be conducted (Barghout et al., 2022)

Together, our findings suggest that targeting the bromodomain of CBP/P300 thereby inhibiting the activation of downstream genes, including responsible drug transporters **(Figure 4.1).** While this approach currently offers combination treatment with the chemotherapeutic agent vincristine, targeting bromodomains holds promising prospects, especially for relapsed patients with acquired drug resistance. Due to the lack of better therapeutic approaches for those patients, inhibition of MDR via epigenetic

machinery might be utilized to develop new therapeutic approaches.

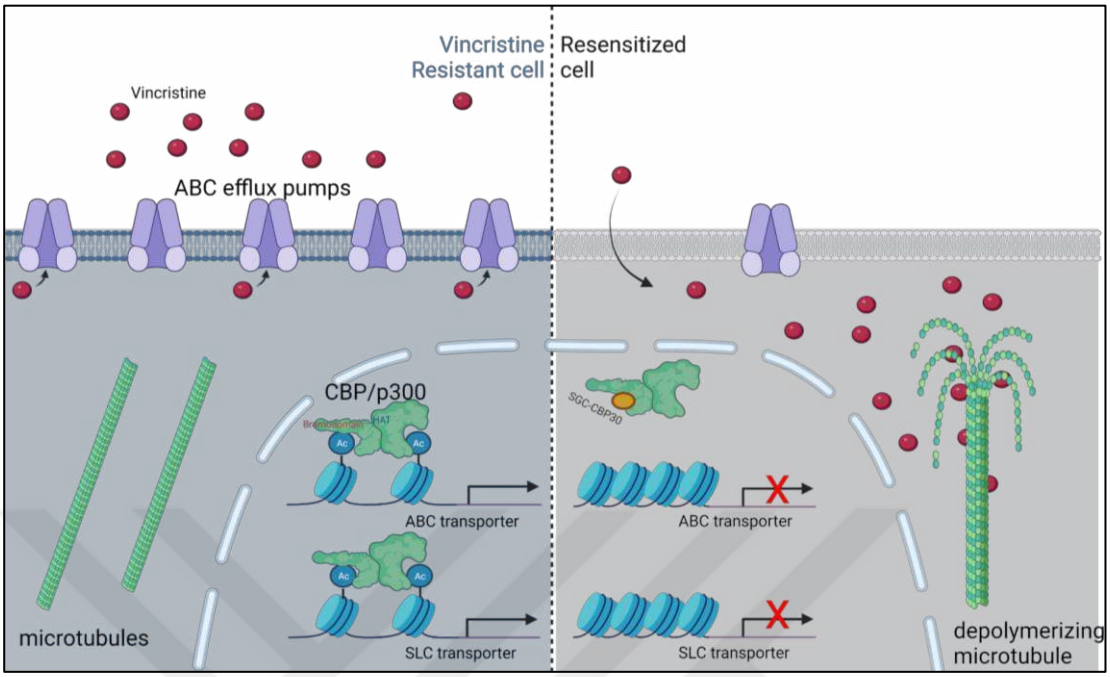


**Figure 4.1: Proposed model for regulation of vincristine resistance by CBP/p300.** Increased activity of CBP/p300 on ABC and SLC transporters such as ABCC3, ABCA4, and SLC14A4 led to increased expression of efflux pumps and acquired drug resistance against vincristine. With the inhibition of the bromodomain of CBP/p300, HAT activity, thus activation of efflux pumps, is decreased, and cells are sensitized to vincristine. Figure created in biorender.com.

**EPIKOL screen identified fitness genes on drug-resistant medulloblastoma cell lines.**

To further investigate epigenetic vulnerabilities of medulloblastoma and the effect of chromatin modifiers on chemotherapy resistance, we utilized EPIKOL screens on parental and vincristine-resistant medulloblastoma cell lines, Daoy, V1-10, and V2-8 in the presence and absence of vincristine. Initially, we repeated the optimization experiments conducted previously for EPIKOL (Ozlem Yedier-Bayram et al., 2022). After confirmation of normal representation of sgRNAs, parental cells were screened with EPIKOL in the presence and absence of vincristine. While the expected depletion of sgRNAs targeting essential genes was confirmed, non-targeting sgRNAs were represented equally in AP and EP groups, supporting the validity of the screen. In addition, in the low-dose vincristine treatment group, *ABCB1* emerged as the top sensitizer gene, providing strong validation for the EPIKOL screen. ABCB1 functions as

the primary transporter responsible for the efflux of vincristine, and although high expression of *ABCB1* in Daoy cells was unexpected (Othman et al., 2014), continued exposure to low-dose vincristine during screening may have induced *ABCB1* expression leading to the selection of the population (Sabnis et al., 2019). Consequently, cells transduced with sgRNAs targeting *ABCB1* were depleted during the screen.

By utilizing the EPIKOL screen on vincristine-resistant cell lines, we aimed to both understand chromatin modifiers that can be targeted to induce cell death even in the absence of vincristine, thus, identify chromatin regulators that regulate the fitness of drug-resistant cells and chromatin modifiers that can be targeted to sensitize cells to vincristine. For both cell lines, we observed good depletion profiles for each treatment group compared to AP when compared to depletion profiles of parental cell line.

The initial validations of the V1-10 essentiality screen revealed three distinct hit genes, which were previously found to be upregulated in medulloblastoma and identified to be crucial for stemness. Notably, the depletion of sgRNAs targeting members of the COMPASS complex was observed in the essentiality screen on V1-10 cells compared to the AP group. The COMPASS complex plays a significant role in regulating H3K4 methylation, an active transcription mark especially critical for establishing enhancer identity, leading differentiation, and development (Fagan & Dingwall, 2019; Ford & Dingwall, 2015). Mutations in KMT members of the COMPASS complex, specifically *MLL2* and *MLL3,* were previously identified in the SHH subtype of MB, inhibiting differentiation and persistence of stemness (Robinson et al., 2012). Similarly, *HCFC1* and *WDR82* were identified as hits in this screen, were previously found to be mutated in MB, and were also listed in DepMap,

Another COMPASS complex hit identified from the essentiality screen was *ASH2L*, which has been associated with drug resistance. In Hodgkin's lymphoma and testicular cancers, inhibition of *ASH2L* sensitized cancer cells to chemotherapeutic agents like etoposide and cisplatin. Additionally, in triple-negative breast cancer, *ASH2L* was found to be involved in migration and metastasis (Batbayar et al., 2023; Constantin & Widmann, 2020). Furthermore, the screen identified Retinoblastoma-binding protein 4 (*RBBP4*) as a hit. *RBBP4* was shown to be upregulated in embryonal cancers, including medulloblastoma and has been shown to regulate the cell cycle, especially for neural

precursors (Schultz-Rogers et al., 2022).

Similarly, on the V2-8 essentiality screen, hits from COMPASS and SWI/SNF complex members were identified. Moreover, two genes previously genes previously studied in the medulloblastoma context and recognized as pan-cancer essential genes in DepMap, namely, *TOP2A* (Zhang et al., 2022) and *PPP4C* (Liao et al., 2020), were shown to affect the fitness of V2-8 cells.

**EPIKOL screen on drug-resistant cell lines validated CBP/p300 as a target to sensitize against vincristine.**

Low-dose EPIKOL screening on drug-resistant cell lines was conducted to identify genes that can be targeted to sensitize against vincristine. To pinpoint genes that sensitize those cells to different doses of vincristine, three different doses of vincristine were utilized throughout the screen, selected specifically for V1-10 and V2-8 cell lines. While MaGECK output confirmed the validity of the screen via depletion of sgRNAs targeting ribosomal genes included in the library, the representation of non-targeting sgRNAs did not change compared to AP. Additionally, sgRNAs targeting ABC transporters, most importantly *ABCB1*, were also depleted for both cell lines, further validating the screen results.

Genes identified as sensitizers for the V1-10 cell line showed less similarity within groups compared to the V2-8 cell line, where sensitizers showed commonality within different treatment groups. CBP was also identified as a hit from the low-dose EPIKOL screen on the V2-8 cell line, while significant depletion on sgRNAs targeting p300 was not detected. Targeting CBP with sgRNAs shown to be depleted in screen also confirmed the sensitization effect, further supporting probe library screen on the same cell lines.

**EPIKOL screen on V2-8 vincristine resistant cell line reveals KEAP1 as a target to overcome drug resistance.**

*KEAP1* was identified as a hit from all vincristine treatment groups compared to the EP group on the V2-8 cell line. It was notably separated from other hits with its high LFC and highly significant p-value (**Figure 3.36**). KEAP1 works as the negative regulator of NRF2 on the protein level as an adaptor protein for the E3 ubiquitin ligase

complex, which regulates the antioxidant response mechanism in the presence of ROS or electrophiles (Kobayashi et al., 2004). Several downstream targets of the KEAP1/NRF2 pathway were identified to be differentially regulated on V2-8 cells compared to parental cells, which also supports the possible role of the path on drug resistance.

While NRF2 is the main target of KEAP1, recent studies showed that KEAP1 has several other interacting partners regulating several different biological processes (Y. Zhang et al., 2020). NRF2 interacts with KEAP1 homodimer with two motifs on the Neh2 domain, namely DLG and ETGE. While the interaction of NRF2 with KEAP1 on the DLG motif is weaker, it is more affected by the conformational change of KEAP1 upon exposure to ROS. Most of the identified substrates of KEAP1 interact with the ETGE motif, which is more potent. From those, Nestin is a class IV intermediate filament, extensively expressed in neural progenitors and positively regulated by NRF2 signaling, which also further activates NRF2 signaling via inhibition of KEAP1-NRF2 interaction (Liu et al., 2022). Significant upregulation of Nestin on V2-8 cells compared to parental cell line was observed.

While loss-of-function mutations, especially on lung and head and neck cancers, have been shown to cause drug resistance due to activation of cytoprotective genes (Islam et al., 2022; Taguchi et al., 2011) KEAP1-KO on V2-8 cells showed significant downregulation in ABC transporters such as *ABCB1* and *ABCA4*, leading sensitization to vincristine and increased apoptosis in our study. However, the knockout of *KEAP1* did not affect parental cell survival. To confirm those findings further, a rescue assay should be conducted by presentation of full-length PAM mutant KEAP1.

Transcriptomic analysis in KEAP1-KO V2-8 cells with two sgRNAs from EPIKOL showed significant differential regulation of around 2000 genes where 95% were mutual, which was expected since downregulation of KEAP1 is expected to constitutively activate NRF2 signaling, which regulates about 2000 genes directly or indirectly through ARE elements on their promoters (McCord et al., 2023). Expectedly, gene sets regulated by NRF2 were positively enriched on GSEA analysis, however, NRF2 targets such as *SOD3*, *GPX4*, and *HIF1α* were downregulated, following a similar pattern shown on RNAseq on V2-8 compared to the parental cell line where some of the NRF2 targets were upregulated while some were downregulated. Interestingly, several histone

proteins were downregulated, which led to the negative enrichment of several gene sets containing those histone proteins. However, no significant change in growth rate in KEAP1-KO cells compared to NT cells was observed on the V2-8 cell line.

**Loss of KEAP1 on vincristine resistant MB cells downregulates BMI1 target genes.**

The top negatively enriched gene sets were from a study where two genes that were known to promote tumorigenesis on medulloblastoma, namely, *BMI1* and *PCGF2,* were knocked down by RNAi on medulloblastoma cell line Daoy (Wiederschain et al., 2007). Genes that were downregulated upon knockdown of BMI1 and PCGF2 in that study were also downregulated on KEAP1-KO V2-8 cells. BMI1 is a part of Polycomb repressive complex 1 (PRC1), which has been associated with the preservation of stemness and reported to be associated with poor prognosis in relapsed medulloblastoma (Bakhshinyan et al., 2019). Additionally, BMI1 was shown to be important for cerebellar development where BMI1 loss leads to severe problems, including hematopoietic and skeletal defects in addition to disorders in balance and behavioral abnormalities in developing mice resulting from defects in cerebellar development (Leung et al., 2004; van der Lugt et al., 1994). Similarly, gene amplification or overexpression of BMI1 has been identified in various cancers, including lung, breast, and B-cell lymphoma. Moreover, depletion of BMI1 via shRNA was shown to adversely affect medulloblastoma cell growth and survival (Wiederschain et al., 2007). Also, chemical inhibition of BMI1 on the xenograft Group 3 MB model was shown to eliminate the tumor completely, providing further evidence of the effect of BMI1 on MB tumorigenesis and development (Bakhshinyan et al., 2019).

Furthermore, *BMI1* has also been studied in a drug-resistant context. Silencing *BMI1* on prostate cancer cells led to sensitization to docetaxel, a drug that inhibits microtubule polymerization. Interestingly, upon silencing of BMI1, KEAP1 was upregulated in the same study (Crea et al., 2011). Conversely, overexpression of BMI1 on B-cell lymphoma has been associated with resistance to etoposide and oxaliplatin through stabilization of survivin (BIRC5) (Bhattacharyya et al., 2012). In addition to that, even though BMI1 has been linked to a repressive PRC1 complex, it has been shown to interact with E-box elements on the promoter of the *ABCB1* gene, inducing its activation via recruiting KAT5 histone acetyltransferase (Banerjee Mustafi et al., 2016).

KEAP1-KO V2-8 cells showed downregulation on BMI1 target genes such as BIRC5 and ABCB1. Additionally, while KO of BMI1 on V2-8 cells resulted in decreased *ABCB1* expression, supporting our hypothesis, overexpression of BMI1 on KEAP1-KO slightly but significantly increased survival in the presence of vincristine, compared to the KEAP1-KO sample. While direct interaction of KEAP1 with BMI1 has not been reported, KEAP1 might be indirectly regulating the function of BMI.

Together, our findings suggest that targeting KEAP1 on the vincristine-resistant medulloblastoma cell line leads to the downregulation of ABCB1 and, thus, sensitization of drug-resistant cells (**Figure 4.2**). According to GSEA analysis, KEAP1 might be regulating the downregulation of *ABCB1* through the regulation of BMI1. These findings offer a novel role of KEAP1 in the regulation of vincristine resistance.

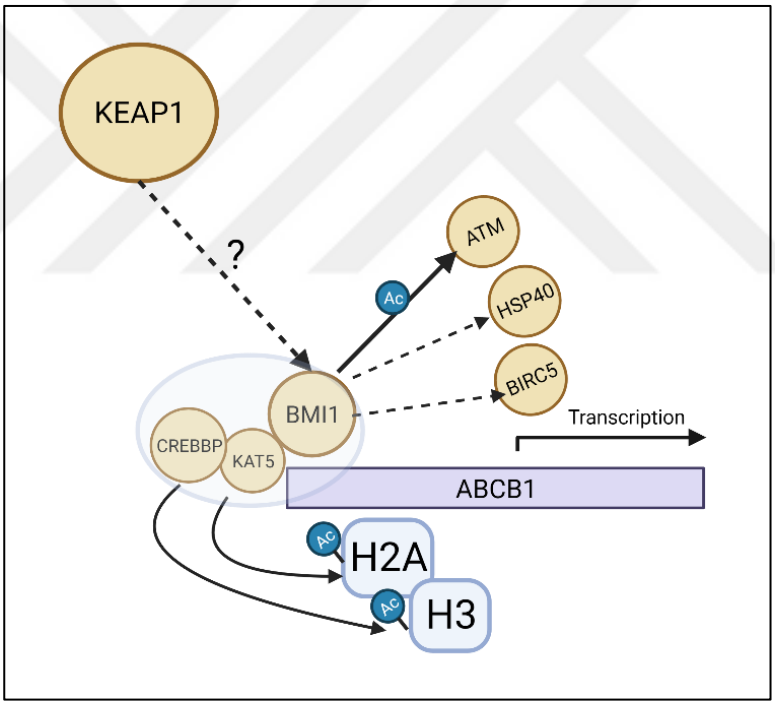


**Figure 4.2: Proposed model for regulation of vincristine resistance by KEAP1.** Inhibition of KEAP1 has been shown to downregulate ABCB1, the primary transporter of vincristine, potentially through regulation of BMI1. Our research demonstrated a negative enrichment of BMI1 targets upon knockout of KEAP1. While BMI1 is known to function in a transcriptional repressor PRC1 complex, its involvement in the activation of *ABCB1* has been shown through the recruitment of KAT5. Figure created in biorender.com.

# BIBLIOGRAPHY

AbdelBaki, M. S., Boue, D. R., Finlay, J. L., & Kieran, M. W. (2018). Desmoplastic nodular medulloblastoma in young children: a management dilemma. *Neuro Oncol*, *20*(8), 1026-1033. https://doi.org/10.1093/neuonc/nox222

Ameratunga, M., Brana, I., Bono, P., Postel-Vinay, S., Plummer, R., Aspegren, J., Korjamo, T., Snapir, A., & de Bono, J. S. (2020). First-in-human Phase 1 open-label study of the BET inhibitor ODM-207 in patients with selected solid tumours. *Br J Cancer*, *123*(12), 1730-1736. https://doi.org/10.1038/s41416-020-01077-z

Ansbro, M. R., Shukla, S., Ambudkar, S. V., Yuspa, S. H., & Li, L. (2013). Screening compounds with a novel high-throughput ABCB1-mediated efflux assay identifies drugs with known therapeutic targets at risk for multidrug resistance interference. *PLoS One*, *8*(4), e60334. https://doi.org/10.1371/journal.pone.0060334

Bakhshinyan, D., Venugopal, C., Adile, A. A., Garg, N., Manoranjan, B., Hallett, R., Wang, X., Mahendram, S., Vora, P., Vijayakumar, T., Subapanditha, M., Singh, M., Kameda-Smith, M. M., Qazi, M., McFarlane, N., Mann, A., Ajani, O. A., Yarascavitch, B., Ramaswamy, V., . . . Singh, S. K. (2019). BMI1 is a therapeutic target in recurrent medulloblastoma. *Oncogene*, *38*(10), 1702-1716. https://doi.org/10.1038/s41388-018-0549-9

Bandopadhayay, P., Bergthold, G., Nguyen, B., Schubert, S., Gholamin, S., Tang, Y., Bolin, S., Schumacher, S. E., Zeid, R., Masoud, S., Yu, F., Vue, N., Gibson, W. J., Paolella, B. R., Mitra, S. S., Cheshier, S. H., Qi, J., Liu, K. W., Wechsler-Reya, R., . . . Cho, Y. J. (2014). BET bromodomain inhibition of MYC-amplified medulloblastoma. *Clin Cancer Res*, *20*(4), 912-925. https://doi.org/10.1158/1078-0432.CCR-13-2281

Banerjee Mustafi, S., Chakraborty, P. K., Naz, S., Dwivedi, S. K., Street, M., Basak, R., Yang, D., Ding, K., Mukherjee, P., & Bhattacharya, R. (2016). MDR1 mediated chemoresistance: BMI1 and TIP60 in action. *Biochim Biophys Acta*, *1859*(8), 983-993. https://doi.org/10.1016/j.bbagrm.2016.06.002

Barghout, S. H., Mann, M. K., Aman, A., Yu, Y., Alteen, M. G., Schimmer, A. D., Schapira, M., Arrowsmith, C. H., & Barsyte-Lovejoy, D. (2022). Combinatorial Anticancer Drug Screen Identifies Off-Target Effects of Epigenetic Chemical Probes. *ACS Chem Biol*, *17*(10), 2801-2816. https://doi.org/10.1021/acschembio.2c00451

Batbayar, G., Ishimura, A., Lyu, H., Wanna-udom, S., Meguro-Horike, M., Terashima, M., Horike, S.-i., Takino, T., & Suzuki, T. (2023). ASH2L, a COMPASS core subunit, is involved in the cell invasion and migration of triple-negative breast cancer cells through the epigenetic control of histone H3 lysine 4 methylation. *Biochemical*

*and Biophysical Research Communications*, *669*, 19-29. https://doi.org/https://doi.org/10.1016/j.bbrc.2023.05.061

Batora, N. V., Giese, M., Sieber, L., Pfister, S. M., Bardwell, V., Kawauchi, D., & Northcott, P. A. (2015). TMOD-01: BCOR IS A NOVEL TUMOR SUPPRESSOR GENE IN SHH-DRIVEN MEDULLOBLASTOMA. *Neuro-Oncology*, *17*(Suppl 5), v226-v226. https://doi.org/10.1093/neuonc/nov237.01

Batora, N. V., Sturm, D., Jones, D. T., Kool, M., Pfister, S. M., & Northcott, P. A. (2014). Transitioning from genotypes to epigenotypes: why the time has come for medulloblastoma epigenomics. *Neuroscience*, *264*, 171-185. https://doi.org/10.1016/j.neuroscience.2013.07.030

Baylin, S. B., & Jones, P. A. (2011). A decade of exploring the cancer epigenome - biological and translational implications. *Nat Rev Cancer*, *11*(10), 726-734. https://doi.org/10.1038/nrc3130

Bernal, A., & Arranz, L. (2018). Nestin-expressing progenitor cells: function, identity and therapeutic implications. *Cell Mol Life Sci*, *75*(12), 2177-2195. https://doi.org/10.1007/s00018-018-2794-z

Bernstock, J. D., Cohen, J. L., Singh, S., Schlappi, C. W., Fiveash, J. B., Johnston, J. M., Fequiere, P., Orr, B. A., Li, R., & Friedman, G. K. (2019). Treatment-induced remission of medulloblastoma using a chemotherapeutic regimen devoid of vincristine in a child with Charcot-Marie-Tooth disease. *Curr Oncol*, *26*(2), e266-e269. https://doi.org/10.3747/co.26.4491

Bhattacharyya, J., Mihara, K., Ohtsubo, M., Yasunaga, S. i., Takei, Y., Yanagihara, K., Sakai, A., Hoshi, M., Takihara, Y., & Kimura, A. (2012). Overexpression of BMI-1 correlates with drug resistance in B-cell lymphoma cells through the stabilization of survivin expression. *Cancer Science*, *103*(1), 34-41. https://doi.org/https://doi.org/10.1111/j.1349-7006.2011.02121.x

Bowers, D. C., Gargan, L., Weprin, B. E., Mulne, A. F., Elterman, R. D., Munoz, L., Giller, C. A., & Winick, N. J. (2007). Impact of site of tumor recurrence upon survival for children with recurrent or progressive medulloblastoma. *J Neurosurg*, *107*(1 Suppl), 5-10. https://doi.org/10.3171/PED-07/07/005

Breslow, D. K., Hoogendoorn, S., Kopp, A. R., Morgens, D. W., Vu, B. K., Kennedy, M. C., Han, K., Li, A., Hess, G. T., Bassik, M. C., Chen, J. K., & Nachury, M. V. (2018). A CRISPR-based screen for Hedgehog signaling provides insights into ciliary function and ciliopathies. *Nature Genetics*, *50*(3), 460-471. https://doi.org/10.1038/s41588-018-0054-7

Brown, H. G., Kepner, J. L., Perlman, E. J., Friedman, H. S., Strother, D. R., Duffner, P. K., Kun, L. E., Goldthwaite, P. T., & Burger, P. C. (2000). "Large cell/anaplastic" medulloblastomas: a Pediatric Oncology Group Study. *J Neuropathol Exp Neurol*,

*59*(10), 857-865. https://doi.org/10.1093/jnen/59.10.857

Brown, R. C., Gunderson, L., & Plenk, H. P. (1977). Medulloblastoma. A review of the LDS hospital experience. *Cancer*, *40*(1), 56-60. https://doi.org/10.1002/1097-0142(197707)40:1<56::aid-cncr2820400111>3.0.co;2-p

Canettieri, G., Di Marcotullio, L., Greco, A., Coni, S., Antonucci, L., Infante, P., Pietrosanti, L., De Smaele, E., Ferretti, E., Miele, E., Pelloni, M., De Simone, G., Pedone, E. M., Gallinari, P., Giorgi, A., Steinkuhler, C., Vitagliano, L., Pedone, C., Schinin, M. E., . . . Gulino, A. (2010). Histone deacetylase and Cullin3-REN(KCTD11) ubiquitin ligase interplay regulates Hedgehog signalling through Gli acetylation. *Nat Cell Biol*, *12*(2), 132-142. https://doi.org/10.1038/ncb2013

Cavalli, F. M. G., Remke, M., Rampasek, L., Peacock, J., Shih, D. J. H., Luu, B., Garzia, L., Torchia, J., Nor, C., Morrissy, A. S., Agnihotri, S., Thompson, Y. Y., Kuzan-Fischer, C. M., Farooq, H., Isaev, K., Daniels, C., Cho, B. K., Kim, S. K., Wang, K. C., . . . Taylor, M. D. (2017). Intertumoral Heterogeneity within Medulloblastoma Subgroups. *Cancer Cell*, *31*(6), 737-754 e736. https://doi.org/10.1016/j.ccell.2017.05.005

Chan, H. M., & La Thangue, N. B. (2001). p300/CBP proteins: HATs for transcriptional bridges and scaffolds. *J Cell Sci*, *114*(Pt 13), 2363-2373. https://www.ncbi.nlm.nih.gov/pubmed/11559745

Chekler, E. L., Pellegrino, J. A., Lanz, T. A., Denny, R. A., Flick, A. C., Coe, J., Langille, J., Basak, A., Liu, S., Stock, I. A., Sahasrabudhe, P., Bonin, P. D., Lee, K., Pletcher, M. T., & Jones, L. H. (2015). Transcriptional Profiling of a Selective CREB Binding Protein Bromodomain Inhibitor Highlights Therapeutic Opportunities. *Chem Biol*, *22*(12), 1588-1596. https://doi.org/10.1016/j.chembiol.2015.10.013

Chen, Q., Yang, B., Liu, X., Zhang, X. D., Zhang, L., & Liu, T. (2022). Histone acetyltransferases CBP/p300 in tumorigenesis and CBP/p300 inhibitors as promising novel anticancer agents. *Theranostics*, *12*(11), 4935-4948. https://doi.org/10.7150/thno.73223

Cheng, Y., He, C., Wang, M., Ma, X., Mo, F., Yang, S., Han, J., & Wei, X. (2019). Targeting epigenetic regulators for cancer therapy: mechanisms and advances in clinical trials. *Signal Transduct Target Ther*, *4*, 62. https://doi.org/10.1038/s41392-019-0095-0

Chevignard, M., Camara-Costa, H., Doz, F., & Dellatolas, G. (2017). Core deficits and quality of survival after childhood medulloblastoma: a review. *Neurooncol Pract*, *4*(2), 82-97. https://doi.org/10.1093/nop/npw013

Choi, J. Y. (2023). Medulloblastoma: Current Perspectives and Recent Advances. *Brain Tumor Res Treat*, *11*(1), 28-38. https://doi.org/10.14791/btrt.2022.0046

Christensen, B. C., Kelsey, K. T., Zheng, S., Houseman, E. A., Marsit, C. J., Wrensch, M. R., Wiemels, J. L., Nelson, H. H., Karagas, M. R., Kushi, L. H., Kwan, M. L., & Wiencke, J. K. (2010). Breast cancer DNA methylation profiles are associated with tumor size and alcohol and folate intake. *PLoS Genet*, *6*(7), e1001043. https://doi.org/10.1371/journal.pgen.1001043

Cleasby, A., Yon, J., Day, P. J., Richardson, C., Tickle, I. J., Williams, P. A., Callahan, J. F., Carr, R., Concha, N., Kerns, J. K., Qi, H., Sweitzer, T., Ward, P., & Davies, T. G. (2014). Structure of the BTB domain of Keap1 and its interaction with the triterpenoid antagonist CDDO. *PLoS One*, *9*(6), e98896. https://doi.org/10.1371/journal.pone.0098896

Cockram, P. E., Kist, M., Prakash, S., Chen, S. H., Wertz, I. E., & Vucic, D. (2021). Ubiquitination in the regulation of inflammatory cell death and cancer. *Cell Death Differ*, *28*(2), 591-605. https://doi.org/10.1038/s41418-020-00708-5

Conery, A. R., Centore, R. C., Neiss, A., Keller, P. J., Joshi, S., Spillane, K. L., Sandy, P., Hatton, C., Pardo, E., Zawadzke, L., Bommi-Reddy, A., Gascoigne, K. E., Bryant, B. M., Mertz, J. A., & Sims, R. J. (2016). Bromodomain inhibition of the transcriptional coactivators CBP/EP300 as a therapeutic strategy to target the IRF4 network in multiple myeloma. *Elife*, *5*. https://doi.org/10.7554/eLife.10483

Constantin, D., & Widmann, C. (2020). ASH2L drives proliferation and sensitivity to bleomycin and other genotoxins in Hodgkin's lymphoma and testicular cancer cells. *Cell Death Dis*, *11*(11), 1019. https://doi.org/10.1038/s41419-020-03231-0

Crea, F., Duhagon Serrat, M. A., Hurt, E. M., Thomas, S. B., Danesi, R., & Farrar, W. L. (2011). BMI1 silencing enhances docetaxel activity and impairs antioxidant response in prostate cancer. *Int J Cancer*, *128*(8), 1946-1954. https://doi.org/10.1002/ijc.25522

Cuadrado, A., Rojo, A. I., Wells, G., Hayes, J. D., Cousin, S. P., Rumsey, W. L., Attucks, O. C., Franklin, S., Levonen, A. L., Kensler, T. W., & Dinkova-Kostova, A. T. (2019). Therapeutic targeting of the NRF2 and KEAP1 partnership in chronic diseases. *Nat Rev Drug Discov*, *18*(4), 295-317. https://doi.org/10.1038/s41573-018-0008-x

Cullinan, S. B., Gordan, J. D., Jin, J. O., Harper, J. W., & Diehl, J. A. (2004). The Keap1-BTB protein is an adaptor that bridges Nrf2 to a Cul3-based E3 ligase: Oxidative stress sensing by a Cul3-Keap1 ligase. *Molecular and Cellular Biology*, *24*(19), 8477-8486. https://doi.org/10.1128/Mcb.24.19.8477-8486.2004

Dawson, M. A., Bannister, A. J., Gottgens, B., Foster, S. D., Bartke, T., Green, A. R., & Kouzarides, T. (2009). JAK2 phosphorylates histone H3Y41 and excludes HP1alpha from chromatin. *Nature*, *461*(7265), 819-822. https://doi.org/10.1038/nature08448

DepMap. (2023). Retrieved 2023-08-03 from https://depmap.org/portal/

Dhalluin, C., Carlson, J. E., Zeng, L., He, C., Aggarwal, A. K., & Zhou, M. M. (1999). Structure and ligand of a histone acetyltransferase bromodomain. *Nature*, *399*(6735), 491-496. https://doi.org/10.1038/20974

Doudna, J. A., & Charpentier, E. (2014). Genome editing. The new frontier of genome engineering with CRISPR-Cas9. *Science*, *346*(6213), 1258096. https://doi.org/10.1126/science.1258096

Eberhart, C. G., Kepner, J. L., Goldthwaite, P. T., Kun, L. E., Duffner, P. K., Friedman, H. S., Strother, D. R., & Burger, P. C. (2002). Histopathologic grading of medulloblastomas: a Pediatric Oncology Group study. *Cancer*, *94*(2), 552-560. https://doi.org/10.1002/cncr.10189

Ecker, J., Oehme, I., Mazitschek, R., Korshunov, A., Kool, M., Hielscher, T., Kiss, J., Selt, F., Konrad, C., Lodrini, M., Deubzer, H. E., von Deimling, A., Kulozik, A. E., Pfister, S. M., Witt, O., & Milde, T. (2015). Targeting class I histone deacetylase 2 in MYC amplified group 3 medulloblastoma. *Acta Neuropathol Commun*, *3*, 22. https://doi.org/10.1186/s40478-015-0201-7

El-Awady, R., Saleh, E., Hashim, A., Soliman, N., Dallah, A., Elrasheed, A., & Elakraa, G. (2016). The Role of Eukaryotic and Prokaryotic ABC Transporter Family in Failure of Chemotherapy. *Front Pharmacol*, *7*, 535. https://doi.org/10.3389/fphar.2016.00535

Ellison, D. W., Dalton, J., Kocak, M., Nicholson, S. L., Fraga, C., Neale, G., Kenney, A. M., Brat, D. J., Perry, A., Yong, W. H., Taylor, R. E., Bailey, S., Clifford, S. C., & Gilbertson, R. J. (2011). Medulloblastoma: clinicopathological correlates of SHH, WNT, and non-SHH/WNT molecular subgroups. *Acta Neuropathol*, *121*(3), 381-396. https://doi.org/10.1007/s00401-011-0800-8

Fagan, R. J., & Dingwall, A. K. (2019). COMPASS Ascending: Emerging clues regarding the roles of MLL3/KMT2C and MLL2/KMT2D proteins in cancer. *Cancer Lett*, *458*, 56-65. https://doi.org/10.1016/j.canlet.2019.05.024

Ford, D. J., & Dingwall, A. K. (2015). The cancer COMPASS: navigating the functions of MLL complexes in cancer. *Cancer Genet*, *208*(5), 178-191. https://doi.org/10.1016/j.cancergen.2015.01.005

Fric, R., Due-Tonnessen, B. J., Lundar, T., Egge, A., Kronen Krossnes, B., Due-Tonnessen, P., Stensvold, E., & Brandal, P. (2020). Long-term outcome of posterior fossa medulloblastoma in patients surviving more than 20 years following primary treatment in childhood. *Sci Rep*, *10*(1), 9371. https://doi.org/10.1038/s41598-020-66328-8

Gajjar, A., Chintagumpala, M., Ashley, D., Kellie, S., Kun, L. E., Merchant, T. E., Woo, S., Wheeler, G., Ahern, V., Krasin, M. J., Fouladi, M., Broniscer, A., Krance, R., Hale, G. A., Stewart, C. F., Dauser, R., Sanford, R. A., Fuller, C., Lau, C., . . .

Gilbertson, R. J. (2006). Risk-adapted craniospinal radiotherapy followed by high-dose chemotherapy and stem-cell rescue in children with newly diagnosed medulloblastoma (St Jude Medulloblastoma-96): long-term results from a prospective, multicentre trial. *Lancet Oncol*, *7*(10), 813-820. https://doi.org/10.1016/S1470-2045(06)70867-1

Ghasemi, M., Turnbull, T., Sebastian, S., & Kempson, I. (2021). The MTT Assay: Utility, Limitations, Pitfalls, and Interpretation in Bulk and Single-Cell Analysis. *Int J Mol Sci*, *22*(23). https://doi.org/10.3390/ijms222312827

Ghosh, S., Taylor, A., Chin, M., Huang, H. R., Conery, A. R., Mertz, J. A., Salmeron, A., Dakle, P. J., Mele, D., Cote, A., Jayaram, H., Setser, J. W., Poy, F., Hatzivassiliou, G., DeAlmeida-Nagata, D., Sandy, P., Hatton, C., Romero, F. A., Chiang, E., . . . Lora, J. M. (2016). Regulatory T Cell Modulation by CBP/EP300 Bromodomain Inhibition. *J Biol Chem*, *291*(25), 13014-13027. https://doi.org/10.1074/jbc.M115.708560

Gilbert, D. F., Erdmann, G., Zhang, X., Fritzsche, A., Demir, K., Jaedicke, A., Muehlenberg, K., Wanker, E. E., & Boutros, M. (2011). A novel multiplex cell viability assay for high-throughput RNAi screening. *PLoS One*, *6*(12), e28338. https://doi.org/10.1371/journal.pone.0028338

Grill, J., Dufour, C., & Kalifa, C. (2006). High-dose chemotherapy in children with newly-diagnosed medulloblastoma. *Lancet Oncol*, *7*(10), 787-789. https://doi.org/10.1016/S1470-2045(06)70872-5

Hahn, M. A., Dickson, K. A., Jackson, S., Clarkson, A., Gill, A. J., & Marsh, D. J. (2012). The tumor suppressor CDC73 interacts with the ring finger proteins RNF20 and RNF40 and is required for the maintenance of histone 2B monoubiquitination. *Hum Mol Genet*, *21*(3), 559-568. https://doi.org/10.1093/hmg/ddr490

Hassan, A. H., Prochasson, P., Neely, K. E., Galasinski, S. C., Chandy, M., Carrozza, M. J., & Workman, J. L. (2002). Function and selectivity of bromodomains in anchoring chromatin-modifying complexes to promoter nucleosomes. *Cell*, *111*(3), 369-379. https://doi.org/10.1016/s0092-8674(02)01005-x

Hayes, J. D., & Dinkova-Kostova, A. T. (2014). The Nrf2 regulatory network provides an interface between redox and intermediary metabolism. *Trends Biochem Sci*, *39*(4), 199-218. https://doi.org/10.1016/j.tibs.2014.02.002

He, F., Antonucci, L., & Karin, M. (2020). NRF2 as a regulator of cell metabolism and inflammation in cancer. *Carcinogenesis*, *41*(4), 405-416. https://doi.org/10.1093/carcin/bgaa039

He, F., Ru, X., & Wen, T. (2020). NRF2, a Transcription Factor for Stress Response and Beyond. *Int J Mol Sci*, *21*(13). https://doi.org/10.3390/ijms21134777

Helming, K. C., Wang, X., & Roberts, C. W. M. (2014). Vulnerabilities of mutant SWI/SNF complexes in cancer. *Cancer Cell*, *26*(3), 309-317. https://doi.org/10.1016/j.ccr.2014.07.018

Henssen, A., Thor, T., Odersky, A., Heukamp, L., El-Hindy, N., Beckers, A., Speleman, F., Althoff, K., Schafers, S., Schramm, A., Sure, U., Fleischhack, G., Eggert, A., & Schulte, J. H. (2013). BET bromodomain protein inhibition is a therapeutic option for medulloblastoma. *Oncotarget*, *4*(11), 2080-2095. https://doi.org/10.18632/oncotarget.1534

Horie, Y., Suzuki, T., Inoue, J., Iso, T., Wells, G., Moore, T. W., Mizushima, T., Dinkova-Kostova, A. T., Kasai, T., Kamei, T., Koshiba, S., & Yamamoto, M. (2021). Molecular basis for the disruption of Keap1-Nrf2 interaction via Hinge & Latch mechanism. *Commun Biol*, *4*(1), 576. https://doi.org/10.1038/s42003-021-02100-6

Huang, J., Chen, M., Xu, E. S., Luo, L., Ma, Y., Huang, W., Floyd, W., Klann, T. S., Kim, S. Y., Gersbach, C. A., Cardona, D. M., & Kirsch, D. G. (2019). Genome-wide CRISPR Screen to Identify Genes that Suppress Transformation in the Presence of Endogenous Kras(G12D). *Sci Rep*, *9*(1), 17220. https://doi.org/10.1038/s41598-019-53572-w

Huang, M., Tailor, J., Zhen, Q., Gillmor, A. H., Miller, M. L., Weishaupt, H., Chen, J., Zheng, T., Nash, E. K., McHenry, L. K., An, Z., Ye, F., Takashima, Y., Clarke, J., Ayetey, H., Cavalli, F. M. G., Luu, B., Moriarity, B. S., Ilkhanizadeh, S., . . . Weiss, W. A. (2019). Engineering Genetic Predisposition in Human Neuroepithelial Stem Cells Recapitulates Medulloblastoma Tumorigenesis. *Cell Stem Cell*, *25*(3), 433-446 e437. https://doi.org/10.1016/j.stem.2019.05.013

Ingram, W. J., Crowther, L. M., Little, E. B., Freeman, R., Harliwong, I., Veleva, D., Hassall, T. E., Remke, M., Taylor, M. D., & Hallahan, A. R. (2013). ABC transporter activity linked to radiation resistance and molecular subtype in pediatric medulloblastoma. *Exp Hematol Oncol*, *2*(1), 26. https://doi.org/10.1186/2162-3619-2-26

Islam, S. S., Qassem, K., Islam, S., Parag, R. R., Rahman, M. Z., Farhat, W. A., Yeger, H., Aboussekhra, A., Karakas, B., & Noman, A. S. M. (2022). Genetic alterations of Keap1 confers chemotherapeutic resistance through functional activation of Nrf2 and Notch pathway in head and neck squamous cell carcinoma. *Cell Death Dis*, *13*(8), 696. https://doi.org/10.1038/s41419-022-05126-8

Itoh, K., Wakabayashi, N., Katoh, Y., Ishii, T., Igarashi, K., Engel, J. D., & Yamamoto, M. (1999). Keap1 represses nuclear activation of antioxidant responsive elements by Nrf2 through binding to the amino-terminal Neh2 domain. *Genes & Development*, *13*(1), 76-86. https://doi.org/DOI 10.1101/gad.13.1.76

Iyer, N. G., Ozdag, H., & Caldas, C. (2004). p300/CBP and cancer. *Oncogene*, *23*(24), 4225-4231. https://doi.org/10.1038/sj.onc.1207118

Jackson, M., Marks, L., May, G. H. W., & Wilson, J. B. (2018). The genetic basis of disease. *Essays Biochem*, *62*(5), 643-723. https://doi.org/10.1042/EBC20170053

Johnston, D. L., Keene, D., Strother, D., Taneva, M., Lafay-Cousin, L., Fryer, C., Scheinemann, K., Carret, A. S., Fleming, A., Afzal, S., Wilson, B., Bowes, L., Zelcer, S., Mpofu, C., Silva, M., Larouche, V., Brossard, J., & Bouffet, E. (2018). Survival Following Tumor Recurrence in Children With Medulloblastoma. *J Pediatr Hematol Oncol*, *40*(3), e159-e163. https://doi.org/10.1097/MPH.0000000000001095

Jones, D. T., Jager, N., Kool, M., Zichner, T., Hutter, B., Sultan, M., Cho, Y. J., Pugh, T. J., Hovestadt, V., Stutz, A. M., Rausch, T., Warnatz, H. J., Ryzhova, M., Bender, S., Sturm, D., Pleier, S., Cin, H., Pfaff, E., Sieber, L., . . . Lichter, P. (2012). Dissecting the genomic complexity underlying medulloblastoma. *Nature*, *488*(7409), 100-105. https://doi.org/10.1038/nature11284

Juraschka, K., & Taylor, M. D. (2019). Medulloblastoma in the age of molecular subgroups: a review. *J Neurosurg Pediatr*, *24*(4), 353-363. https://doi.org/10.3171/2019.5.PEDS18381

Kageyama, S., Saito, T., Obata, M., Koide, R. H., Ichimura, Y., & Komatsu, M. (2018). Negative Regulation of the Keap1-Nrf2 Pathway by a p62/Sqstm1 Splicing Variant. *Mol Cell Biol*, *38*(7). https://doi.org/10.1128/MCB.00642-17

Kalifa, C., & Grill, J. (2005). The therapy of infantile malignant brain tumors: current status? *J Neurooncol*, *75*(3), 279-285. https://doi.org/10.1007/s11060-005-6752-x

Katsuoka, F., Motohashi, H., Ishii, T., Aburatani, H., Engel, J. D., & Yamamoto, M. (2005). Genetic evidence that small maf proteins are essential for the activation of antioxidant response element-dependent genes. *Mol Cell Biol*, *25*(18), 8044-8051. https://doi.org/10.1128/MCB.25.18.8044-8051.2005

Katsuragi, Y., Ichimura, Y., & Komatsu, M. (2016). Regulation of the Keap1–Nrf2 pathway by p62/SQSTM1. *Current Opinion in Toxicology*, *1*, 54-61. https://doi.org/https://doi.org/10.1016/j.cotox.2016.09.005

Kobayashi, A., Kang, M. I., Okawa, H., Ohtsuji, M., Zenke, Y., Chiba, T., Igarashi, K., & Yamamoto, M. (2004). Oxidative stress sensor Keap1 functions as an adaptor for Cul3-based E3 ligase to regulate proteasomal degradation of Nrf2. *Mol Cell Biol*, *24*(16), 7130-7139. https://doi.org/10.1128/MCB.24.16.7130-7139.2004

Komatsu, M., Kurokawa, H., Waguri, S., Taguchi, K., Kobayashi, A., Ichimura, Y., Sou, Y. S., Ueno, I., Sakamoto, A., Tong, K. I., Kim, M., Nishito, Y., Iemura, S., Natsume, T., Ueno, T., Kominami, E., Motohashi, H., Tanaka, K., & Yamamoto, M. (2010). The selective autophagy substrate p62 activates the stress responsive transcription factor Nrf2 through inactivation of Keap1. *Nat Cell Biol*, *12*(3), 213-223. https://doi.org/10.1038/ncb2021

Kool, M., Korshunov, A., Remke, M., Jones, D. T., Schlanstein, M., Northcott, P. A., Cho, Y. J., Koster, J., Schouten-van Meeteren, A., van Vuurden, D., Clifford, S. C., Pietsch, T., von Bueren, A. O., Rutkowski, S., McCabe, M., Collins, V. P., Backlund, M. L., Haberler, C., Bourdeaut, F., . . . Pfister, S. M. (2012). Molecular subgroups of medulloblastoma: an international meta-analysis of transcriptome, genetic aberrations, and clinical data of WNT, SHH, Group 3, and Group 4 medulloblastomas. *Acta Neuropathol*, *123*(4), 473-484. https://doi.org/10.1007/s00401-012-0958-8

Korshunov, A., Sahm, F., Stichel, D., Schrimpf, D., Ryzhova, M., Zheludkova, O., Golanov, A., Lichter, P., Jones, D. T. W., von Deimling, A., Pfister, S. M., & Kool, M. (2018). Molecular characterization of medulloblastomas with extensive nodularity (MBEN). *Acta Neuropathol*, *136*(2), 303-313. https://doi.org/10.1007/s00401-018-1840-0

Kulikowski, E., Rakai, B. D., & Wong, N. C. W. (2021). Inhibitors of bromodomain and extra-terminal proteins for treating multiple human diseases. *Med Res Rev*, *41*(1), 223-245. https://doi.org/10.1002/med.21730

Lafay-Cousin, L., & Dufour, C. (2022). High-Dose Chemotherapy in Children with Newly Diagnosed Medulloblastoma. *Cancers (Basel)*, *14*(3). https://doi.org/10.3390/cancers14030837

Lau, A. T., Lee, S. Y., Xu, Y. M., Zheng, D., Cho, Y. Y., Zhu, F., Kim, H. G., Li, S. Q., Zhang, Z., Bode, A. M., & Dong, Z. (2011). Phosphorylation of histone H2B serine 32 is linked to cell transformation. *J Biol Chem*, *286*(30), 26628-26637. https://doi.org/10.1074/jbc.M110.215590

Leung, C., Lingbeek, M., Shakhova, O., Liu, J., Tanger, E., Saremaslani, P., van Lohuizen, M., & Marino, S. (2004). Bmi1 is essential for cerebellar development and is overexpressed in human medulloblastomas. *Nature*, *428*(6980), 337-341. https://doi.org/10.1038/nature02385

Li, P., Lee, E. H., Du, F., Gordon, R. E., Yuelling, L. W., Liu, Y., Ng, J. M., Zhang, H., Wu, J., Korshunov, A., Pfister, S. M., Curran, T., & Yang, Z. J. (2016). Nestin Mediates Hedgehog Pathway Tumorigenesis. *Cancer Res*, *76*(18), 5573-5583. https://doi.org/10.1158/0008-5472.CAN-16-1547

Li, W., Xu, H., Xiao, T., Cong, L., Love, M. I., Zhang, F., Irizarry, R. A., Liu, J. S., Brown, M., & Liu, X. S. (2014). MAGeCK enables robust identification of essential genes from genome-scale CRISPR/Cas9 knockout screens. *Genome Biol*, *15*(12), 554. https://doi.org/10.1186/s13059-014-0554-4

Li, X., Zhang, D., Hannink, M., & Beamer, L. J. (2004). Crystal structure of the Kelch domain of human Keap1. *J Biol Chem*, *279*(52), 54750-54758. https://doi.org/10.1074/jbc.M410073200

Liao, H., Cai, J., Liu, C., Shen, L., Pu, X., Yao, Y., Han, B., Yu, T., Cheng, S. Y., & Yue, S. (2020). Protein phosphatase 4 promotes Hedgehog signaling through dephosphorylation of Suppressor of fused. *Cell Death Dis*, *11*(8), 686. https://doi.org/10.1038/s41419-020-02843-w

Liu, S., Pi, J., & Zhang, Q. (2022). Signal amplification in the KEAP1-NRF2-ARE antioxidant response pathway. *Redox Biol*, *54*, 102389. https://doi.org/10.1016/j.redox.2022.102389

Lokumcu, L. (2017). *Assessing the function of chromatin modifying enzymes in medulloblastoma* (Publication Number 473056) Koc University].

Long, J., Li, B., Rodriguez-Blanco, J., Pastori, C., Volmar, C. H., Wahlestedt, C., Capobianco, A., Bai, F., Pei, X. H., Ayad, N. G., & Robbins, D. J. (2014). The BET bromodomain inhibitor I-BET151 acts downstream of smoothened protein to abrogate the growth of hedgehog protein-driven cancers. *J Biol Chem*, *289*(51), 35494-35502. https://doi.org/10.1074/jbc.M114.595348

Louis, D. N., Perry, A., Reifenberger, G., von Deimling, A., Figarella-Branger, D., Cavenee, W. K., Ohgaki, H., Wiestler, O. D., Kleihues, P., & Ellison, D. W. (2016). The 2016 World Health Organization Classification of Tumors of the Central Nervous System: a summary. *Acta Neuropathol*, *131*(6), 803-820. https://doi.org/10.1007/s00401-016-1545-1

Louis, D. N., Perry, A., Wesseling, P., Brat, D. J., Cree, I. A., Figarella-Branger, D., Hawkins, C., Ng, H. K., Pfister, S. M., Reifenberger, G., Soffietti, R., von Deimling, A., & Ellison, D. W. (2021). The 2021 WHO Classification of Tumors of the Central Nervous System: a summary. *Neuro Oncol*, *23*(8), 1231-1251. https://doi.org/10.1093/neuonc/noab106

Lv, J., Xie, M., Zhao, S., Qiu, W., Wang, S., & Cao, M. (2021). Nestin is essential for cellular redox homeostasis and gastric cancer metastasis through the mediation of the Keap1–Nrf2 axis. *Cancer Cell International*, *21*(1), 603. https://doi.org/10.1186/s12935-021-02184-4

Martin, A. M., Raabe, E., Eberhart, C., & Cohen, K. J. (2014). Management of pediatric and adult patients with medulloblastoma. *Curr Treat Options Oncol*, *15*(4), 581-594. https://doi.org/10.1007/s11864-014-0306-4

Martino, E., Casamassima, G., Castiglione, S., Cellupica, E., Pantalone, S., Papagni, F., Rui, M., Siciliano, A. M., & Collina, S. (2018). Vinca alkaloids and analogues as anti-cancer agents: Looking back, peering ahead. *Bioorg Med Chem Lett*, *28*(17), 2816-2826. https://doi.org/10.1016/j.bmcl.2018.06.044

Martirosian., V., & Neman., J. (2018). - Medulloblastoma: Challenges and advances in treatment and research. *Cancer Rep*, *2*(3).

McCord, J. M., Gao, B., & Hybertson, B. M. (2023). The Complex Genetic and Epigenetic Regulation of the Nrf2 Pathways: A Review. *Antioxidants (Basel)*, *12*(2). https://doi.org/10.3390/antiox12020366

McDermott, M., Eustace, A. J., Busschots, S., Breen, L., Crown, J., Clynes, M., O'Donovan, N., & Stordal, B. (2014). In vitro Development of Chemotherapy and Targeted Therapy Drug-Resistant Cancer Cell Lines: A Practical Guide with Case Studies. *Front Oncol*, *4*, 40. https://doi.org/10.3389/fonc.2014.00040

Menyhart, O., Giangaspero, F., & Gyorffy, B. (2019). Molecular markers and potential therapeutic targets in non-WNT/non-SHH (group 3 and group 4) medulloblastomas. *J Hematol Oncol*, *12*(1), 29. https://doi.org/10.1186/s13045-019-0712-y

Merk, D. J., Ohli, J., Merk, N. D., Thatikonda, V., Morrissy, S., Schoof, M., Schmid, S. N., Harrison, L., Filser, S., Ahlfeld, J., Erkek, S., Raithatha, K., Andreska, T., Weisshaar, M., Launspach, M., Neumann, J. E., Shakarami, M., Plenker, D., Marra, M. A., . . . Schuller, U. (2018). Opposing Effects of CREBBP Mutations Govern the Phenotype of Rubinstein-Taybi Syndrome and Adult SHH Medulloblastoma. *Dev Cell*, *44*(6), 709-724 e706. https://doi.org/10.1016/j.devcel.2018.02.012

Millard, N. E., & De Braganca, K. C. (2016). Medulloblastoma. *J Child Neurol*, *31*(12), 1341-1353. https://doi.org/10.1177/0883073815600866

Mohammad, F., & Helin, K. (2017). Oncohistones: drivers of pediatric cancers. *Genes Dev*, *31*(23-24), 2313-2324. https://doi.org/10.1101/gad.309013.117

Moi, P., Chan, K., Asunis, I., Cao, A., & Kan, Y. W. (1994). Isolation of NF-E2-related factor 2 (Nrf2), a NF-E2-like basic leucine zipper transcriptional activator that binds to the tandem NF-E2/AP1 repeat of the beta-globin locus control region. *Proc Natl Acad Sci U S A*, *91*(21), 9926-9930. https://doi.org/10.1073/pnas.91.21.9926

Mu, X., Springer, J. E., & Bowser, R. (1997). FAC1 expression and localization in motor neurons of developing, adult, and amyotrophic lateral sclerosis spinal cord. *Exp Neurol*, *146*(1), 17-24. https://doi.org/10.1006/exnr.1997.6508

Mujtaba, S., He, Y., Zeng, L., Yan, S., Plotnikova, O., Sachchidanand, Sanchez, R., Zeleznik-Le, N. J., Ronai, Z., & Zhou, M. M. (2004). Structural mechanism of the bromodomain of the coactivator CBP in p53 transcriptional activation. *Mol Cell*, *13*(2), 251-263. https://doi.org/10.1016/s1097-2765(03)00528-8

Nicodeme, E., Jeffrey, K. L., Schaefer, U., Beinke, S., Dewell, S., Chung, C. W., Chandwani, R., Marazzi, I., Wilson, P., Coste, H., White, J., Kirilovsky, J., Rice, C. M., Lora, J. M., Prinjha, R. K., Lee, K., & Tarakhovsky, A. (2010). Suppression of inflammation by a synthetic histone mimic. *Nature*, *468*(7327), 1119-1123. https://doi.org/10.1038/nature09589

Northcott, P. A., Buchhalter, I., Morrissy, A. S., Hovestadt, V., Weischenfeldt, J., Ehrenberger, T., Grobner, S., Segura-Wang, M., Zichner, T., Rudneva, V. A., Warnatz, H. J., Sidiropoulos, N., Phillips, A. H., Schumacher, S., Kleinheinz, K., Waszak, S. M., Erkek, S., Jones, D. T. W., Worst, B. C., . . . Lichter, P. (2017). The whole-genome landscape of medulloblastoma subtypes. *Nature*, *547*(7663), 311-317. https://doi.org/10.1038/nature22973

Northcott, P. A., Jones, D. T., Kool, M., Robinson, G. W., Gilbertson, R. J., Cho, Y. J., Pomeroy, S. L., Korshunov, A., Lichter, P., Taylor, M. D., & Pfister, S. M. (2012). Medulloblastomics: the end of the beginning. *Nat Rev Cancer*, *12*(12), 818-834. https://doi.org/10.1038/nrc3410

Northcott, P. A., Pfister, S. M., & Jones, D. T. (2015). Next-generation (epi)genetic drivers of childhood brain tumours and the outlook for targeted therapies. *Lancet Oncol*, *16*(6), e293-302. https://doi.org/10.1016/S1470-2045(14)71206-9

Northcott, P. A., Robinson, G. W., Kratz, C. P., Mabbott, D. J., Pomeroy, S. L., Clifford, S. C., Rutkowski, S., Ellison, D. W., Malkin, D., Taylor, M. D., Gajjar, A., & Pfister, S. M. (2019). Medulloblastoma. *Nat Rev Dis Primers*, *5*(1), 11. https://doi.org/10.1038/s41572-019-0063-6

Ogura, T., Tong, K. I., Mio, K., Maruyama, Y., Kurokawa, H., Sato, C., & Yamamoto, M. (2010). Keap1 is a forked-stem dimer structure with two large spheres enclosing the intervening, double glycine repeat, and C-terminal domains. *Proc Natl Acad Sci U S A*, *107*(7), 2842-2847. https://doi.org/10.1073/pnas.0914036107

Orr, B. A. (2020). Pathology, diagnostics, and classification of medulloblastoma. *Brain Pathol*, *30*(3), 664-678. https://doi.org/10.1111/bpa.12837

Ostrom, Q. T., Gittleman, H., Truitt, G., Boscia, A., Kruchko, C., & Barnholtz-Sloan, J. S. (2018). CBTRUS Statistical Report: Primary Brain and Other Central Nervous System Tumors Diagnosed in the United States in 2011-2015. *Neuro Oncol*, *20*(suppl_4), iv1-iv86. https://doi.org/10.1093/neuonc/noy131

Othman, R. T., Kimishi, I., Bradshaw, T. D., Storer, L. C., Korshunov, A., Pfister, S. M., Grundy, R. G., Kerr, I. D., & Coyle, B. (2014). Overcoming multiple drug resistance mechanisms in medulloblastoma. *Acta Neuropathol Commun*, *2*, 57. https://doi.org/10.1186/2051-5960-2-57

Ottensmeier, H., Schlegel, P. G., Eyrich, M., Wolff, J. E., Juhnke, B. O., von Hoff, K., Frahsek, S., Schmidt, R., Faldum, A., Fleischhack, G., von Bueren, A., Friedrich, C., Resch, A., Warmuth-Metz, M., Krauss, J., Kortmann, R. D., Bode, U., Kuhl, J., & Rutkowski, S. (2020). Treatment of children under 4 years of age with medulloblastoma and ependymoma in the HIT2000/HIT-REZ 2005 trials: Neuropsychological outcome 5 years after treatment. *PLoS One*, *15*(1), e0227693. https://doi.org/10.1371/journal.pone.0227693

Packer, R. J., Goldwein, J., Nicholson, H. S., Vezina, L. G., Allen, J. C., Ris, M. D., Muraszko, K., Rorke, L. B., Wara, W. M., Cohen, B. H., & Boyett, J. M. (1999). Treatment of children with medulloblastomas with reduced-dose craniospinal radiation therapy and adjuvant chemotherapy: A Children's Cancer Group Study. *J Clin Oncol*, *17*(7), 2127-2136. https://doi.org/10.1200/JCO.1999.17.7.2127

Park, I. G., Jeon, M., Kim, H., & Lee, J. M. (2022). Coordinated methyl readers: Functional communications in cancer. *Semin Cancer Biol*, *83*, 88-99. https://doi.org/10.1016/j.semcancer.2021.03.015

Parkes, J., Hendricks, M., Ssenyonga, P., Mugamba, J., Molyneux, E., Schouten-van Meeteren, A., Qaddoumi, I., Fieggen, G., Luna-Fineman, S., Howard, S., Mitra, D., Bouffet, E., Davidson, A., Bailey, S., & Siop, P. (2015). SIOP PODC adapted treatment recommendations for standard-risk medulloblastoma in low and middle income settings. *Pediatr Blood Cancer*, *62*(4), 553-564. https://doi.org/10.1002/pbc.25313

Parsons, D. W., Li, M., Zhang, X., Jones, S., Leary, R. J., Lin, J. C., Boca, S. M., Carter, H., Samayoa, J., Bettegowda, C., Gallia, G. L., Jallo, G. I., Binder, Z. A., Nikolsky, Y., Hartigan, J., Smith, D. R., Gerhard, D. S., Fults, D. W., VandenBerg, S., . . . Velculescu, V. E. (2011). The genetic landscape of the childhood cancer medulloblastoma. *Science*, *331*(6016), 435-439. https://doi.org/10.1126/science.1198056

Pickar-Oliver, A., & Gersbach, C. A. (2019). The next generation of CRISPR-Cas technologies and applications. *Nat Rev Mol Cell Biol*, *20*(8), 490-507. https://doi.org/10.1038/s41580-019-0131-5

Pugh, T. J., Weeraratne, S. D., Archer, T. C., Pomeranz Krummel, D. A., Auclair, D., Bochicchio, J., Carneiro, M. O., Carter, S. L., Cibulskis, K., Erlich, R. L., Greulich, H., Lawrence, M. S., Lennon, N. J., McKenna, A., Meldrim, J., Ramos, A. H., Ross, M. G., Russ, C., Shefler, E., . . . Cho, Y. J. (2012). Medulloblastoma exome sequencing uncovers subtype-specific somatic mutations. *Nature*, *488*(7409), 106-110. https://doi.org/10.1038/nature11329

Quinlan, A., & Rizzolo, D. (2017). Understanding medulloblastoma. *JAAPA*, *30*(10), 30-36. https://doi.org/10.1097/01.JAA.0000524717.71084.50

Ramaswamy, V., Remke, M., Adamski, J., Bartels, U., Tabori, U., Wang, X., Huang, A., Hawkins, C., Mabbott, D., Laperriere, N., Taylor, M. D., & Bouffet, E. (2016). Medulloblastoma subgroup-specific outcomes in irradiated children: who are the true high-risk patients? *Neuro Oncol*, *18*(2), 291-297. https://doi.org/10.1093/neuonc/nou357

Ramaswamy, V., Remke, M., Bouffet, E., Bailey, S., Clifford, S. C., Doz, F., Kool, M., Dufour, C., Vassal, G., Milde, T., Witt, O., von Hoff, K., Pietsch, T., Northcott, P. A., Gajjar, A., Robinson, G. W., Padovani, L., Andre, N., Massimino, M., . . .

Pomeroy, S. L. (2016). Risk stratification of childhood medulloblastoma in the molecular era: the current consensus. *Acta Neuropathol*, *131*(6), 821-831. https://doi.org/10.1007/s00401-016-1569-6

Rasmussen, K. D., & Helin, K. (2016). Role of TET enzymes in DNA methylation, development, and cancer. *Genes Dev*, *30*(7), 733-750. https://doi.org/10.1101/gad.276568.115

Riccio, A., Aaltonen, L. A., Godwin, A. K., Loukola, A., Percesepe, A., Salovaara, R., Masciullo, V., Genuardi, M., Paravatou-Petsotas, M., Bassi, D. E., Ruggeri, B. A., Klein-Szanto, A. J., Testa, J. R., Neri, G., & Bellacosa, A. (1999). The DNA repair gene MBD4 (MED1) is mutated in human carcinomas with microsatellite instability. *Nature Genetics*, *23*(3), 266-268. https://doi.org/10.1038/15443

Robinson, G., Parker, M., Kranenburg, T. A., Lu, C., Chen, X., Ding, L., Phoenix, T. N., Hedlund, E., Wei, L., Zhu, X., Chalhoub, N., Baker, S. J., Huether, R., Kriwacki, R., Curley, N., Thiruvenkatam, R., Wang, J., Wu, G., Rusch, M., . . . Gilbertson, R. J. (2012). Novel mutations target distinct subgroups of medulloblastoma. *Nature*, *488*(7409), 43-48. https://doi.org/10.1038/nature11213

Robinson, G. W., Rudneva, V. A., Buchhalter, I., Billups, C. A., Waszak, S. M., Smith, K. S., Bowers, D. C., Bendel, A., Fisher, P. G., Partap, S., Crawford, J. R., Hassall, T., Indelicato, D. J., Boop, F., Klimo, P., Sabin, N. D., Patay, Z., Merchant, T. E., Stewart, C. F., . . . Northcott, P. A. (2018). Risk-adapted therapy for young children with medulloblastoma (SJYC07): therapeutic and molecular outcomes from a multicentre, phase 2 trial. *Lancet Oncol*, *19*(6), 768-784. https://doi.org/10.1016/S1470-2045(18)30204-3

Rossetto, D., Avvakumov, N., & Cote, J. (2012). Histone phosphorylation: a chromatin modification involved in diverse nuclear events. *Epigenetics*, *7*(10), 1098-1108. https://doi.org/10.4161/epi.21975

Roussel, M. F., & Stripay, J. L. (2018). Epigenetic Drivers in Pediatric Medulloblastoma. *Cerebellum*, *17*(1), 28-36. https://doi.org/10.1007/s12311-017-0899-9

Sabel, M., Fleischhack, G., Tippelt, S., Gustafsson, G., Doz, F., Kortmann, R., Massimino, M., Navajas, A., von Hoff, K., Rutkowski, S., Warmuth-Metz, M., Clifford, S. C., Pietsch, T., Pizer, B., Lannering, B., & Group, S.-E. B. T. (2016). Relapse patterns and outcome after relapse in standard risk medulloblastoma: a report from the HIT-SIOP-PNET4 study. *J Neurooncol*, *129*(3), 515-524. https://doi.org/10.1007/s11060-016-2202-1

Sabnis, D. H., Storer, L. C. D., Liu, J. F., Jackson, H. K., Kilday, J. P., Grundy, R. G., Kerr, I. D., & Coyle, B. (2019). A role for ABCB1 in prognosis, invasion and drug resistance in ependymoma. *Sci Rep*, *9*(1), 10290. https://doi.org/10.1038/s41598-019-46700-z

Sahlgren, C. M., Pallari, H. M., He, T., Chou, Y. H., Goldman, R. D., & Eriksson, J. E. (2006). A nestin scaffold links Cdk5/p35 signaling to oxidant-induced cell death. *EMBO J*, *25*(20), 4808-4819. https://doi.org/10.1038/sj.emboj.7601366

Sanson, K. R., Hanna, R. E., Hegde, M., Donovan, K. F., Strand, C., Sullender, M. E., Vaimberg, E. W., Goodale, A., Root, D. E., Piccioni, F., & Doench, J. G. (2018). Optimized libraries for CRISPR-Cas9 genetic screens with multiple modalities. *Nat Commun*, *9*(1), 5416. https://doi.org/10.1038/s41467-018-07901-8

Schoonover, S., Davies, P., & Bowser, R. (1996). Immunolocalization and redistribution of the FAC1 protein in Alzheimer's disease. *J Neuropathol Exp Neurol*, *55*(4), 444-455. https://doi.org/10.1097/00005072-199604000-00007

Schroeder, K., & Gururangan, S. (2014). Molecular variants and mutations in medulloblastoma. *Pharmgenomics Pers Med*, *7*, 43-51. https://doi.org/10.2147/PGPM.S38698

Schubeler, D. (2015). Function and information content of DNA methylation. *Nature*, *517*(7534), 321-326. https://doi.org/10.1038/nature14192

Schultz-Rogers, L. E., Thayer, M. L., Kambakam, S., Wierson, W. A., Helmer, J. A., Wishman, M. D., Wall, K. A., Greig, J. L., Forsman, J. L., Puchhalapalli, K., Nair, S., Weiss, T. J., Luiken, J. M., Blackburn, P. R., Ekker, S. C., Kool, M., & McGrail, M. (2022). Rbbp4 loss disrupts neural progenitor cell cycle regulation independent of Rb and leads to Tp53 acetylation and apoptosis. *Dev Dyn*, *251*(8), 1267-1290. https://doi.org/10.1002/dvdy.467

Schwalbe, E. C., Lindsey, J. C., Nakjang, S., Crosier, S., Smith, A. J., Hicks, D., Rafiee, G., Hill, R. M., Iliasova, A., Stone, T., Pizer, B., Michalski, A., Joshi, A., Wharton, S. B., Jacques, T. S., Bailey, S., Williamson, D., & Clifford, S. C. (2017). Novel molecular subgroups for clinical classification and outcome prediction in childhood medulloblastoma: a cohort study. *Lancet Oncol*, *18*(7), 958-971. https://doi.org/10.1016/S1470-2045(17)30243-7

Seligson, D. B., Horvath, S., McBrian, M. A., Mah, V., Yu, H., Tze, S., Wang, Q., Chia, D., Goodglick, L., & Kurdistani, S. K. (2009). Global levels of histone modifications predict prognosis in different cancers. *Am J Pathol*, *174*(5), 1619-1628. https://doi.org/10.2353/ajpath.2009.080874

Shanmugam, M. K., Arfuso, F., Arumugam, S., Chinnathambi, A., Jinsong, B., Warrier, S., Wang, L. Z., Kumar, A. P., Ahn, K. S., Sethi, G., & Lakshmanan, M. (2018). Role of novel histone modifications in cancer. *Oncotarget*, *9*(13), 11414-11426. https://doi.org/10.18632/oncotarget.23356

Sharma, S., Kelly, T. K., & Jones, P. A. (2010). Epigenetics in cancer. *Carcinogenesis*, *31*(1), 27-36. https://doi.org/10.1093/carcin/bgp220

Sharma, S., & Petsalaki, E. (2018). Application of CRISPR-Cas9 Based Genome-Wide Screening Approaches to Study Cellular Signalling Mechanisms. *Int J Mol Sci*, *19*(4). https://doi.org/10.3390/ijms19040933

Shorstova, T., Foulkes, W. D., & Witcher, M. (2021). Achieving clinical success with BET inhibitors as anti-cancer agents. *Br J Cancer*, *124*(9), 1478-1490. https://doi.org/10.1038/s41416-021-01321-0

Siegfried, A., Bertozzi, A. I., Bourdeaut, F., Sevely, A., Loukh, N., Grison, C., Miquel, C., Lafon, D., Sevenet, N., Pietsch, T., Dufour, C., & Delisle, M. B. (2016). Clinical, pathological, and molecular data on desmoplastic/nodular medulloblastoma: case studies and a review of the literature. *Clin Neuropathol*, *35*(3), 106-113. https://doi.org/10.5414/NP300205

Skubnik, J., Pavlickova, V. S., Ruml, T., & Rimpelova, S. (2021). Vincristine in Combination Therapy of Cancer: Emerging Trends in Clinics. *Biology (Basel)*, *10*(9). https://doi.org/10.3390/biology10090849

Strachan, G. D., Morgan, K. L., Otis, L. L., Caltagarone, J., Gittis, A., Bowser, R., & Jordan-Sciutto, K. L. (2004). Fetal Alz-50 clone 1 interacts with the human orthologue of the Kelch-like Ech-associated protein. *Biochemistry*, *43*(38), 12113-12122. https://doi.org/10.1021/bi0494166

Strachowska, M., Gronkowska, K., Michlewska, S., & Robaszkiewicz, A. (2021). CBP/p300 Bromodomain Inhibitor-I-CBP112 Declines Transcription of the Key ABC Transporters and Sensitizes Cancer Cells to Chemotherapy Drugs. *Cancers (Basel)*, *13*(18). https://doi.org/10.3390/cancers13184614

Subramanian, A., Kuehn, H., Gould, J., Tamayo, P., & Mesirov, J. P. (2007). GSEA-P: a desktop application for Gene Set Enrichment Analysis. *Bioinformatics*, *23*(23), 3251-3253. https://doi.org/10.1093/bioinformatics/btm369

Taguchi, K., Motohashi, H., & Yamamoto, M. (2011). Molecular mechanisms of the Keap1-Nrf2 pathway in stress response and cancer evolution. *Genes Cells*, *16*(2), 123-140. https://doi.org/10.1111/j.1365-2443.2010.01473.x

Tang, Y., Gholamin, S., Schubert, S., Willardson, M. I., Lee, A., Bandopadhayay, P., Bergthold, G., Masoud, S., Nguyen, B., Vue, N., Balansay, B., Yu, F., Oh, S., Woo, P., Chen, S., Ponnuswami, A., Monje, M., Atwood, S. X., Whitson, R. J., . . . Cho, Y. J. (2014). Epigenetic targeting of Hedgehog pathway transcriptional output through BET bromodomain inhibition. *Nat Med*, *20*(7), 732-740. https://doi.org/10.1038/nm.3613

Taylor, L., Wade, P. K., Johnson, J. E. C., Aldighieri, M., Morlando, S., Di Leva, G., Kerr, I. D., & Coyle, B. (2023). Drug Resistance in Medulloblastoma Is Driven by YB-1, ABCB1 and a Seven-Gene Drug Signature. *Cancers (Basel)*, *15*(4). https://doi.org/10.3390/cancers15041086

Taylor, M. D., Northcott, P. A., Korshunov, A., Remke, M., Cho, Y. J., Clifford, S. C., Eberhart, C. G., Parsons, D. W., Rutkowski, S., Gajjar, A., Ellison, D. W., Lichter, P., Gilbertson, R. J., Pomeroy, S. L., Kool, M., & Pfister, S. M. (2012). Molecular subgroups of medulloblastoma: the current consensus. *Acta Neuropathol*, *123*(4), 465-472. https://doi.org/10.1007/s00401-011-0922-z

Thomas, A., & Noel, G. (2019). Medulloblastoma: optimizing care with a multidisciplinary approach. *J Multidiscip Healthc*, *12*, 335-347. https://doi.org/10.2147/JMDH.S167808

Tiberi, L., Bonnefont, J., van den Ameele, J., Le Bon, S. D., Herpoel, A., Bilheu, A., Baron, B. W., & Vanderhaeghen, P. (2014). A BCL6/BCOR/SIRT1 complex triggers neurogenesis and suppresses medulloblastoma by repressing Sonic Hedgehog signaling. *Cancer Cell*, *26*(6), 797-812. https://doi.org/10.1016/j.ccell.2014.10.021

Tonelli, C., Chio, I. I. C., & Tuveson, D. A. (2018). Transcriptional Regulation by Nrf2. *Antioxid Redox Signal*, *29*(17), 1727-1745. https://doi.org/10.1089/ars.2017.7342

Tong, K. I., Katoh, Y., Kusunoki, H., Itoh, K., Tanaka, T., & Yamamoto, M. (2006). Keap1 recruits Neh2 through binding to ETGE and DLG motifs: characterization of the two-site molecular recognition model. *Mol Cell Biol*, *26*(8), 2887-2900. https://doi.org/10.1128/MCB.26.8.2887-2900.2006

Triscott, J., Yip, S., Johnston, D., Michaud, J., Rassekh, S. R., Hukin, J., Dunn, S., & Dunham, C. (2021). Histologic Correlates of Molecular Group 4 Pediatric Medulloblastoma: A Retrospective Canadian Review. *Pediatr Dev Pathol*, *24*(4), 309-317. https://doi.org/10.1177/10935266211001986

van der Lugt, N. M., Domen, J., Linders, K., van Roon, M., Robanus-Maandag, E., te Riele, H., van der Valk, M., Deschamps, J., Sofroniew, M., van Lohuizen, M., & et al. (1994). Posterior transformation, neurological abnormalities, and severe hematopoietic defects in mice with a targeted deletion of the bmi-1 proto-oncogene. *Genes Dev*, *8*(7), 757-769. https://doi.org/10.1101/gad.8.7.757

Varan, A. (2011). Risk-adapted chemotherapy in childhood medulloblastoma. *Expert Rev Anticancer Ther*, *11*(5), 771-780. https://doi.org/10.1586/era.10.222

Visconti, R., Della Monica, R., & Grieco, D. (2016). Cell cycle checkpoint in cancer: a therapeutically targetable double-edged sword. *J Exp Clin Cancer Res*, *35*(1), 153. https://doi.org/10.1186/s13046-016-0433-9

Vo, N., & Goodman, R. H. (2001). CREB-binding protein and p300 in transcriptional regulation. *J Biol Chem*, *276*(17), 13505-13508. https://doi.org/10.1074/jbc.R000025200

Volkel, P., & Angrand, P. O. (2007). The control of histone lysine methylation in

epigenetic regulation. *Biochimie*, *89*(1), 1-20. https://doi.org/10.1016/j.biochi.2006.07.009

Wakabayashi, N., Itoh, K., Wakabayashi, J., Motohashi, H., Noda, S., Takahashi, S., Imakado, S., Kotsuji, T., Otsuka, F., Roop, D. R., Harada, T., Engel, J. D., & Yamamoto, M. (2003). Keap1-null mutation leads to postnatal lethality due to constitutive Nrf2 activation. *Nature Genetics*, *35*(3), 238-245. https://doi.org/10.1038/ng1248

Wang, J. C., Lu, Q. Y., Cai, J. Y., Wang, Y., Lai, X. F., Qiu, Y., Huang, Y. N., Ke, Q., Zhang, Y. N., Guan, Y. J., Wu, H. X., Wang, Y. Y., Liu, X., Shi, Y., Zhang, K., Wang, M. S., & Xiang, A. P. (2019). Nestin regulates cellular redox homeostasis in lung cancer through the Keap1-Nrf2 feedback loop. *Nature Communications*, *10*. https://doi.org/ARTN 5043
10.1038/s41467-019-12925-9

Wei, L., Lee, D., Law, C. T., Zhang, M. S., Shen, J., Chin, D. W., Zhang, A., Tsang, F. H., Wong, C. L., Ng, I. O., Wong, C. C., & Wong, C. M. (2019). Genome-wide CRISPR/Cas9 library screening identified PHGDH as a critical driver for Sorafenib resistance in HCC. *Nat Commun*, *10*(1), 4681. https://doi.org/10.1038/s41467-019-12606-7

Wiederschain, D., Chen, L., Johnson, B., Bettano, K., Jackson, D., Taraszka, J., Wang, Y. K., Jones, M. D., Morrissey, M., Deeds, J., Mosher, R., Fordjour, P., Lengauer, C., & Benson, J. D. (2007). Contribution of polycomb homologues Bmi-1 and Mel-18 to medulloblastoma pathogenesis. *Mol Cell Biol*, *27*(13), 4968-4979. https://doi.org/10.1128/MCB.02244-06

Wijaya, J., Fukuda, Y., & Schuetz, J. D. (2017). Obstacles to Brain Tumor Therapy: Key ABC Transporters. *Int J Mol Sci*, *18*(12). https://doi.org/10.3390/ijms18122544

Wilkens, S. (2015). Structure and mechanism of ABC transporters. *F1000Prime Rep*, *7*, 14. https://doi.org/10.12703/P7-14

Williamson, D., Schwalbe, E. C., Hicks, D., Aldinger, K. A., Lindsey, J. C., Crosier, S., Richardson, S., Goddard, J., Hill, R. M., Castle, J., Grabovska, Y., Hacking, J., Pizer, B., Wharton, S. B., Jacques, T. S., Joshi, A., Bailey, S., & Clifford, S. C. (2022). Medulloblastoma group 3 and 4 tumors comprise a clinically and biologically significant expression continuum reflecting human cerebellar development. *Cell Rep*, *40*(5), 111162. https://doi.org/10.1016/j.celrep.2022.111162

Wippold, F. J., 2nd, & Perry, A. (2006). Neuropathology for the neuroradiologist: rosettes and pseudorosettes. *AJNR Am J Neuroradiol*, *27*(3), 488-492. https://www.ncbi.nlm.nih.gov/pubmed/16551982

Wu, K. C., Cui, J. Y., & Klaassen, C. D. (2012). Effect of graded Nrf2 activation on phase-I and -II drug metabolizing enzymes and transporters in mouse liver. *PLoS*

*One*, *7*(7), e39006. https://doi.org/10.1371/journal.pone.0039006

Yamamoto, T., Suzuki, T., Kobayashi, A., Wakabayashi, J., Maher, J., Motohashi, H., & Yamamoto, M. (2008). Physiological significance of reactive cysteine residues of Keap1 in determining Nrf2 activity. *Mol Cell Biol*, *28*(8), 2758-2770. https://doi.org/10.1128/MCB.01704-07

Yedier-Bayram, O., Gokbayrak, B., Kayabolen, A., Aksu, A. C., Cavga, A. D., Cingoz, A., Kala, E. Y., Karabiyik, G., Gunsay, R., Esin, B., Morova, T., Uyulur, F., Syed, H., Philpott, M., Cribbs, A. P., Kung, S. H. Y., Lack, N. A., Onder, T. T., & Bagci-Onder, T. (2022). EPIKOL, a chromatin-focused CRISPR/Cas9-based screening platform, to identify cancer-specific epigenetic vulnerabilities. *Cell Death Dis*, *13*(8), 710. https://doi.org/10.1038/s41419-022-05146-4

Yedier-Bayram, O., Gokbayrak, B., Kayabolen, A., Aksu, A. C., Cavga, A. D., Cingöz, A., Kala, E. Y., Karabiyik, G., Günsay, R., Esin, B., Morova, T., Uyulur, F., Syed, H., Philpott, M., Cribbs, A. P., Kung, S. H. Y., Lack, N. A., Onder, T. T., & Bagci-Onder, T. (2022). EPIKOL, a chromatin-focused CRISPR/Cas9-based screening platform, to identify cancer-specific epigenetic vulnerabilities. *Cell Death & Disease*, *13*(8), 710. https://doi.org/10.1038/s41419-022-05146-4

Yi, J., & Wu, J. (2018). Epigenetic regulation in medulloblastoma. *Mol Cell Neurosci*, *87*, 65-76. https://doi.org/10.1016/j.mcn.2017.09.003

Zhang, D. D., Lo, S. C., Cross, J. V., Templeton, D. J., & Hannink, M. (2004). Keap1 is a redox-regulated substrate adaptor protein for a Cul3-dependent ubiquitin ligase complex. *Mol Cell Biol*, *24*(24), 10941-10953. https://doi.org/10.1128/MCB.24.24.10941-10953.2004

Zhang, H., Zhu, D., Zhang, Z., Kaluz, S., Yu, B., Devi, N. S., Olson, J. J., & Van Meir, E. G. (2020). EZH2 targeting reduces medulloblastoma growth through epigenetic reactivation of the BAI1/p53 tumor suppressor pathway. *Oncogene*, *39*(5), 1041-1048. https://doi.org/10.1038/s41388-019-1036-7

Zhang, Y., Jiang, C., Li, H., Lv, F., Li, X., Qian, X., Fu, L., Xu, B., & Guo, X. (2015). Elevated Aurora B expression contributes to chemoresistance and poor prognosis in breast cancer. *Int J Clin Exp Pathol*, *8*(1), 751-757. https://www.ncbi.nlm.nih.gov/pubmed/25755770

Zhang, Y., Shi, Z., Zhou, Y., Xiao, Q., Wang, H., & Peng, Y. (2020). Emerging Substrate Proteins of Kelch-like ECH Associated Protein 1 (Keap1) and Potential Challenges for the Development of Small-Molecule Inhibitors of the Keap1-Nuclear Factor Erythroid 2-Related Factor 2 (Nrf2) Protein-Protein Interaction. *J Med Chem*, *63*(15), 7986-8002. https://doi.org/10.1021/acs.jmedchem.9b01865

Zhang, Y., Yang, H., Wang, L., Zhou, H., Zhang, G., Xiao, Z., & Xue, X. (2022). TOP2A correlates with poor prognosis and affects radioresistance of medulloblastoma. *Front*

*Oncol*, *12*, 918959. https://doi.org/10.3389/fonc.2022.918959

Zhao, Z., & Shilatifard, A. (2019). Epigenetic modifications of histones in cancer. *Genome Biol*, *20*(1), 245. https://doi.org/10.1186/s13059-019-1870-5

Zhu, P., Zhou, W., Wang, J., Puc, J., Ohgi, K. A., Erdjument-Bromage, H., Tempst, P., Glass, C. K., & Rosenfeld, M. G. (2007). A histone H2A deubiquitinase complex coordinating histone acetylation and H1 dissociation in transcriptional regulation. *Mol Cell*, *27*(4), 609-621. https://doi.org/10.1016/j.molcel.2007.07.024

Zhu, Y., Wang, Z., Li, Y., Peng, H., Liu, J., Zhang, J., & Xiao, X. (2023). The Role of CREBBP/EP300 and Its Therapeutic Implications in Hematological Malignancies. *Cancers (Basel)*, *15*(4). https://doi.org/10.3390/cancers15041219

Zucconi, B. E., Luef, B., Xu, W., Henry, R. A., Nodelman, I. M., Bowman, G. D., Andrews, A. J., & Cole, P. A. (2016). Modulation of p300/CBP Acetylation of Nucleosomes by Bromodomain Ligand I-CBP112. *Biochemistry*, *55*(27), 3727-3734. https://doi.org/10.1021/acs.biochem.6b00480

Zwergel, C., Romanelli, A., Stazi, G., Besharat, Z. M., Catanzaro, G., Tafani, M., Valente, S., & Mai, A. (2018). Application of Small Epigenetic Modulators in Pediatric Medulloblastoma. *Front Pediatr*, *6*, 370. https://doi.org/10.3389/fped.2018.00370